INFORMATION TO USERS

This material was produced from a microfilm copy of the original document. While the most advanced technological means to photograph and reproduce this document have been used, the quality is heavily dependent upon the quality of the original submitted.

The following explanation of techniques is provided to help you understand markings or patterns which may appear on this reproduction.

1. The sign or "target" for pages apparently lacking from the document photographed is "Missing Page(s)". If it was possible to obtain the missing page(s) or section, they are spliced into the film along with adjacent pages. This may have necessitated cutting thru an image and duplicating adjacent pages to insure you complete continuity.

2. When an image on the film is obliterated with a large round black mark, it is an indication that the photographer suspected that the copy may have moved during exposure and thus cause a blurred image. You will find a good image of the page in the adjacent frame.

3. When a map, drawing or chart, etc., was part of the material being photographed the photographer followed a definite method in "sectioning" the material. It is customary to begin photoing at the upper left hand corner of a large sheet and to continue photoing from left to right in equal sections with a small overlap. If necessary, sectioning is continued again — beginning below the first row and continuing on until complete.

4. The majority of users indicate that the textual content is of greatest value, however, a somewhat higher quality reproduction could be made from "photographs" if essential to the understanding of the dissertation. Silver prints of "photographs" may be ordered at additional charge by writing the Order Department, giving the catalog number, title, author and specific pages you wish reproduced.

5. PLEASE NOTE: Some pages may have indistinct print. Filmed as received.

Xerox University Microfilms
300 North Zeeb Road
Ann Arbor, Michigan 48106

FLOW PATTERNS, "ROLLING MOTIONS," AND THICKNESS OF THE NEUTRAL HYDROGEN IN THE GALAXY

by

LANCE WALLACE

A dissertation submitted to the Graduate Faculty in Physics in partial fulfillment of the requirements for the degree of Doctor of Philosophy, the City University of New York.

1974

This manuscript has been read and accepted for the Graduate Faculty in Physics in satisfaction of the dissertation requirement for the degree of Doctor of Philosophy.

5/21/74
date

Chi Yuan
Chairman of Examining Committee

5/21/74
date

Marvin Mittleman
Executive Officer

(Supervisory Committee)

Marvin H. Mittleman

R.B. Stothers

Leon Cohen

W.W. Roberts, Jr.

The City University of New York

ABSTRACT

FLOW PATTERNS, "ROLLING MOTIONS," AND THICKNESS OF THE NEUTRAL HYDROGEN IN THE GALAXY

by

LANCE WALLACE

Adviser: Professor Chi Yuan

PART I: The detailed 3-dimensional velocity and density fields of the neutral hydrogen in the Galaxy are obtained from a linear solution of the perturbed equations of fluid dynamics. The results of applying an integrated form of the boundary conditions on the mass flux in the vertical direction yield a unique density contrast between spiral arm and interarm regions which depends on the strength of the spiral field at that point. Using current "best" values of galactic parameters, we find the density contrast near the 10-kpc circle to be in the ratio of 5:1. The density contrast varies with distance from the plane, falling at first and then rising until the limiting distance of the linear approximation (about 300 pcs) is reached. The vertical flow of the gas is extremely small, and is probably not observable.

PART II: The results of Part I are utilized to provide a numerical model of the gaseous component of the Galaxy, from which brightness-temperature contour maps can be produced by computer and compared to observations. Such maps are used to test and confirm a conjecture that the "rolling motions" observed in the spiral arms for the past decade, and thought to involve energies of 10^{50} ergs per kpc length of the arm, are only apparent motions resulting from a combination of the displacement of the arms from the galactic plane with the differential rotation of the Galaxy.

ABSTRACT (continued)

PART III: The apparent increase in thickness of the Galaxy with distance from the sun is established with the aid of several previous studies and from new measurements of the thickness from a variety of large-scale 21-cm surveys of the Galaxy. The increase in thickness is apparent in every survey; it appears to be linear and to have a magnitude of 30-40 pcs/kpc. Assuming this "distance effect" is an illusion of some sort, we can remove it from consideration and arrive at improved estimates of the thickness of the Galaxy. These new estimates are considerably smaller than previous estimates. Possible causes of the "distance effect" are enumerated, discussed, and (in some cases) eliminated.

TABLE OF CONTENTS

LIST OF ILLUSTRATIONS

(Note: Captions immediately precede each diagram and are numbered C-1 through C-35. Diagrams are located immediately following the pages of the text on which they are discussed.)

LIST OF ILLUSTRATIONS (Continued)

INTRODUCTION

The first fully successful theory of galactic spiral structure was advanced in 1964 by C. C. Lin and Frank Shu. Known as the density wave theory, it accounted for the galactic spiral arms as a rigidly rotating spiral wave, through which the hydrogen gas and stars pass in roughly circular stream lines and at varying speeds (agreeing with the observed rotation curve of the Galaxy) depending on their radial distance from the galactic center. By postulating that the spiral pattern was a wave composed at different times of different particles of gas and stars rather than a material concentration consisting of the same gas and stars over long periods of time, Lin and Shu avoided the major pitfall of the previous theories--the so-called "winding dilemma" caused by the differential rotation of the Galaxy, which would force any unreplenished material spiral arms to be wound up into 25 or 50 turns over the lifetime of the Galaxy.

To make the problem mathematically tractable, Lin and Shu treated the Galaxy as a two-dimensional fluid, justifying their approximation by the observation that the radius of the Galaxy is roughly 50 times the thickness.

Later, in his unpublished thesis, Shu considered the effects of the thickness of the Galaxy in an integrated form, finding that the finite thickness could be accommodated in the original theory by the introduction of a "reduction factor" which would take into account both the reduced gravitational potential when the gas and stars are allowed to spread out from the plane, and the reduced "response" (or density redistribution) of both components to their own gravitational field according to the Poisson and Boltzmann equations.

With the introduction of a large-scale spiral shock wave (Roberts 1969), the density-wave theory brought an impressive list of observed phenomena into the confines of a single theoretical structure (Lin, Shu, and Yuan, 1969; Yuan, 1969; Roberts and Yuan, 1970) and made several predictions regarding systematic motion of the gas and synchrotron radiation along the postulated shock wave that have since been fulfilled. Thus the theory has been rapidly accepted by the astrophysical community.

Nonetheless, certain questions cannot be answered by the theory in its present state. Among these questions are

(1) What are the streamlines of the hydrogen gas and the magnitudes of its vertical motion? (The answer to this question may throw light on the observed

influx of gas at low velocities near the galactic poles; it would also allow 3-dimensional numerical models of the Galaxy to be constructed and then used to prepare theoretical profiles and contour line diagrams of the brightness temperature of the gas due to 21-cm line emission to be compared with observations.)

(2) How does the magnitude and phase of the horizontal motions of the gas change with distance from the plane?

(3) What is the density variation of the gas with distance from the galactic plane? (Answers to the last two questions could determine limits to the distance from the galactic plane at which stars could be born.)

(4) What is the theoretical thickness of the Galaxy, and how does it depend on such elements as the strength of the Galactic spiral gravitational field and the magnitude of the dispersion velocity of the gas? Also, how does this theoretical thickness compare with observed values? (Answers to these questions could determine limits to the strength of the Galactic magnetic field and the cosmic-ray energy density, assuming that these quantities contribute to "holding up" the gas.)

(5) How can such observations as the "rolling motion" of the spiral arms around their longitudinal axes be accounted for by known physical mechanisms?

All these questions have in common the requirement that a detailed study be made of the full 3-dimensional response of the gas to a 3-dimensional spiral gravitational field. A stellar spiral field satisfying the requirements of the Boltzmann and Poisson equations was constructed by Vandervoort in 1970 and will be used as the basis for such a detailed study in Part I of the following thesis. In Part II, we will apply the results of Part I to the study of a particular problem, the "rolling motion" of the gas, and will find an unexpected solution to that problem. Finally, in Part III, another aspect of the vertical structure of the Galaxy will be examined--its thickness, as determined from 21-cm line observations--and we will give the first quantitative discussion of a heliocentric "distance effect" which has gone almost completely unnoticed and which leads to considerable overestimates of the Galactic thickness.

LARGE-SCALE THREE-DIMENSIONAL BEHAVIOR OF THE DENSITY AND FLOW PATTERNS OF THE NEUTRAL GALACTIC HYDROGEN

In this section, we shall solve the fluid equations determining the large-scale density variations and the full three-dimensional flow patterns of the neutral hydrogen in the Galaxy. To do so, we make two basic assumptions:

(1) The velocities in the radial, azimuthal, and z-directions may be treated as perturbations on a basis state of pure circular rotation. Since the circular velocity at the position of the sun is 250 km/sec while the peculiar velocities are $\sim$ 10 km/sec, this seems to be a particularly good assumption.

(2) The flow of the gas is determined entirely by the stellar potential, and the response of the gas (i.e., its changes in density distribution) to the stellar potential will not change the total potential significantly. In the vicinity of the sun, the gas probably has less than 15% of the mass of the stars, so this assumption also appears to be well-founded. However, at greater distances from the galactic center, the gaseous component may have a relatively larger proportion of the mass; for these areas, the assumption that the response of the gas will not change the potential significantly would have to be re-examined.

The equations of continuity, motion, and state for the gas are

$$\frac{\partial u_\varpi}{\partial t} + u_\varpi \frac{\partial u_\varpi}{\partial \varpi} + \frac{u_\vartheta}{\varpi}\frac{\partial u_\varpi}{\partial \vartheta} + u_z \frac{\partial u_\varpi}{\partial z} - \frac{u_\vartheta^2}{\varpi} = \frac{-1}{\rho}\frac{\partial P}{\partial \varpi} - \frac{\partial \gamma}{\partial \varpi}$$

$$\frac{\partial u_\vartheta}{\partial t} + u_\varpi \frac{\partial u_\vartheta}{\partial \varpi} + \frac{u_\vartheta}{\varpi}\frac{\partial u_\vartheta}{\partial \vartheta} + u_z \frac{\partial u_\vartheta}{\partial z} + \frac{u_\vartheta u_\varpi}{\varpi} = \frac{-1}{\rho\varpi}\frac{\partial P}{\partial \vartheta} - \frac{1}{\varpi}\frac{\partial \gamma}{\partial \vartheta}$$

$$\frac{\partial u_z}{\partial t} + u_\varpi \frac{\partial u_z}{\partial \varpi} + \frac{u_\vartheta}{\varpi}\frac{\partial u_z}{\partial \vartheta} + u_z \frac{\partial u_z}{\partial z} = -\frac{1}{\rho}\frac{\partial P}{\partial z} - \frac{\partial \gamma}{\partial z}$$

$$\frac{\partial \rho}{\partial t} + \frac{1}{\varpi}\frac{\partial}{\partial \varpi}(\varpi u_\varpi \rho) + \frac{1}{\varpi}\frac{\partial}{\partial \vartheta}(\rho u_\vartheta) + \frac{\partial}{\partial z}(\rho u_z) = 0$$

$$P = a^2 \rho$$

Here γ, the stellar potential, is taken from Vandervoort (1970) and consists of an axisymmetric portion $\gamma^{(0)}$:

$$\gamma^{(0)} = \gamma_\infty(\varpi, 0) + 2\pi G \sigma_* \Delta \ln(2\cosh z/\Delta)$$

where γ_∞ is the potential due to an infinitesimal disk of surface density σ_*, and the second term is due to a finite disk of half-thickness Δ;

and a spiral portion $\gamma^{(1)}$:

$$\gamma^{(1)} = N_0(\varpi)\,\mathrm{sech}^{|k|\Delta}\frac{z}{\Delta}\, e^{i(\omega t - m\vartheta + \Phi(\varpi))}$$

in which N_0 is the amplitude of the potential, $k \equiv \frac{d\Phi}{d\varpi}$ is the local (radial) wavenumber of the spiral whose phase is $\Phi(\varpi)$, and ω is taken to be a real number to insure the maintenance in time of the spiral wave. (If the spiral pattern has m arms and rotates at an angular velocity of Ω_p, then $\omega = m\Omega_p$.)

Now we impose a spiral perturbation of the same form as the spiral potential on our unknowns $\underset{\sim}{u}$ and $\rho(\varpi, z, \theta)$:

$$\underset{\sim}{u} = \underset{\sim}{u}^{(0)}_{(\varpi,z)} + \underset{\sim}{u}^{(1)}_{(\varpi,z)} e^{i(\omega t - m\theta + \Phi(\varpi))}; \quad \rho = \rho^{(0)}_{(\varpi,z)} + \rho^{(1)}_{(\varpi,z)} e^{i(\omega t - m\theta + \Phi(\varpi))}$$

where $\underset{\sim}{u}^{(1)}$ and $\rho^{(1)}$ vary slowly compared to the phase term $\Phi(\varpi)$.

For $\underset{\sim}{u}^{(0)}$ we take a basis state of pure circular rotation:

$$\underset{\sim}{u}^{(0)} = (0, u_{\theta_0}(\varpi), 0)$$

The zero-order equations then reduce to

$$-u_{\theta_0}^2/\varpi = -\frac{a^2}{\rho^{(0)}} \partial\rho^{(0)}/\partial\varpi - \frac{\partial\gamma^{(0)}}{\partial\varpi}$$

$$0 = -a^2/\rho^{(0)} \partial\rho^{(0)}/\partial z - \frac{\partial\gamma^{(0)}}{\partial z}$$

The solution for the axisymmetric gas density $\rho^{(0)}$ is

$$\rho^{(0)} = \rho_0 \operatorname{sech}^2 z/\Delta$$

where $\beta^2 \equiv \frac{2\pi G \sigma_* \Delta}{a^2} = \frac{2\langle v_z^2 \rangle}{a^2}$

Since $\langle v_z^2 \rangle$, the stellar dispersion velocity, is of the order of 20 km/sec, and a shall be taken here as of the order of 10 km/sec, consisting of contributions from the gaseous dispersion velocity, and contributions to the pressure from the magnetic field and cosmic rays, the value of β^2 in the local region is around 8; thus the gas has a far smaller scale height than the stars, which fall off as $\operatorname{sech}^2 \frac{z}{\Delta}$. Farther out, assuming a^2 remains roughly constant, the value of β^2 drops rapidly, and we would expect an increase in the thickness of the gas layer in the outer regions. Such an increase is in fact observed, and we show in a later section that the magnitude of the observed increase agrees extremely well with the calculated behavior of β^2.

Closer in toward the center of the galaxy, a constant value of a^2 would lead to increased values of β^2 and a corresponding decrease in the thickness of the gas layer, which is not observed. Therefore for the regions interior to the sun we may either let $\underline{a}$ increase toward the center or alternately choose β^2 = constant to match the observed relatively constant value for the thickness of the gas layer. The first alternative--increasing the value of $\underline{a}$ toward the center--is supported by the observations of Burton (1969), Shane (1970) and others, who find that the behavior of the velocity dispersion σ_v of the gas may be described by a linear function of the radius:

$$\sigma_v = 9.0 - 0.4\,\varpi$$

Of course, σ_v as defined is one component of our $\underline{a}$.

The shape of the $\operatorname{sech}^2 \beta \frac{z}{\Delta}$ curve is close to that of a Gaussian, but is wider at the wings. Thus it matches the observations a bit better than a Gaussian (see Schmidt 1957). However, the widening at the wings observed by Schmidt is even greater than that supplied by the $\operatorname{sech}^2 \beta \frac{z}{\Delta}$ curve.

At this point, we may distinguish the following two cases:

(1) The spiral perturbation density of the gas is far smaller than the axisymmetric density: $\rho^{(1)} << \rho^{(0)}$ In this case, the actual density increase in the arm regions is small, perhaps too small to allow for efficient star formation. This case may correspond to the SO galaxies, which are flattened in the manner of spiral galaxies but show no spiral structure.

(2) The spiral component of the gas may be nearly comparable in size to the axisymmetric component: $\rho^{(1)} \lesssim \rho^{(0)}$ Here the density contrast between the arm and interarm regions (i.e., the ratio $(\rho^{(0)} + \rho^{(1)})/(\rho^{(0)} - \rho^{(1)})$ is larger. We shall see later that this assumption probably more nearly corresponds to the case of our own galaxy.

Case I: $\rho^{(1)} << \rho^{(0)}$

In this case, there is a completely formal linear analysis, with both unknowns ($\rho^{(1)}$ and $\underset{\sim}{u}^{(1)}$) being much smaller than the quantities $\rho^{(0)}$ and $\underset{\sim}{u}^{(0)}$. We now assume that the spiral pattern rotates like a rigid body at the angular velocity Ω_p, and we write the first-order equations in the rotating system of reference. In this system, $\frac{\partial \underset{\sim}{u}}{\partial t} = f\underset{\sim}{u}$, where $f \equiv \omega - m\Omega = m(\Omega_p - \Omega)$ is the frequency with which a gaseous element encounters the same configuration of spiral arms. (For a spiral pattern of m arms, this is m times the frequency with which it encounters the same spiral arm.)

In the system rotating with the spiral pattern, then, we have the following equations for $\rho^{(1)}$ and $\underset{\sim}{u}^{(1)}$:

$$if\, u_{\varpi}^{(1)} - 2\Omega\, u_{\vartheta}^{(1)} = -i\, k\, \gamma^{(1)}$$

$$if\, u_{\vartheta}^{(1)} + \kappa^2/2\Omega\, u_{\varpi}^{(1)} = 0$$

$$if\, \rho^{(0)} u_z^{(1)} + \rho^{(1)} \frac{\partial \gamma^{(0)}}{\partial z} = -\rho^{(0)} \frac{\partial \gamma^{(1)}}{\partial z}$$

$$i\, k\, \rho^{(0)} u_{\varpi}^{(1)} + \partial/\partial z\, (\rho^{(0)} u_z^{(1)}) = 0$$

Here $\kappa = 2\Omega\left(1 + \frac{\varpi}{2\Omega}\frac{d\Omega}{d\varpi}\right)^{1/2}$ is the epicyclic frequency of the stars. Note that several terms which are formally first-order terms have been dropped because in actuality they are insignificant compared to the other first-order terms.

The four equations break into two sets of two, and we may solve the first two for $u_{\varpi}^{(1)}$ and $u_{\vartheta}^{(1)}$ immediately:

$$u_{\varpi}^{(1)} = \frac{kf}{\kappa^2 - f^2}\, \gamma^{(1)}$$

$$u_{\vartheta}^{(1)} = i\, \frac{k\, \kappa^2/2\Omega}{\kappa^2 - f^2}\, \gamma^{(1)}$$

We now fix the magnitude of the spiral potential in order to arrive at a quantitative estimate of the behavior of the above perturbation velocities. The magnitude of the spiral potential in the vicinity of the sun appears to be about 5% of the mean gravitational potential (see Yuan 1969) and using that figure we find that $|N_0| \sim 170$ (km/sec)^2. For values of $\underline{k} = -1.5$ (the negative sign depicts a trailing arm), $\underline{f} \equiv m(\Omega_p - \Omega) = 2(25 - 13.5) = -23$ km/sec/kpc, and $\kappa = 32$ km/sec/kpc, we find that the systematic radial velocity of the gas in the plane has a value in the vicinity of the sun of about

$$u_{\varpi}^{(1)} \sim -12 \text{ km/sec}$$

This is quite close, but a little too high, to the values of 6-10 km/sec usually cited in the literature. A similar calculation for $u_{\theta}^{(1)}$ shows a value of $\sim$ 10 km/sec. The phases of the two components of the velocity agree with those previously found in the two-dimensional studies of Lin, Shu, and Yuan (1969): the radial component is toward the galactic center in the arms and away from the center in the interarm regions, while the azimuthal component is against the direction of rotation inside the arms and with the rotation outside the arms. Thus the present set of equations has succeeded in reproducing the behavior of the planar components of the velocity already found by two-dimensional studies and gives hope that the results for the remaining two components will also be trustworthy.

The final two equations may now be written

$$i f \mu + \frac{1}{\rho^{(0)}} \frac{\partial}{\partial z} j_z = \frac{i k^2 f}{k^2 - f^2} \gamma^{(1)}$$

$$a^2 \frac{\partial \mu}{\partial z} + i f \rho^{(0)} j_z = -\frac{\partial \gamma^{(1)}}{\partial z}$$

where we have changed to the more convenient variables j_z (the mass flux or "current" in the z-direction) and $\mu \equiv \rho^{(1)}/\rho^{(0)}$ (the ratio of the spiral density component to the axisymmetric component).

We see at once from the above that for a plane-symmetric density and potential distribution, j_z must go to zero at $z = 0$. That is, <u>the gas cannot cross the galactic plane,</u> unlike the stars, which oscillate freely through it.

Secondly, again from qualitative consideration of the equations, we can determine that the phases of the z-motion are such that <u>the gas swoops toward the plane as it approaches a spiral arm and is released to rise away from the plane after it passes through the arm</u>. (Recall that we are considering the case $\rho^{(1)} \ll \rho^{(0)}$; for Case II, in which $\rho^{(1)} \lesssim \rho^{(0)}$, this conclusion is modified. See below.)

<u>Boundary Conditions.</u> To solve the equations analytically, we must first settle on the proper boundary conditions for the Galaxy. This question has been treated by several authors without, perhaps, a completely satisfactory conclusion. The best-known treatment is that of Goldreich and Lynden-Bell, whose boundary conditions for an isothermal atmosphere are

$$\frac{\rho^{(1)}}{\rho^{(0)}} \longrightarrow 0 \quad \text{as} \quad z \longrightarrow \pm\infty$$

$$\rho^{(0)} u_z^{(1)} \Big|_{-\infty}^{\infty} = 0$$

Their second condition appears to be a somewhat weakened statement of conservation of mass: that is, any mass flowing in at $z = -\infty$, say, must flow out again at $z = +\infty$, to avoid matter sinks or sources. Their first condition, while appearing reasonable at first glance, may in fact be too stringent--it appears to throw out the interesting

kinds of behavior studied by Landau and Lifschitz and others (internal gravity waves), in which a density perturbation grows with increasing height in an exponential atmosphere. Moreover, the boundary conditions as given by Goldreich and Lynden-Bell will probably not allow symmetry around the plane except in special instances; for requiring symmetry puts a third boundary condition and overspecifies the system of equations.

For these reasons, we prefer the following boundary conditions:

$$\rho^{(1)}(z) = \rho^{(1)}(-z)$$

$$j_z \left(\equiv \rho^{(0)} u_z^{(1)} \right) \longrightarrow 0 \quad \text{as} \quad z \longrightarrow \pm \infty$$

(Note that the condition of symmetry around the plane immediately requires that j_z be an odd function of z. Then Goldreich and Lynden-Bell's boundary condition on j_z reduces to the one given above, since $j_z(+\infty) = -j_z(-\infty)$.)

The basic difference between Goldreich and Lynden-Bell's boundary conditions and ours is that we demand symmetry around the plane but allow $\rho^{(1)}/\rho^{(0)}$ to increase without bound, while they demand that $\rho^{(1)}/\rho^{(0)}$ go to zero while sacrificing symmetry around the plane. Of course, in our treatment, at some value of z the value of $\mu \equiv \rho^{(1)}/\rho^{(0)}$ exceeds 1, and the original assumption of smallness is violated. However, to anticipate for the moment our numerical results, the point at which μ becomes equal to 1 is usually in the region $z \sim 500$ pcs. Since most of the gas is concentrated to within the first 200 pcs of the plane, it seems that any effects occurring around 500 pcs will be insignificant; this is our justification

for treating Vandervoort's "local" spiral potential, expected to apply out to about z = 300 pcs, as being good out to infinity, and applying boundary conditions at infinity to arrive at an analytical solution.

It turns out to be necessary for the later numerical analysis of these equations to transform the second boundary condition by integrating the equation of continuity over z:

$$if \int_{-\infty}^{\infty} \rho^{(1)} dz + \dot{z}\Big|_{-\infty}^{+\infty} = \frac{-i k^2 f}{k^2 - f^2} \int_{-\infty}^{\infty} \rho^{(0)} \gamma^{(1)} dz$$

$$\text{or} \quad \int_{-\infty}^{\infty} \rho^{(1)} dz = \frac{-k^2}{k^2 - f^2} \int_{-\infty}^{\infty} \rho^{(0)} \gamma^{(1)} dz$$

We can compare this result, obtained for a differentially-rotating disk with a spiral perturbation, to the result obtained by Lynden-Bell and Goldreich for a uniformly-rotating disk and a plane-wave perturbation:

$$\int_{-\infty}^{\infty} \rho^{(1)} dz = \frac{k^2}{4\Omega^2 - \omega^2} \int_{-\infty}^{\infty} \rho^{(0)} \left[\gamma^{(1)} - a^2 \frac{\rho^{(1)}}{\rho^{(0)}} \right] dz$$

(Here our potential is negative and theirs is positive, which accounts for the difference in sign.) Their ω is essentially our f (both quantities measure the frequency with which a gaseous element encounters the density wave), but their Ω, the constant angular velocity of the disk, has been replaced by our $\kappa/2$ (half the epicyclic frequency), a quantity that varies with radius from the center. We are lacking their term involving $\frac{\rho^{(1)}}{\rho^{(0)}}$, because we are now treating the "pressureless" case $\rho^{(1)} \ll \rho^{(0)}$. Later we will allow $\rho^{(1)}$ to become of the order of $\rho^{(0)}$ (Case II below) and then we will find a result essentially similar to that of Goldreich and Lynden-Bell. This is the crucial formulation of the boundary condtion that will allow a complete numerical

solution of the equations.

An easy way of satisfying the boundary condition is to have $\rho^{(1)}$ be proportional to $\rho^{(0)}\psi^{(1)}$ everywhere. This is perhaps what impelled Shu to state that $\rho^{(1)} \propto \rho^{(0)}\psi^{(1)}$. However, if we let $\rho^{(1)} \propto \rho^{(0)}\psi^{(1)}$ and plug back into the equations for j_z and for μ, we find that only for a special sort of potential, namely one that is linear in z, can we have $\rho^{(1)} \propto \rho^{(0)}\psi^{(1)}$ everywhere. As it turns out, the spiral potential (sech $\frac{|k|\Delta}{\Delta} z$) near the plane varies quite slowly and uniformly in z, due to the small value of $|k|\Delta$, so that in fact it is not too bad an approximation to say that $\rho^{(1)} \propto \rho^{(0)}\psi^{(1)}$ at least close to the plane. However, it is more accurate to say that the spiral perturbation density decreases faster than $\rho^{(0)}\psi^{(1)}$ near the plane and slower than $\rho^{(0)}\psi^{(1)}$ away from the plane.

Analytic Solution. The complete set of equations with the boundary conditions discussed immediately above can be solved formally in an analytic fashion, but we have not succeeded in presenting the results in a useful fashion. Therefore the calculations have been banished to the appendix.

Case II: $\rho^{(1)} \lesssim \rho^{(0)}$

We now consider the case in which a well-defined contrast between the spiral arms and the interarm region is displayed by the gas. The full set of equations is now the following:

$$if u_\omega^{(1)} - 2\Omega u_\theta^{(1)} = -ik a^2 \frac{\rho^{(1)}}{\rho^{(0)}} - ik \gamma^{(1)}$$

$$if u_\theta^{(1)} + \kappa^2/2\Omega u_\omega^{(1)} = 0$$

$$if \rho^{(0)} u_z^{(1)} = -a^2 \frac{\partial \rho^{(1)}}{\partial z} - \rho^{(0)} \frac{\partial \gamma^{(1)}}{\partial z} - \rho^{(1)} \frac{\partial \gamma^{(0)}}{\partial z}$$

$$if \rho^{(1)} + \partial/\partial z (\rho^{(0)} u_z^{(1)}) + ik \rho^{(0)} u_\omega^{(1)} = 0$$

where new terms involving $\rho^{(1)}$ have made their appearance in the first and third equations of the set. Again we consider the first two equations and solve for the planar components of the velocity:

$$u_\omega^{(1)} = \frac{kf}{\kappa^2 - f^2} \left[a^2 \frac{\rho^{(1)}}{\rho^{(0)}} + \gamma^{(1)} \right]$$

$$u_\theta^{(1)} = \frac{-\kappa^2}{2if\Omega} u_\omega^{(1)}$$

The expression for the radial component $u_\omega^{(1)}$ may be compared to that obtained in Case I, where it was proportional to the spiral potential $\gamma^{(1)}$ alone. Since $\rho^{(1)}$ and $\gamma^{(1)}$ are of opposite phases, the radial velocity is reduced by the addition of the pressure term. For values of $\mu_0 \equiv \left. \frac{\rho^{(1)}}{\rho^{(0)}} \right|_{z=0}$

ranging from 0.5 to 0.9 (and using previous values for $\underline{a}$ and $\rho^{(1)}$), the magnitude of the radial systematic motion varies from 9 km/sec to 6 km/sec. The excellent agreement of these values with those observed in our Galaxy is an indication that the Milky Way is likely to be described by the present set of equations more closely than by the equations of Case I (small density contrast).

The remaining two equations for j_z and for μ may be written:

$$\frac{\partial \mu}{\partial z} = \frac{-if}{\rho^{(0)} a^2} j_z - \frac{1}{a^2} \frac{\partial \rho^{(1)}}{\partial z}$$

$$\partial j_z / \partial z = -if \rho^{(0)} \left[(1+x)\mu + x \frac{\rho^{(1)}}{a^2} \right]$$

where $x = k^2 a^2 / \kappa^2 - f^2$.

Before turning to the numerical solution of these equations, we consider the qualitative effect of retaining the pressure term. First we note that there is now a critical value of μ_o past which the direction of flow of the gas changes sign with respect to the position of the spiral arms:

$$\mu_{crit} = \frac{-x}{1+x} \frac{\rho^{(1)}|_{z=0}}{a^2} = \frac{-x}{1+x} \frac{1}{a^2} \eta \frac{\omega - \Omega^2}{k}$$

where η ($\sim 5\%$) is the fractional strength of the spiral field $\frac{\partial \pi^{(1)}}{\partial \varpi}$ compared to the axisymmetric component $\frac{\partial \pi^{(0)}}{\partial \varpi}$. In case I, no matter what the value of μ_o, the direction of j_z was such that the gas flow was toward the plane as it approached a spiral arm. In the present case, this is still true for values of $\mu_o < \mu_{crit}$; but for values of

$\mu_o \tilde{>} \mu_{crit}$, the direction of j_z is reversed close to the plane but remains as before for higher values of z; and finally for values of μ_o sufficiently greater than μ_{crit}, (i.e., μ_o greater than μ_{crit} by a few percent), the direction of j_z is reversed for all values of z. That is, the gas flow is away from the plane as it approaches a spiral arm. Which of these three possibilities is actually the case must be decided by application of the boundary condition, which fixes the value of μ_o. We note that the third possibility mentioned above, gas flow away from the plane as it approaches a spiral arm, would be physically unacceptable if the flow in the vertical direction were a major component of the gas motion, since then the volume density of the gas would be decreasing as it enters a spiral arm. However, to anticipate once again the results obtained in numerical analysis, it turns out that the velocities in the z-direction as determined by the application of the integrated form of the boundary condition, are so small that they have essentially no effect on the volume density of the gas. Therefore, a flow pattern of the type exemplified by the third possibility above, in which a slight expansion in the vertical direction is coupled with a compression in the radial direction, is certainly not ruled out by physical arguments.

In summary, the effect of considering the pressure term (that is, allowing $\rho^{(1)}$ to approach the magnitude of $\rho^{(0)}$) has been to reduce the magnitude of the systematic motion in the plane and to provide extra possibilities for the vertical portion of the flow pattern.

Numerical Solution. The numerical solution of our two coupled first-order inhomogeneous ordinary differential equations for j_z and μ can be carried out by starting at $z = 0$ by requiring $j_z(0) = 0$, and determining the correct value of μ_0 by applying the condition that $jz(\infty)$ go to 0 at $z = \pm \infty$; or, in integrated form,

$$\int_{-\infty}^{\infty} \rho^{(1)} dz = \frac{-\chi}{1+\chi} \frac{1}{a^2} \int_{-\infty}^{\infty} \rho^{(0)} \gamma^{(1)} dz$$

In practice, this means that we require

$$\int_0^{\xi_\infty} \rho^{(1)} d\xi = \frac{-\chi}{1+\chi} \frac{1}{a^2} \rho_0 N_0 \int_0^{\xi_\infty} \operatorname{sech}^{\beta^2+|h|\Delta} \xi \, d\xi$$

where ξ_∞ is some reasonable number such as 2.

An iteration technique, starting with arbitrary values for μ_0 and pinching down on the correct value by comparing the left and right-hand-sides of the integrated boundary condition, can determine μ_0 to several decimal places in a few seconds of computer time.

The result of several score computer-generated solutions to the equations above, using a number of different values of ϖ and the associated "best" values of the parameters at that radius, is consistently

$$\frac{\mu_0}{\mu_{CRIT}} = 1.04 \pm 0.02$$

It appears, therefore, that we have a powerful method for determining the proper density contrast between arm and interarm regions in the plane as a function of ω: namely, that $\mu_0 \sim 1.04 \mu_{CRIT}$. Since the density contrast is a subject of considerable uncertainty, with estimates ranging all the way from essentially no contrast (Piddington) to contrasts of 20:1 or larger (Weaver), this appears to be one of the most potentially useful results of the present work. This effect is discussed further below.

The above result also insures that the vertical component of the velocity is virtually as small as possible. Order-of-magnitude arguments concerning the velocity component in the z-direction allow a velocity on the order of a few km/sec, which would have definite observational results. However, the present result appears to limit velocities in the z-direction to a few tenths of a km/sec, at least in the areas of high gas density near the plane. This is an unpleasant result in the sense that it has no observational consequences, and therefore cannot be corroborated in a direct manner. If true, however, it lightens the load for model-galaxy builders, since it implies that z-motions need not be considered even in high-latitude studies.

Finally, the near-equality of $\mu_{0\ corr}$ and μ_{crit} dictate that the flow-pattern of the gas is very close to the transition region in which the gas near the plane

flows slightly away from the plane as it approaches a spiral arm, while the gas farther from the plane may or may not reverse this pattern: the value of $\mu_{0\,corr}$ is so close to the critical multiple of μ_{crit} that a choice of which possibility is the correct one seems extremely difficult. However, the choice between the two patterns of flow has been made far less important by the fact that the velocity in the z-direction has been limited so drastically by the application of the integrated form of the boundary condition; the most important aspect of the flow pattern in the vertical direction is not its direction or phase with respect to the spiral arms but rather its extraordinary smallness: the streamlines of the gas are almost perfectly flat near the plane, and even 100 pcs up they vary up and down by less than 10 pcs. (See Fig. 1).

Density Contrast. We have found that the proper choice for the arm-interarm density contrast in the plane is always just a few percent larger than the value of μ_{crit}. Therefore, by studying the dependence of μ_{crit} on the parameters that determine its magnitude, we may hope to narrow down the limits between which it can vary, and arrive at some quantitative predictions which future observations may confirm or deny. μ_{crit} depends on the following parameters:

(1) k, the local wave number;

(2) a, the effective sonic speed;

(3) κ, the epicyclic frequency;

(4) Ω_p, the pattern speed; and

(5) η, the strength of the spiral component of the gravitational field.

FIGURE 1

Vertical behavior of the gas streamlines for the case in which the spiral gas density $\rho^{(1)}$ is considered small in comparison to the axisymmetric gas density (Case I). The flow is extremely flat near the plane but oscillates more strongly in the rarefied portions far from the plane. The points marked 0 and 2π corresponds to successive spiral arms encountered by the gas in its trip around the galaxy. As it approaches an arm, it is pulled downward by gravitational force; after passing through the arm, it is released to rise away from the plane.

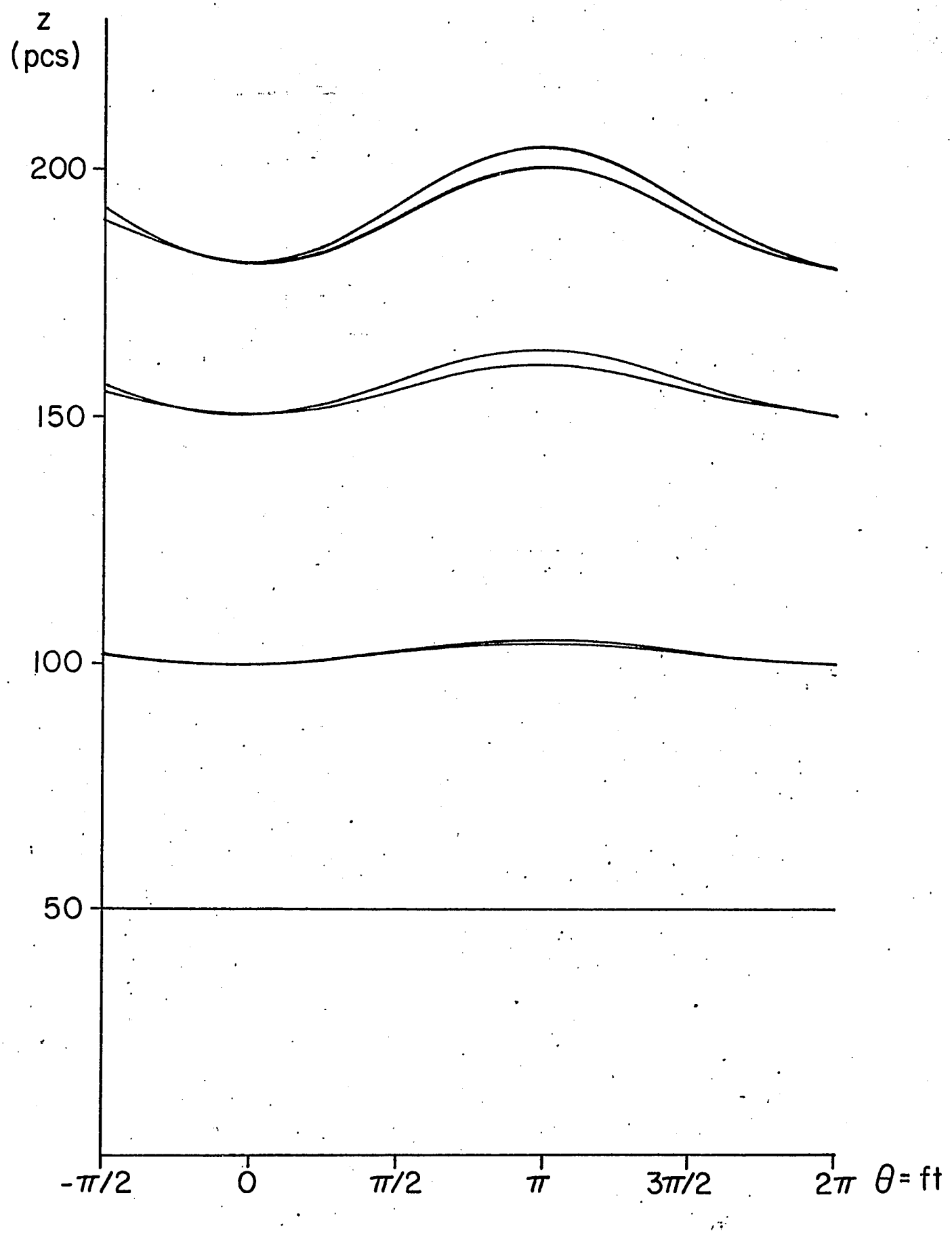
z
(pcs)
200
150
100
50
-π/2
0
π/2
π
3π/2
2π
θ = ft

Using the "best" values of these parameters, namely

$k = 1.6$ kpc^{-1} (corresponding to a pitch angle of 7^{o})

$a = 10$ km/sec

$K = 32$ km/sec/kpc

$\eta = 5\%$

$\Omega_p = 13.5$ km/sec/kpc

we find μ_{crit} in the vicinity of the sun is about 0.67. This corresponds to a density contrast of about 5:1. Choosing what seem to us to be outer limits to the values of the parameters such that μ_{crit} will be reduced to a minimum, namely

$k = 0.9$ kpc^{-1} (pitch angle for the arms of 12^{o})

$a = 12$ km/sec

$K = 32$ km/sec/kpc

$\eta = 4\%$

$\Omega_p = 14.5$ km/sec/kpc

we find that μ_{min} is about 0.33. That is, <u>the minimum density contrast between arm and interarm regions in the vicinity of the sun is 2:1</u>. This result seems to us to be a strong theoretical argument against the contention of Piddington (1973) that the spiral arms of the Galaxy may show little relation to concentrations of neutral hydrogen.

We have less luck in finding an upper limit to μ_{crit} in the vicinity of the sun. Once again choosing outer limits to the parameters such that this time μ_{crit} reaches a maximum value, namely

$k = 1.8$ kpc^{-1} (pitch angle of 6°)

$a = 8$ km/sec

$K = 32$ km/sec/kpc

$\eta = 5\%$

$\Omega_{\rho} = 12.5$ km/sec/kpc

we find that $\mu_{max} = 0.94$, which corresponds to a density contrast of 33:1. Since this is larger than the highest previous estimates, we have not succeeded in placing a strict upper limit on the density contrast.

However, it should be noted that these upper and lower limits on μ_{crit} cannot be attained unless our best estimates of the values of four distinct parameters are all off in precisely the right direction. Probably it is reasonable to place limits on the value of μ_{crit} between 0.5 and 0.8; that is, the density contrast between arm and interarm regions near the sun is not less than 3:1 nor more than 9:1.

The behavior of the density contrast as a function of distance from the galactic center is displayed in Table . The density contrast appears to increase with distance from the center, in qualitative agreement with observations.

The rather high values for μ_{crit} for $\varpi \gtrsim 10$ kpc present a problem: our "small" perturbation quantity $\rho_0^{(1)}$ is of the order of 0.6-0.8 times the magnitude of the zero-order axisymmetric density $\rho_0^{(0)}$! (The subscripts refer to the values in the plane--z = 0.) Might this not invalidate the entire linear analysis? The answer is no, for two reasons. First, the linear approach has

given values for the streaming motions in the plane in full agreement with the original two-dimensional treatment of Lin and Shu and the later extension to an integrated version of the three-dimensional problem by Shu (1967). Second, the value of μ_0 evaluated in the plane is a local maximum; as we move away from the plane, the value of μ_0 falls steadily, reaching a minimum of from 0.05 to 0.37 at heights ranging from 250-500 pcs. (See Fig. 2) Thus, throughout most of the region of interest ($0 < z \lesssim 300$ pcs) the perturbation quantity is indeed small.

Velocity in the z-direction. We have seen that a major result of applying the integrated form of the second boundary condition is that j_z and therefore u_z are sharply reduced. Numerical studies in which the boundary condition was not applied gave typical values for j_z of about 1-2 atoms/cm^3 km/sec, with u_z typically increasing to values of 10 km/sec at $z \sim 200$ pcs. With the strict application of the boundary condition, however, both quantities are reduced to about 10% of these values.

As mentioned above, this result means that the streamlines of the gas are virtually parallel to the plane, an important point for the construction of galactic models. Secondly, the small values obtained for j_z appear to remove the possibility that the observed low-velocity influx of mass at the poles could be due to the normal circulation pattern of the gas.

FIGURE 2

Using presently-accepted values for various galactic parameters leads to this picture of increasing density contrast between arm and interarm regions with increasing distance from the center. (ϖ = 9, 10, and 11 kpc) The behavior of the arm-interarm density contrast with increasing distance from the plane is qualitatively similar in all three cases.

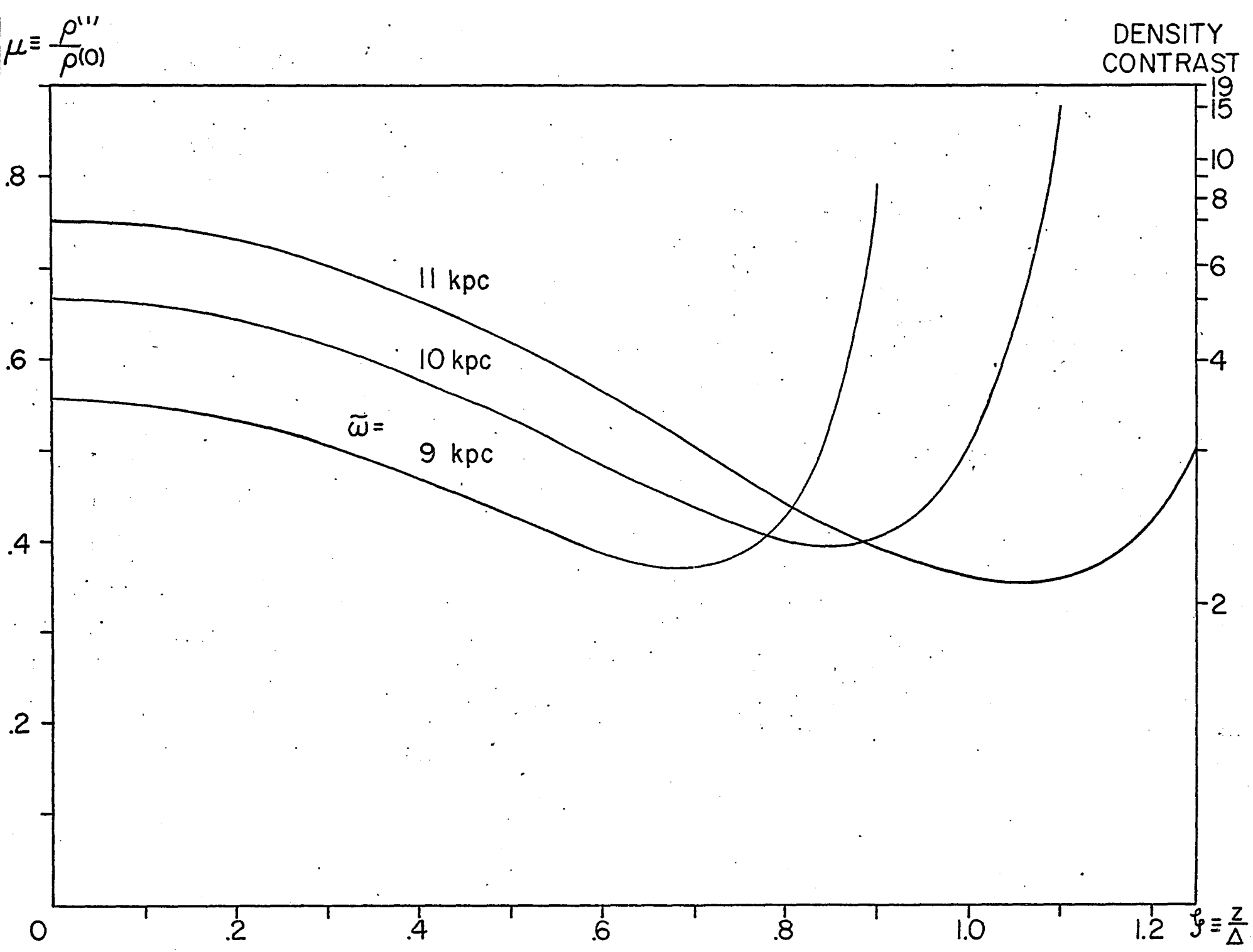
$\mu \equiv \frac{\rho'''}{\rho(0)}$
DENSITY CONTRAST
19
15
10
8
6
4
2
.8
.6
.4
.2
11 kpc
10 kpc
$\tilde{\omega}$ =
9 kpc
0
.2
.4
.6
.8
1.0
1.2
$\vartheta \equiv \frac{z}{\Delta}$

FIGURE 3

Results of the numerical solution for the behavior with increasing distance from the plane of the spiral component of the density $\rho^{(1)}$. The variation with z of the axisymmetric component of the gas density $\rho^{(0)}$ and the spiral component of the stellar potential $g_0^{(1)}$ are also shown. Shu's 1967 approximation to the behavior of the perturbation quantity $\frac{\rho^{(1)}}{\rho^{(0)}}$ would follow the curve for the stellar potential $g_0^{(1)}$; the actual behavior of $\frac{\rho^{(1)}}{\rho^{(0)}}$ in this linear approximation is as shown. This curve begins to blow up at about z = 400 pcs, marking the limit of the region in which the linear approximation is still valid.

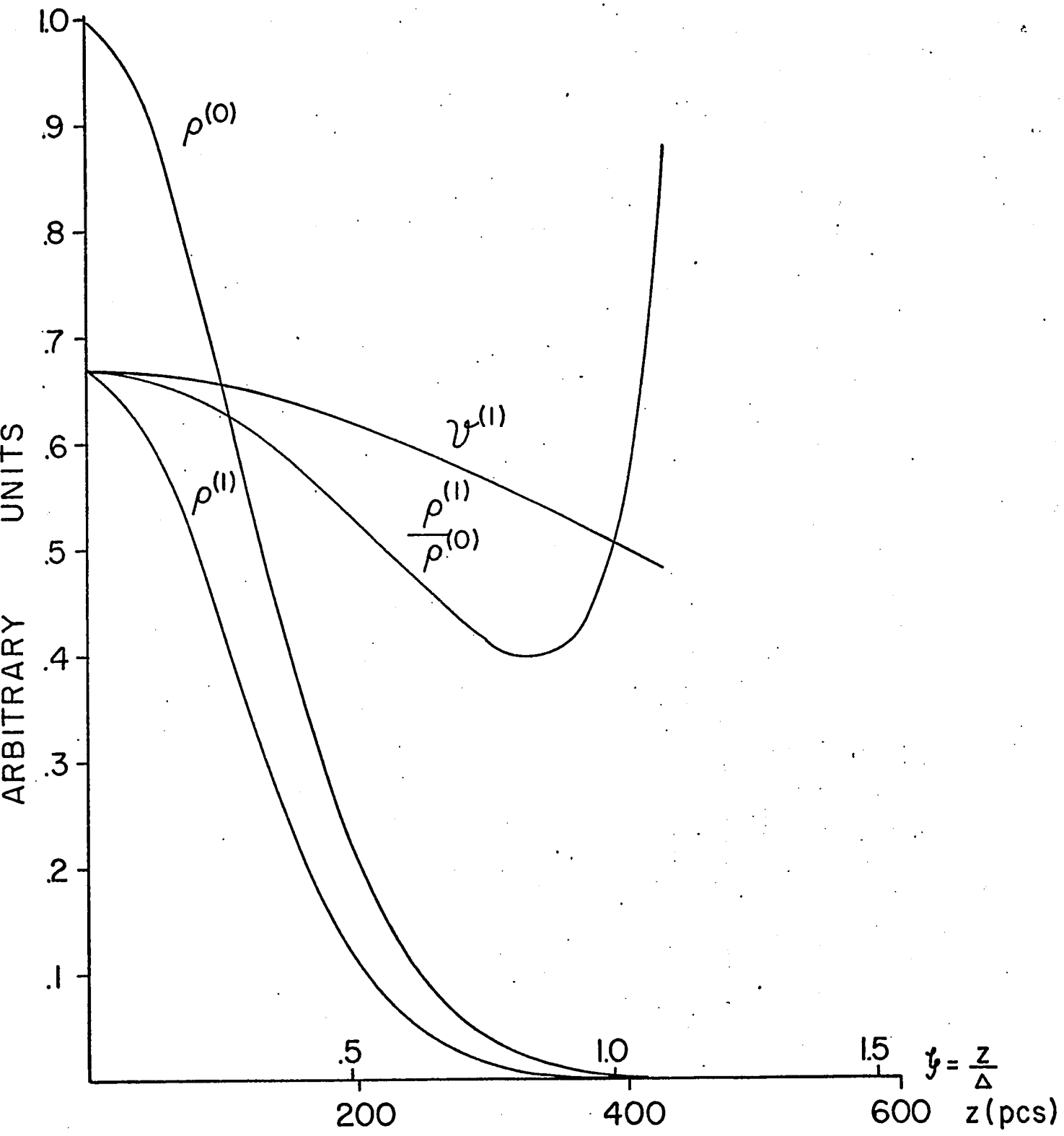
1.0
.9
.8
.7
.6
.5
.4
.3
.2
.1
ARBITRARY UNITS
$\rho^{(0)}$
$v^{(1)}$
$\rho^{(1)}$
$\frac{\rho^{(1)}}{\rho^{(0)}}$
.5
1.0
1.5
$\eta = \frac{z}{\Delta}$
200
400
600
z (pcs)

FIGURE 4

Vertical component of the gas flow for the case in which the spiral gas density is allowed to approach the value of the axisymmetric gas density (Case II). The horizontal axis is the height above the plane in units of Δ (300 pcs); the vertical axis is the mass flux in the z-direction in units of atoms/cm^3 • km/sec. All values are determined at the outer edge of a spiral arm. The two curves for $\mu_o < \mu_{crit}$ are similar to the behavior of the gas flow in Case I, with the gas moving away from the plane as it leaves the gravitational attraction of the arm. Note that as μ_o approaches more closely the value of μ_{crit}, the allowed values of the velocity fall by roughly a factor of 10. However, the phase remains the same for $\mu_o = \mu_{crit}$, with the gas going downward into the spiral arm and upward after passing through it. For μ_o sufficiently greater than μ_{crit} however, the phase reverses and the gas is pushed upward as it enters the spiral arm and falls back down after leaving the arm region. This behavior occurs because the pressure term, which opposes the gravitational term, has surpassed it in strength. Which of these possible types of behavior is actually the case must be determined by the boundary conditions set on the mass flux and the spiral density.

VERTICAL MASS FLUX FOR VALUES OF $\mu_o \gtrless \mu_{CRIT}$

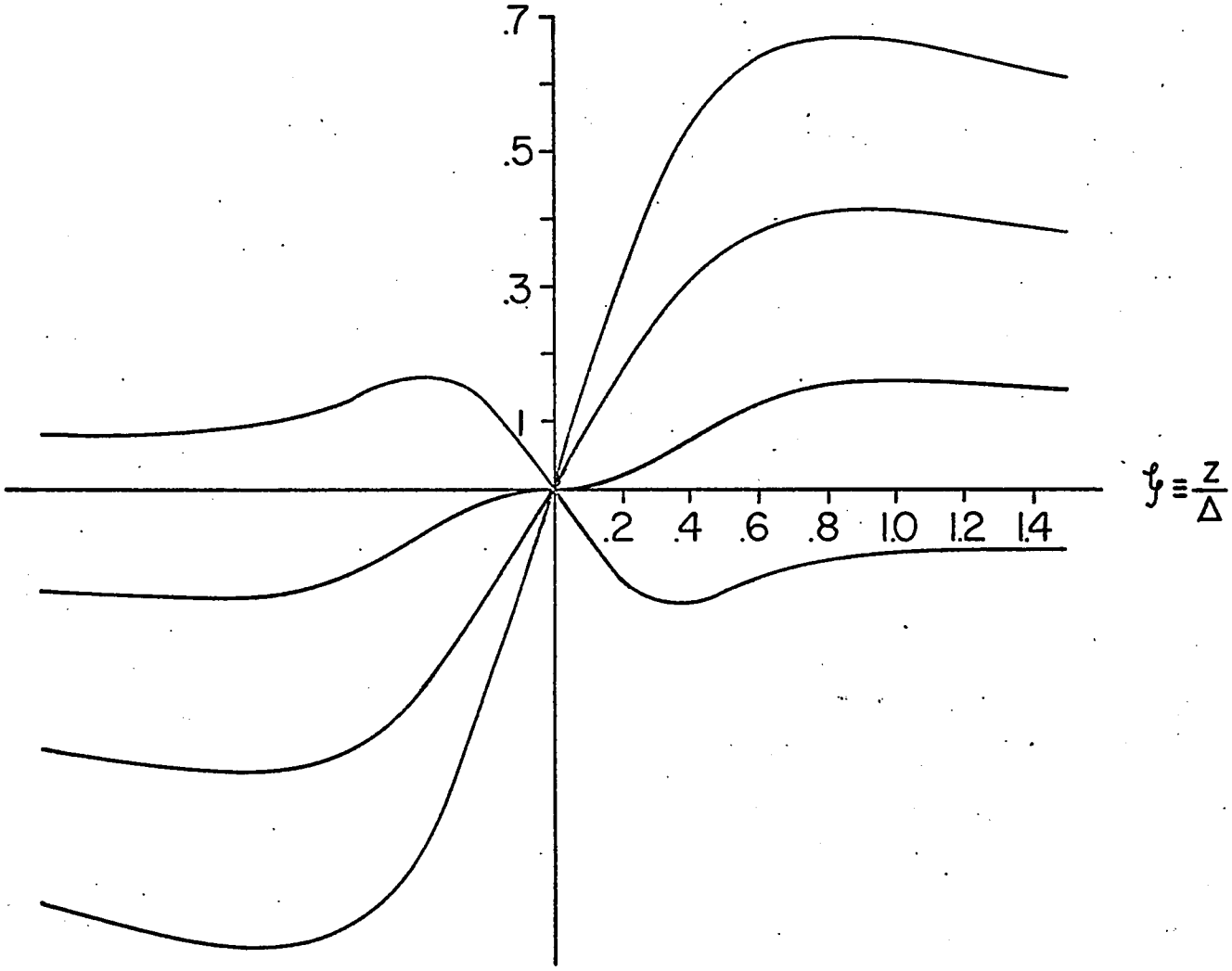

FIGURE 5

Same as the previous figure, but with μ_o only slightly greater than μ_{crit}. Here the pressure term is sufficiently strong to force a reversal of phase near the plane, but further from the plane the phase of the flow is as before.

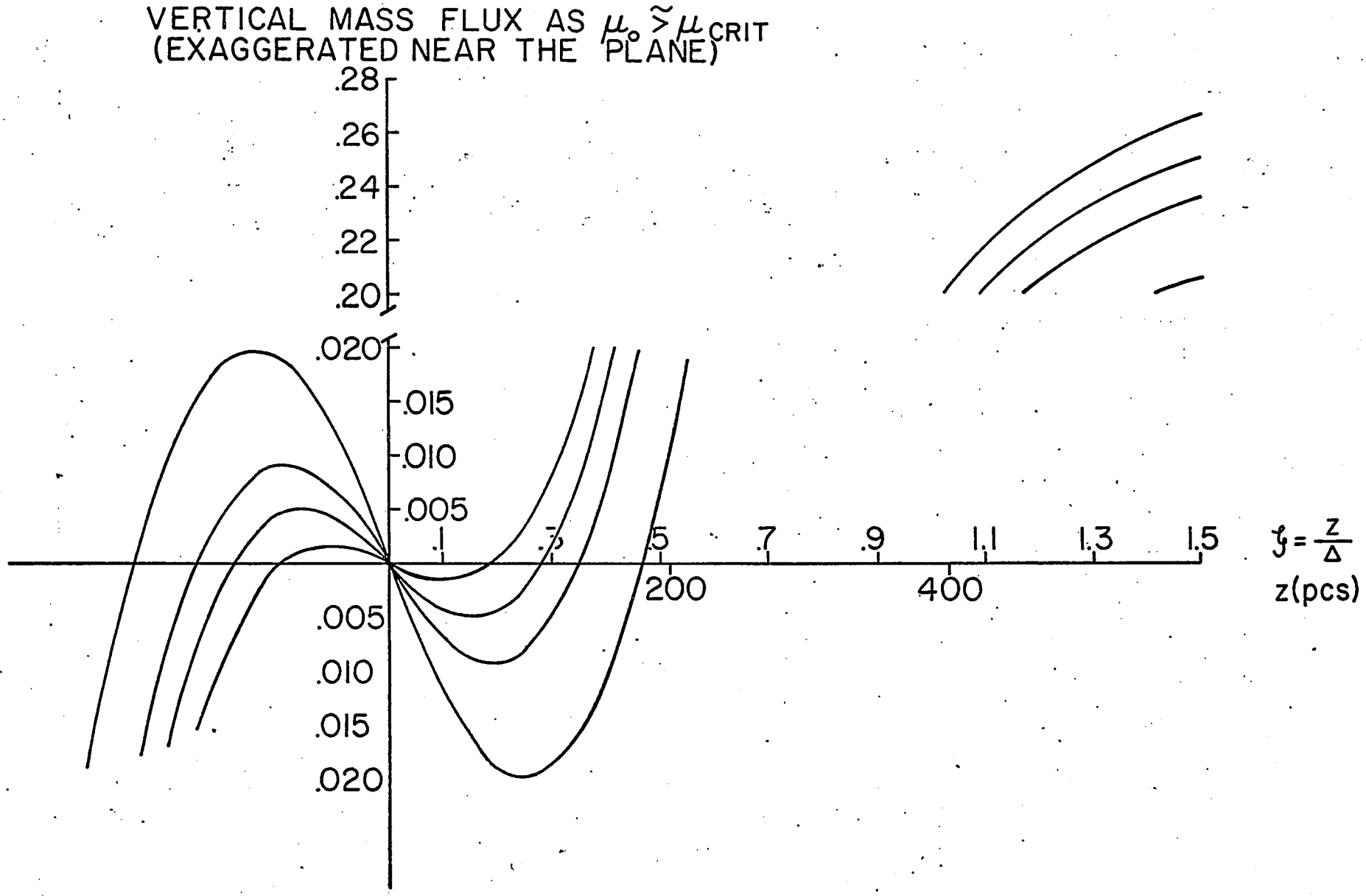
VERTICAL MASS FLUX AS $\mu_o \gtrsim \mu_{CRIT}$
(EXAGGERATED NEAR THE PLANE)
.28
.26
.24
.22
.20
.020
.015
.010
.005
.005
.010
.015
.020
.1
.3
.5
.7
.9
1.1
1.3
1.5
200
400
$\zeta = \frac{z}{\Delta}$
z(pcs)

FIGURE 6A

Calculated thicknesses of the gas in arm and interarm regions. Here the axisymmetric gas density behaves as $\mathrm{sech}^{\beta^2} \frac{z}{\Delta}$, the spiral gas density is determined numerically from the fluid equations and boundary conditions discussed in the text, and the density contrast is that determined from a choice of the "best" galactic parameters in the vicinity of the sun. (i.e., the density contrast is 5:1, and $\mu_{crit} = 0.67$). There appears to be a slight (25 pc) increase in thickness in the interarm regions.

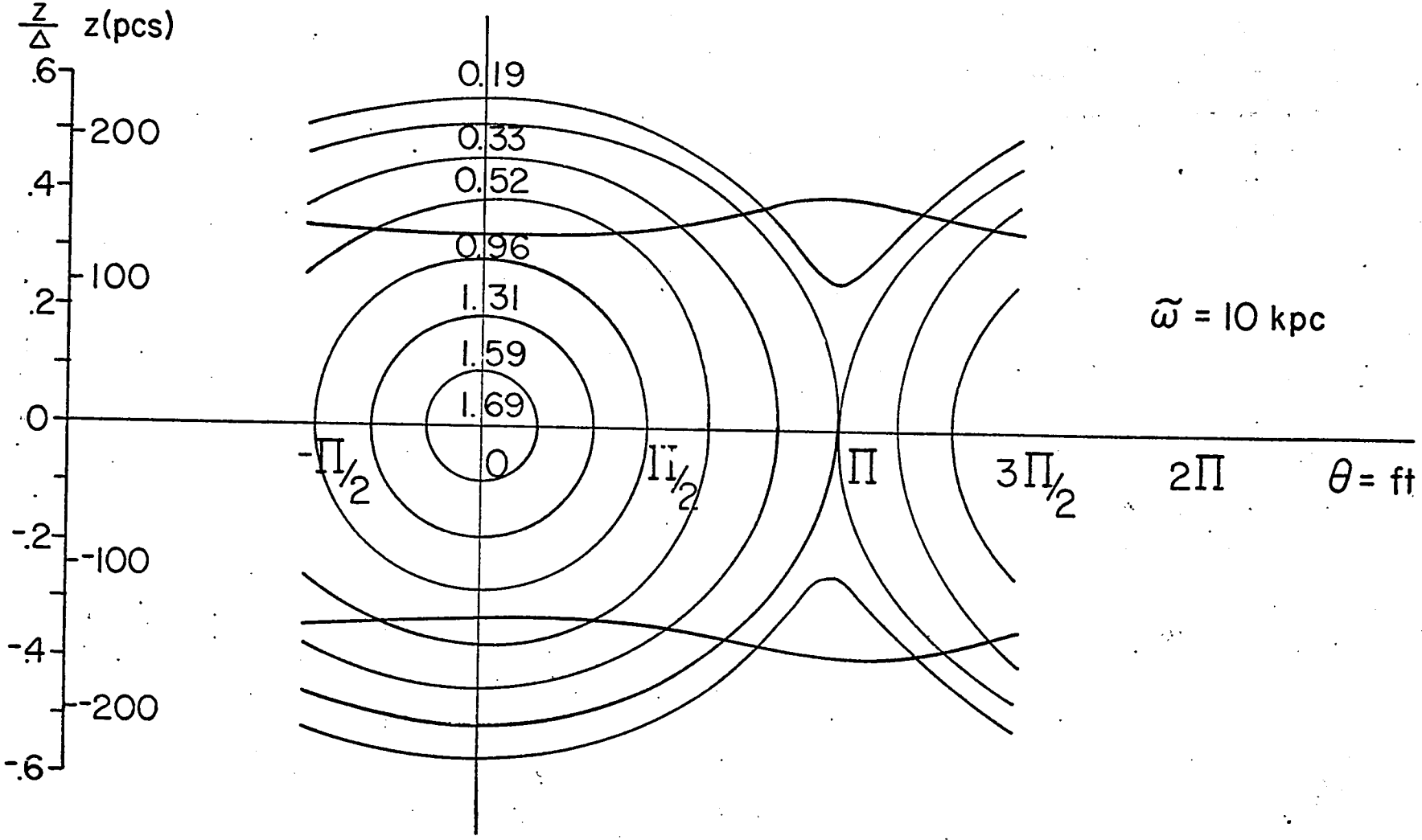
z/Δ
z(pcs)
.6
200
.4
100
.2
0
-.2
-100
-.4
-200
-.6
0.19
0.33
0.52
0.96
1.31
1.59
1.69
0
-Π/2
Π/2
Π
3Π/2
2Π
θ = ft
ω̃ = 10 kpc

FIGURE 6B

Same as the previous figure, but we are now at a galactic radius of 12 kpc. Using the "best" galactic parameters available at this radius results in a value for μ_{crit} of 0.79, corresponding to an arm-interarm density contrast of 9:1. Here the increase in thickness of the interarm regions is spectacular--about 75 pcs.

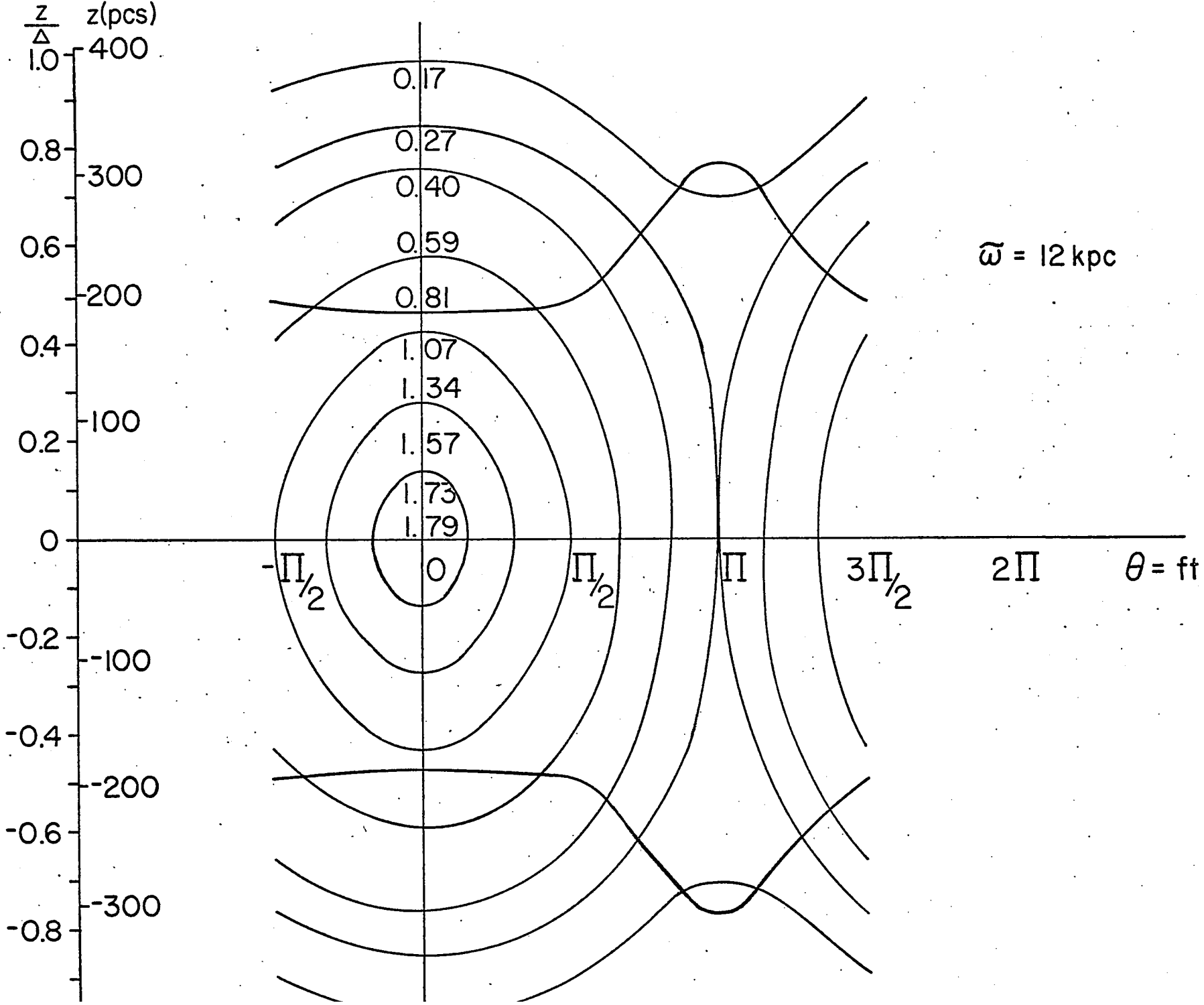
z/Δ
z(pcs)
1.0
400
0.8
300
0.6
200
0.4
100
0.2
0
-0.2
-100
-0.4
-200
-0.6
-300
-0.8
0.17
0.27
0.40
0.59
0.81
1.07
1.34
1.57
1.73
1.79
-Π/2
0
Π/2
Π
3Π/2
2Π
θ = ft
ω̃ = 12 kpc

We are also interested in the behavior of $u_\varpi^{(1)}$ and $u_\vartheta^{(1)}$ away from the plane. Unlike their behavior in Case I, in which they fell off with distance from the plane in proportion to the decrease of the spiral potential, we find them to be remarkably constant over a distance of about 200 pcs from the plane, decreasing in absolute magnitude by only about 5%. This result invalidates a suggestion of Harten's (1971) concerning the cause of the "rolling motion" in spiral arms which depended on a rapid decrease in the magnitude of $u_\varpi^{(1)}$ away from the plane.

The behavior of $u_\varpi^{(1)}$ away from the plane also has an effect on the formation of stars, according to Roberts' ideas concerning large-scale spiral shock waves located on the inner edges of the spiral arms. Since, in his view, the efficiency of shock formation depends on the strength of the shock, which in turn depends on the density and velocity of the gas perpendicular to the shock, the behavior of μ and $u_\varpi^{(1)}$ with vertical distance from the plane is essential to the study of the vertical extent of the shock wave. A means of putting limits on the distance from the plane that a star can be born appears to be within reach.

Velocity Dispersion of the Gas. The velocity dispersion of the interstellar medium is a subject of intense interest, since it gives information about the temperature and structure of the interstellar gas. Several methods of determining the velocity dispersion of the gas have been used, including Gaussian analysis of the observations (Shane 1971, Burton 1970, Takakubo 1967). This method suffers from the fact that the components identified by eye from the brightness-temperature profiles may bear no relation to actual physical components of the interstellar gas. Another method involves measuring the extent into the "forbidden" area of the latitude-velocity diagrams of gas observed at the cardinal points; but this method fails because of the existence of systematic motions of unknown magnitude. Here we discuss a third method, which does not give precise values of the velocity dispersion but which may be useful in identifying any large-scale variations of the velocity dispersion with distance from the galactic center.

The basic idea is to measure the velocity width associated with the tangent points of the gas, and then to translate this width into a velocity dispersion using computer models of the galaxy. The actual values of the velocity dispersion so found will depend on the accuracy of the model; but the variation of the values with distance from the galactic center should be considerably less model-dependent.

To carry out this program, we must first be able to locate, on any given latitude-velocity diagram, the actual maximum velocity, corresponding to the tangent point. A priori, it might appear that a density peak located 10 or even 20 km/sec from the true maximum velocity of the gas would tend to mask the actual point of ocurrence of the maximum velocity. However, because of the fact that we are integrating for large distances along nearly constant velocity at this point, the effect of the velocity plateau completely overwhelms nearby density peaks. That is, it is our contention that the brightness-temperature peak at highest velocity in the observed maps of the inner regions is, in every case, due to the effect of the velocity plateau without regard to the density of the associated gas. Of course, this statement can easily be checked, by comparing the velocities of the observed brightness-temperature peaks with those of the Schmidt model. If the difference between the two values is both small and consistent for all longitudes then the hypothesis above is correct. The results of our own measurements from the observations of Henderson and Kerr in the northern sky and Kerr in the southern are given in Figs. 7A, 7B. The Henderson observations were presented with a more extended velocity axis than those of Kerr and should therefore show less scatter and be more reliable; these measurements show a highly constant difference

FIGURE 7A

A comparison of the maximum velocities associated with a brightness-temperature peak, and the velocities at the half-maximum points on the steeply-falling part of the curve, as read directly from observations of Henderson (1966) and Kerr (1969), with Schmidt's 1965 model for the motion of the gas in the Northern Sky. The good agreement of the two curves indicates that is generally safe to consider the "innermost" (maximum-velocity) brightness temperature peak on a b-v diagram as representing not a spiral arm but rather a case of a large contribution to the optical depth caused by a slow change in velocity of the gas over a considerable distance. (This is the "velocity stretching" discussed by Burton (1970).) This in turn indicates that it may be all right to take the distance in velocity between the brightness temperature peak and the half-maximum contours (vertical distance between the two dashed lines) as being proportional to the velocity dispersion of the gas. Note the gradual decrease in the velocity dispersion with increasing longitude (increasing distance from the center), agreeing with theoretical considerations and with earlier observational results.

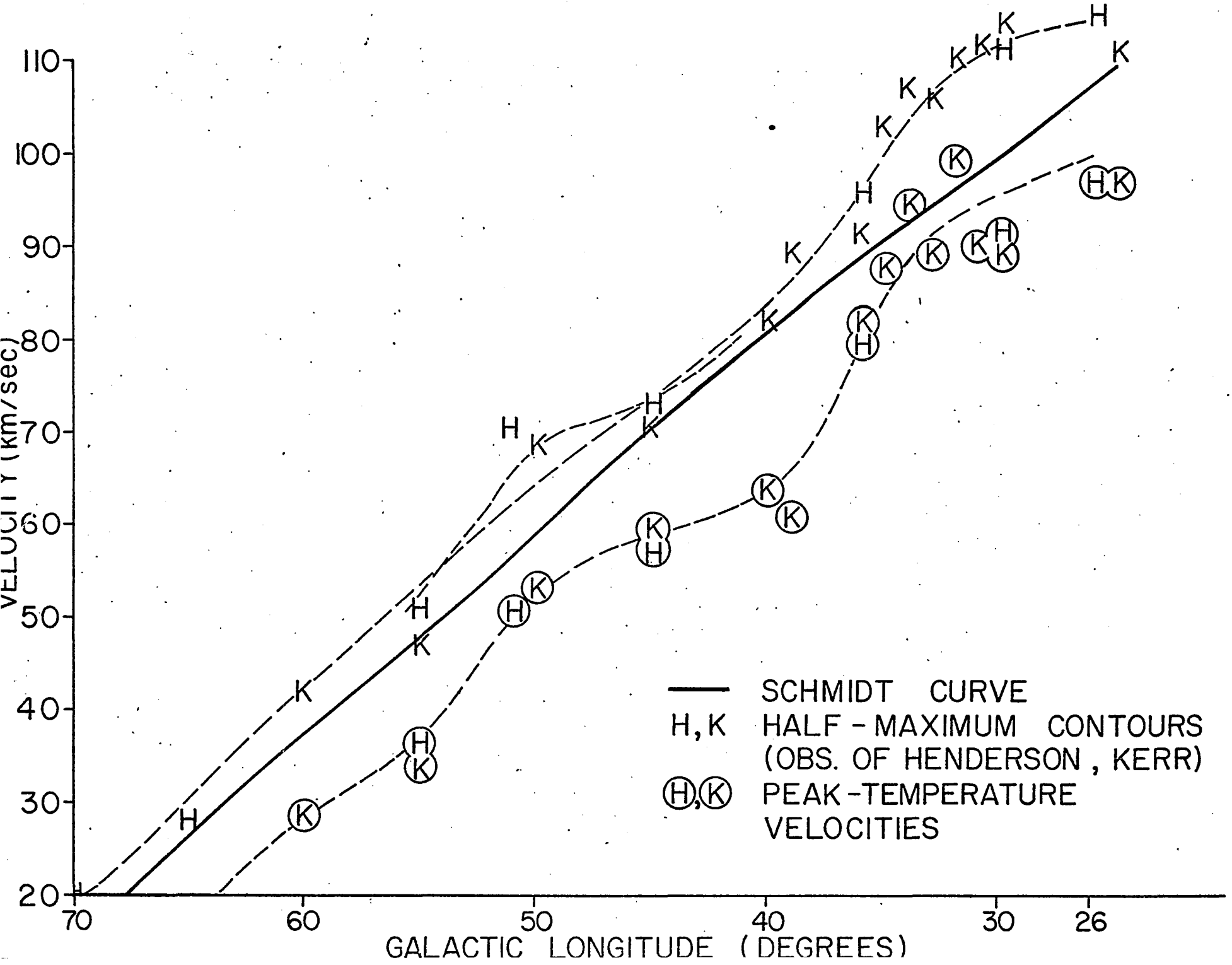
110
100
90
80
70
60
50
40
30
20
VELOCITY (km/sec)
70
60
50
40
30
26
GALACTIC LONGITUDE (DEGREES)
SCHMIDT CURVE
H, K HALF-MAXIMUM CONTOURS (OBS. OF HENDERSON, KERR)
(H),(K) PEAK-TEMPERATURE VELOCITIES

FIGURE 7B

Same as the previous figure for the case of the Southern Sky (observations taken from Kerr (1969). Once again the distance between the dashed lines appears to be a good indicator of the velocity dispersion, but there is no longer a clear increase in the velocity dispersion as we approach the center.

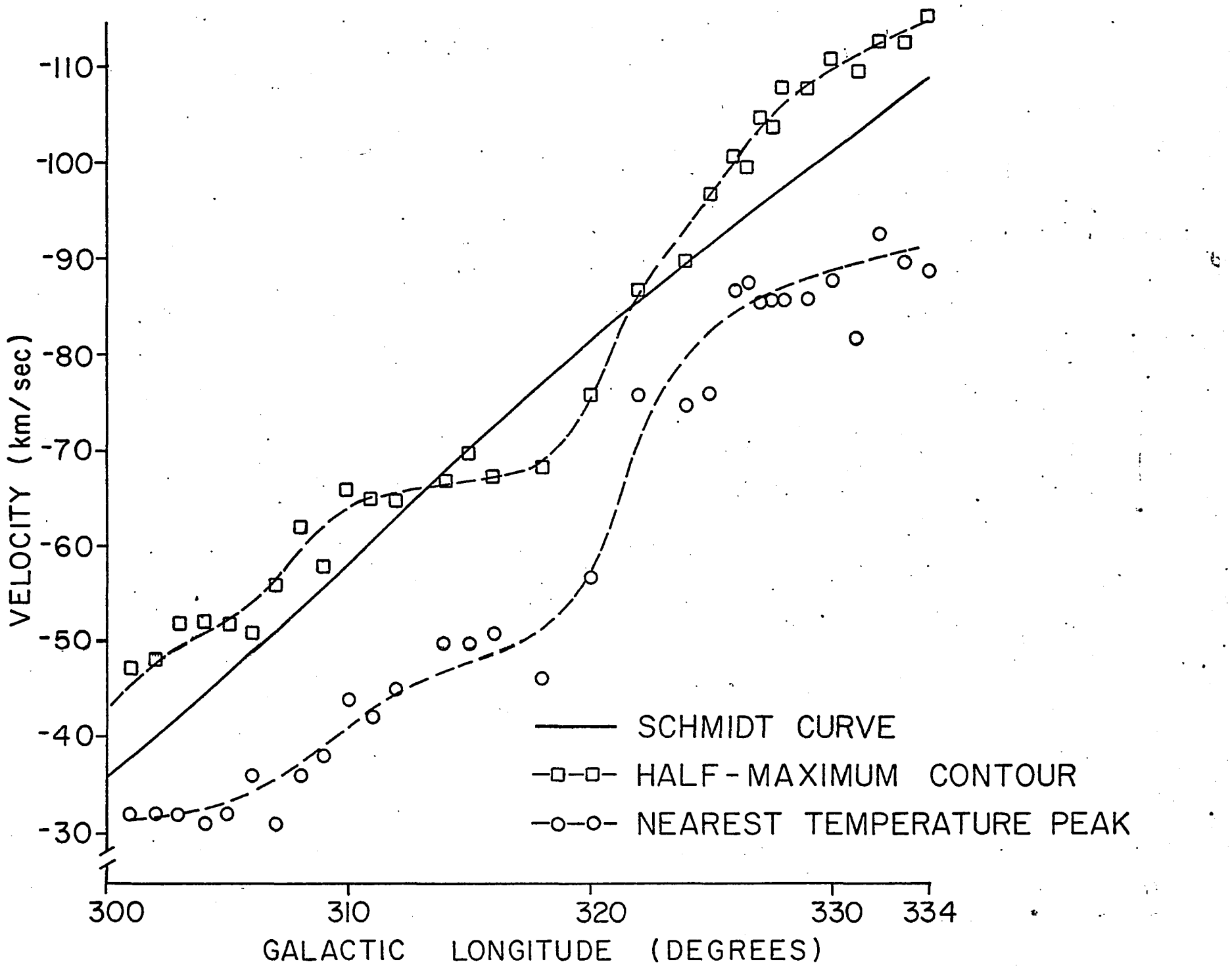
-110
-100
-90
-80
-70
-60
-50
-40
-30
VELOCITY (km/sec)
300
310
320
330
334
GALACTIC LONGITUDE (DEGREES)
SCHMIDT CURVE
HALF-MAXIMUM CONTOUR
NEAREST TEMPERATURE PEAK

between the maximum-velocity temperature peak and the Schmidt-model velocity of between 10 and 14 km/sec. The results from Kerr's observations are less uniform, probably because of his cramped format, but even here the difference between the two velocities is usually about 5-10 km/sec, except in the region $l = 310^{\circ}$-325°.

Thus we can locate the point of maximum velocity on a given latitude-velocity diagram to considerable accuracy simply by adding a value of about 10 km/sec to the value for the velocity of the highest-velocity brightness-temperature peak. This means that we can measure the velocity spread from the peak tempearature to the half-maximum point and be quite confident that this spread is produced essentially by the velocity dispersion of the gas, and not by other factors such as a density concentration located, say, 10 km/sec away from the actual velocity maximum, which would give unreasonably high values to the velocity dispersion.

To test this idea further, a number of computer runs were made with density contrasts varying between 2:1 and 9:1 and with values for the velocity dispersion ranging between 3 and 16 km/sec. Results showed that the peak brightness temperature was consistently within 8 km/sec of the actual velocity maximum, with an average difference of 5 km/sec. The velocity spread from peak temperature to half-maximum appeared to reflect the actual velocity dispersion with great consistency. Of 18 measurements, 15 showed a ratio of the velocity spread ΔV to the velocity dispersion σ_v of between 1.7 and 2.0. This

ratio exhibited no dependence on the magnitude of the velocity dispersion or on the longitude of the observations.

Thus the computer tests confirm the impression from the observations that the peak brightness temperature at highest velocity on the inner-region latitude-velocity maps is a good indicator of the actual maximum velocity of the gas and suggest further that the velocity spread ΔV between the peak velocity and the half-maximum velocity should be divided by a number of the order of 1.8 or 1.9 to give the velocity dispersion of the gas at that point. Measurements show that the absolute value of the velocity difference ΔV in the northern sky lies around 16 km/sec. (10 measurements from Henderson gave an average of 15.6 km/sec; 15 values from Kerr gave 15.8 km/sec.) If the divisor of 1.8 or 1.9 indicated above is correct, this corresponds to a velocity dispersion of between 8 and 9 km/sec, which is somewhat higher than the values found by most previous investigators. However, in view of the uncertainties involved in setting up a computer model of the galaxy, not too much faith can be rested in the absolute magnitude derived for the velocity dispersion. We are more interested in the variation of the velocity dispersion with distance from the center of the galaxy. Here we find that the more reliable values of Henderson show a fairly steady decrease in magnitude of ΔV from about 19 km/sec at low

longitudes (closer to the center) to 13 km/sec at high ones; the Kerr values were scattered too widely to detect such a decrease. The Henderson results indicate a decrease in the velocity dispersion σ_v from about 10 km/sec at ϖ = 5 kpc to about 7 km/sec at ϖ = 9 kpc. This result agrees qualitatively with the decrease of velocity dispersion outward observed by Shane and Burton and expected theoretically (the velocity dispersion must be larger toward the center in order to maintain the thickness of the gaseous disk against the increased gravitational force of the stars). However, the values are somewhat larger than the values suggested by Burton ($9.0 - 0.4\varpi$), and somewhat smaller than those suggested by Yuan ($\sigma_v = 80/\varpi$).

As a further check, the values for the velocity dispersion suggested by Burton and Yuan were used to construct theoretical latitude-velocity maps by the computer, from which maps the velocity spread ΔV was measured. Burton's function for the velocity dispersion gave measured values of ΔV of about 13 km/sec at $l = 30^\circ$ ranging down to 10 km/sec at 65°. Compared to the observed range (19-13) these values are about 30% too low. On the other hand, Yuan's value for the velocity dispersion gave a range for the velocity spread ΔV of 30 to 16 km/sec--about 50% too high.

Measurements of the velocity spread ΔV made from Kerr's southern sky observations differed from the northern sky observations of both Henderson and Kerr in magnitude, being about 20% larger. 32 measurements of ΔV in the region $l = 300\text{-}334^{\circ}$ yielded a value of about 19.5 km/sec, with no apparent dependence on longitude. This would lead to a velocity dispersion of about 11 km/sec, quite a bit greater than the dispersion of 7-10 km/sec found in the northern sky. The reason for the discrepancy is not clear.

To summarize, we have conjectured that the difference in velocity between the peak brightness temperature and the half-maximum temperature near the tangent-point region as found directly from the latitude-velocity maps of the inner part of the galactic disk, may provide a simple and consistent measure of the velocity dispersion of the gas at that point. We have tested the conjecture on a numerical model for widely-varying density contrasts and velocity dispersions, and found a highly consistent ratio for the velocity spread ΔV to the velocity dispersion σ_v of 1.7 to 2.0. The values of the velocity dispersion in best agreement to the observations range from 10 km/sec at low longitudes to 7 km/sec at high longitudes in the northern sky, and average to about 11 km/sec in the southern sky.

"ROLLING MOTIONS" IN SPIRAL ARMS

A number of investigators have noticed an apparent asymmetry associated with the spiral arms: the upper parts of the arm appear to have a different radial velocity than the lower parts. Taken at face value, these observations imply some sort of "rolling" of the arm about its own axis, and the term "rolling motion" to describe this phenomenon has come into common use.

The first to point this out was Rougoor, in his study of the "3-kpc" arm. (1964) Subsequently, prominent rolling motions were discovered in every major spiral feature. Observations of rolling motion were made by McGee and Milton (1964), Henderson (1967), Burton (1966), Shane (1967), Harten (1971), and Fujimoto (1972). Spiral arms in which the rolling motion was noted include the Scutum and Sagittarius arms in the northern sky (Shane); Norma and the southern Sagittarius arm in the southern sky and Perseus in the northern sky (Harten); the "Outer Arm" in the Northern sky (Fujimoto). I have made new measurements of rolling motion for all these features and also for outer arms beyond Perseus using the observations of Kerr (1969) Hindman and Kerr (1970), Henderson (1966), Lindblad (1972), Shane (1971), and Burton (1970). A complete set of tables of all my measurements, and graphs comparing them to previous work, is included in this section.

The magnitudes of the observed motion are usually of the order of one kn/sec/degree of latitude, although Burton, Fujimoto, and Harten seem to find considerably larger and more consistent values than Shane or the present investigators. Using reasonable estimates for the amount of gas involved, it is possible to estimate the energy of the phenomenon, and both Shane and Fujimoto have done so. Their results agree rather well:

$$\text{Energy per kpc length of feature} = 10^{50\text{-}51} \text{ ergs}$$

Previous Theories of Rolling Motion. Fujimoto and Miyamoto theorized that the rolling motion of the gas is caused by a helical magnetic field surrounding the spiral arms and forcing some of the gas to follow helical paths around the circumference of the arm. One main difficulty with this explanation was their use of circular arms rather than spiral ones, leaving unraised and unanswered the question of how the gas would complete a more or less circular streamline if it were confined to the spiral arm. A second difficulty is the proposed helical magnetic field. Although Mathewson has brought forth some observational evidence for such a field in the local regions (within 500 pcs) the weight of the evidence seems to be on the side of a planar or random field.

Harten applied two-dimensional density wave theory plus some speculations on its extension to three dimensions to arrive at a variety of mechanisms for producing radial and azimuthal (shear) motions; however, the treatment of the three-dimensional gas flow in the earlier parts of this

thesis indicate that a number of Harten's speculations (such as the idea that the radial motions would sharply decrease away from the plane) were mistaken, thus invalidating all of his mechanisms for producing true asymmetric motions.

Both of the above theories postulate that the rolling motion is real. By contrast, the present treatment will show that a simple geometric effect invariably produces the appearance of rolling motion whenever an arm is displaced from the plane. Both the magnitude and sign of the observed rolling motion can be adequately reproduced by reasonable choices of a few parameters. A complete description of the geometric mechanism responsible for the appearance of rolling motion will be given in the section following the discussion of the observations.

To prove this idea, velocity-latitude diagrams have been drawn up by a computer to illustrate the dependence of the magnitude and sign of the rolling motion on the height of the arm above the plane, the velocity dispersion of the gas, the size of the systematic velocities predicted by density-wave theory, and other variables. This allows a direct comparison with observations. The details of the computer model of the galaxy are discussed elsewhere in this thesis.

Observations of Rolling Motion. I shall first discuss my own measurements of "rolling motion," and then, in figures and tables, compare them to previous results. The measurement procedure is as follows: from available latitude-velocity (b-V) contour maps, an attempt is made to estimate the "tilt" of all the brightness-temperature peaks appearing on a particular diagram, in much the same manner as described in Harten (1971). For example, in Fig. 16 , it is clear that the slope dV/db of the feature at $V = +20$ km/sec is large and negative. In the case of a regular feature such as this one, measurements made from neighboring contour lines will give roughly the same result. However, in more irregular features, measurements of different contour lines will give widely different results, and often no unambiguous value for dV/db can be found. Moreover, there is a fair degree of subjectivity involved. Different observers sometimes get widely varying results, sometimes even disagreeing about the sign of the gradient. As an example of the difficulty, consider the papers of Burton (1970) and Shane (1971) on the region containing the Sagittarius and Scutum arms. Shane studied two sections of the Sagittarius arm which flanked the sections studied by Burton. Although the same observing equipment was used, and even the same Gaussian analysis computer program, Burton's values for dV/db were far more consistent from one longitude to the next, and were almost 300% larger than Shane's; the average value of dV/db found by Burton was -2.3 km/sec, compared to Shane's average value of -0.8. It is most unlikely that

these differences reflect a real change in this quantity along the arm, since as noted above, Burton's region was bracketed by Shane's.

The main source of this type of confusion is the irregularity of the latitude-velocity diagrams, arising from the spotty or discrete nature of the interstellar region. The result of these irregularities is to make the measurement of rolling motion essentially a statistical phenomenon. For example, a single value of dV/db should reflect an average of several measurements made from different contour lines. The rather continuous and slowly-changing behavior of dV/db found by Harten, Fujimoto, and Burton is, in my opinion, a reflection of a choice on the part of the observer leading to some systematic bias: for example, Harten's choice of the 15%-maximum-intensity contour line as the one to measure from, or Fujimoto's choice of latitudes 1° and -1° as the upper and lower limits from which to measure dV/db. (The latter choice ignores altogether the problem of centering one's measurements on the center of the arm; indeed, the center of one of the arms investigated by Fujimoto lay entirely outside his region of inspection!)

A common situation that leads to greatly magnified and erroneous values of dV/db is the case in which two intensity maxima, possibly corresponding to individual clouds, are displaced slightly from each other in both latitude and velocity. Then, even though neither one individually shows signs of a rolling motion, the contour lines enveloping both maxima may yield enormous values of dV/db.
This appears to be the case in one of the diagrams most widely reproduced as an example of rolling motion: the

FIGURE 8

An oft-reproduced section of the Perseus arm that appears to show a tremendous rolling motion. (Observations from Henderson 1966). Diagrams at neighboring longitudes indicate, however, that in fact two features are involved in a close approach here. The dashed lines indicate the "ridge lines" of the two features, as printed out automatically by the computer and augmented by the present author. The features, considered separately, actually have a rather small "rolling motion" of about -1 km/sec/degree.

8

longitude 121° diagram from Westerhout (1967). Diagrams at neighboring longitudes indicate that here two major features are experiencing a close approach. Each one individually has a much smaller rolling motion than the two together, as can be seen in the "ridge lines" drawn in automatically on the Henderson observations (Fig. 8).

To sum up, it appears that attempting to measure the rolling motion of the spiral arms from b-V maps is an inherently difficult and uncertain enterprise. Different observers will estimate the slopes of identical regions in rather different fashion. On the other hand, as noted by Harten and confirmed by the present investigation, there is a high degree of reproducibility of results of measurements made at different times by the same observer. And, finally, as can be seen in the accompanying diagrams, there is a fair degree of agreement among different observers for the behavior of the rolling motion in the outer regions of the Galaxy. Therefore we shall treat the observations of the outer arms separately from those for the inner arms.

To make discussion of our results as clear as possible, a diagram is provided (Fig. 9) showing the spiral pattern adopted in the present work with the conventional names of the spiral features displayed. The inner arms consist of the Sagittarius and Norma-Scutum arms; the outer arms are designated the Perseus arm, the Outer arm, the Carina feature (following the nomenclature of Harten. It is the extension of Bok's optical Carina feature into higher longitudes.), and the Far Outer arm. Nonetheless, to

FIGURE 9

Spiral arm pattern adopted for the study of rolling motions. Scutum, Sagittarius, Perseus and the Outer arms cross the sun-center line at distances of 5.5, 8.3, 12.5, and 14.5 kpc. The two-armed pattern becomes a 4-armed pattern at about 10.5 kpc, with the Carina and Outer arms beginning there. The "local" or Orion arm is treated as a material concentration only.

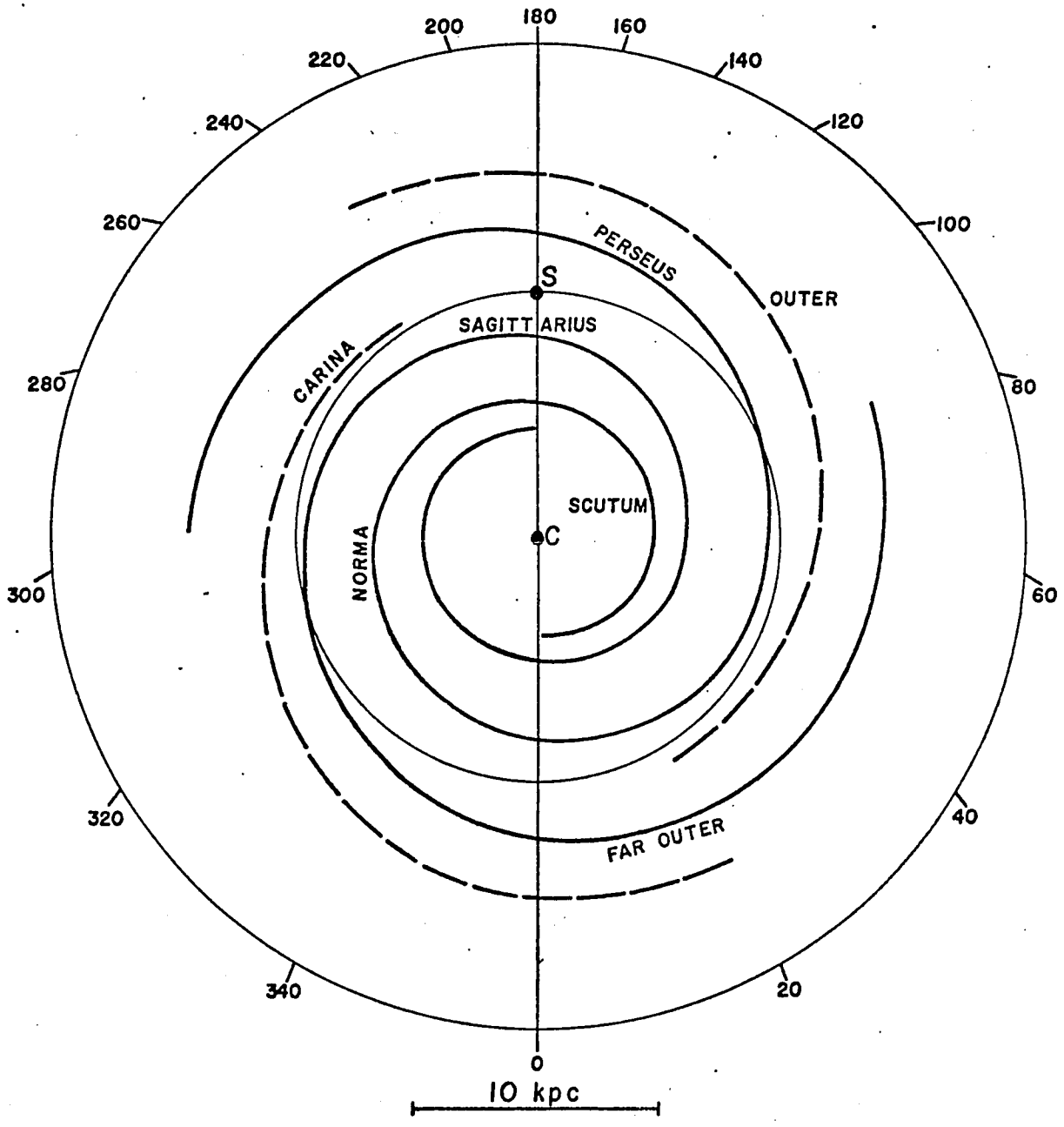
180
200
160
220
140
240
120
260
100
280
80
300
60
320
40
340
20
0
PERSEUS
OUTER
S
SAGITTARIUS
CARINA
SCUTUM
C
NORMA
FAR OUTER
10 kpc

allow for the possibility that some observers may have different ideas about which regions should be given which names, I have included in the tables the velocity and latitude of the feature considered, which will allow an unambiguous identification of it. I strongly recommend that future measurements of rolling motion include this information, since the lack of it in certain previous studies has led to considerable uncertainty as to which feature was being considered.

Observations: Outer Arms

The main observational material for these regions are the surveys by Henderson (1966), Kerr (1969), and Hindman and Kerr (1970). Westerhout's 1967 survey, done in equatorial coordinates, is unsuitable for the present purposes, which require measurements to be made at constant galactic longitude. Kerr's survey is also far less suited for dV/db measurements than those of Henderson or Hindman and Kerr, since the latitude extent is small (-2° to $+2^{\circ}$, which does not include the region of greatest deformation of the Galaxy on the southern side), and the velocity scale is cramped. These factors combine to give greater scatter and somewhat larger values of $|dV/db|$ than the corresponding values for the northern sky determined from Henderson's data. On the other hand, Kerr made finer intervals of longitude in his observations, which allows the continuity of the spiral features to be better established. The details of the measurements are listed in Tables I-IV; comparisons with Harten's measurements are shown in Fig. 10. Some general remarks on individual arms follow.

FIGURE 10

Measured rolling motions for several outer arms. Filled dots: present measurements; open circles: measurements of Harten. Note the predominance of negative values. (The units of dv/db are km/sec/degree.)

ROLLING MOTION

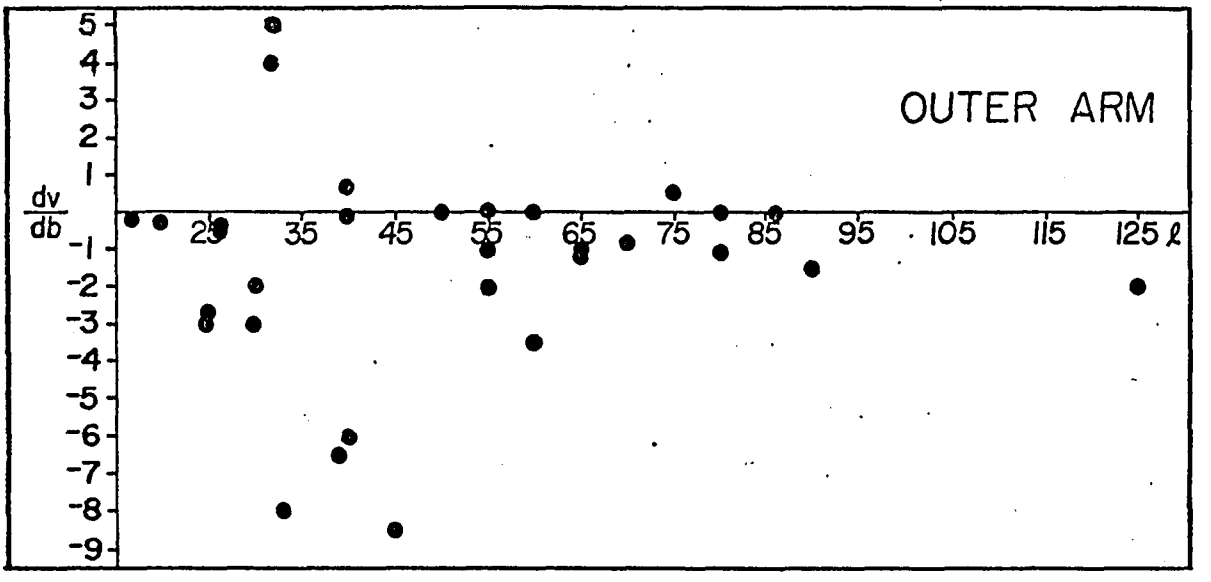

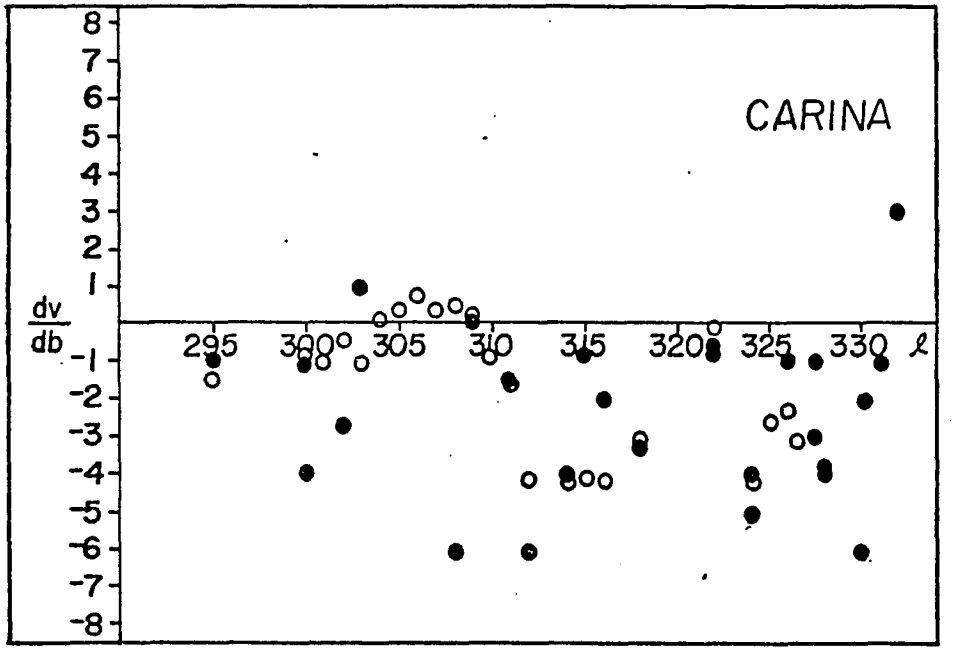

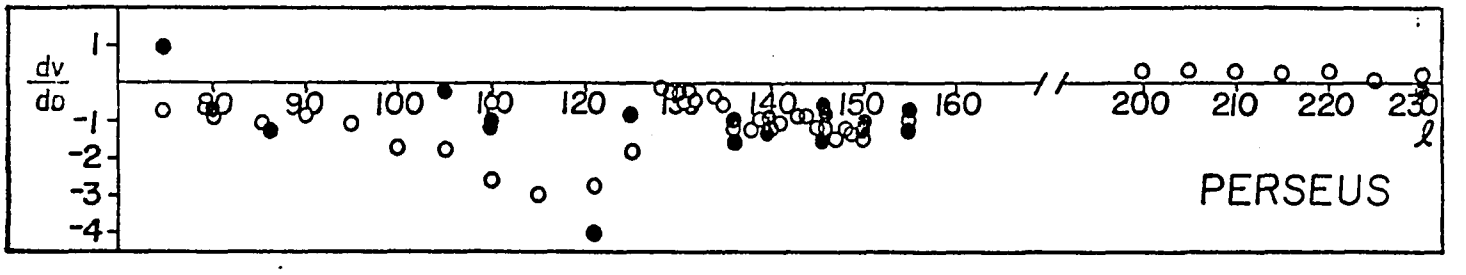

Outer Arm. This feature, which can be followed from $l = 25^{\circ}$ to $l = 125^{\circ}$ very well, (and possibly extended to 150°) exhibits very prominent and systematic rolling motions. It is the most suitable feature for the examination of the mechanism proposed in this paper for two reasons: it is located throughout its length in regions of considerable height above the plane and also in regions where the deformation of the Galaxy has its greatest slope; and secondly, in this longitude range, the bending of the plane is very uniform and approximates very closely the sin L law adopted in the numerical model of the Galaxy. Thus we expect the observations to agree not only in magnitude and sign with the values predicted, but also to change with longitude at least qualitatively in the manner expected.

Northern Perseus Arm. Measurements of rolling motions here are highly reliable, because of the large extent in latitude. Such measurements show almost unbroken negative values of dV/db hovering around -1 km/sec/degree from $l = 110^{\circ}$-155°, where the arm begins to merge gradually with the local branch, forming a single feature in the latitude-velocity diagram at about $l = 165^{\circ}$. Nonetheless, a problem of interpretation arises around $l = 120^{\circ}$ when a branch from the Outer arm appears to approach closely and partly merge with the Perseus feature. The rolling motion of each separately is considerably smaller than the maximum value of about -3 km/sec/degree found by both Harten and the present observers for the combined feature between $l = 115^{\circ}$ and 125°. Moreover, the deformation of the Galaxy beyond $l = 105^{\circ}$ becomes so complicated that it is no longer represented very well

by the simple sin L law in the numerical model. For these reasons, the Perseus arm is not as suitable a testing ground for the proposed mechanism as the Outer arm.

Southern Perseus arm. Sturctural features are extremely complicated in this region. The nodal line of the bending of the Galactic plane appears in the direction $l \sim 190^{\circ}$. This region is the only case among all the outer arms where the rolling motion gradients are often positive.

Carina. This feature could be followed in the observations of Kerr from $l = 295^{\circ}$ to $l = 333^{\circ}$. As mentioned above, Kerr's format results in larger scatter in the measurements. The overall behavior is similar to that of the other outer arms: a consistently negative dV/db of average magnitude -1.5 km/sec/deg.

To sum up, more than 100 measurements of rolling motion carried out on four major spiral arm features in the outer regions of the Galaxy show a systematic, rather uniformly negative, value of dv/db that is remarkably uniform from one arm to the next and in both hemispheres, and whose magnitude hovers about a mean value of -1 to -2 km/sec/deg.

Observations: Inner Arms

In the inner regions, the observations of rolling motion are complicated by several factors:

(1) Distance ambiguity. Inside the 10-kpc circle, any given brightness temperature has been built up by contributions from two distinct areas. Unless the contribution of one area is far less than that of the other, the measurement of dV/db using the brightness-temperature contour lines will have no meaning. Of course, the variation of intensity with latitude and the effect of the pitch angle of a spiral arm may help in resolving some of the ambiguity. But in most cases, this ambiguity simply cannot be completely removed.

(2) Tangent point. Along the tangent point, because of the very slow change of the velocity, an immense distance along the line of sight contributes to the observed brightness temperature. Again the value of dV/db is almost meaningless, since it does not refer to a single well-delimited region. This effect has caused immense difficulty in interpreting the measurements. All the previous measurements (Burton, Shane, and Harten) have shown large values with rapid swings in the sign and magnitude of dV/db near these points. In fact, it is this very behavior that convinced Harten of the existence of "shearing" motions in addition to what he called "tumbling" motions along the spiral arms. But in our view, measurements near the tangent point must carry little weight because of the effect described.

In spite of these effects, we shall present our measurements of rolling motion in the inner arms in Tables V-XII. Comparison with previous work is made in Fig. 11. Comments on individual arms follow.

Northern Sagittarius Arm. This feature was exhaustively studied by Burton and Shane. However, as described above, and as indicated in Fig. 11, their measurements of the rolling motion seem to disagree violently, with Burton finding much larger and more consistently negative values in his longitude region (43-55°) than Shane in his (22-42°). Our own measurements have a larger scatter but seem to fall generally closer to those of Shane.

Scutum. Here our measurements appear to agree with those of Shane in indicating generally negative values for the near arm and mixed values for the far arm.

3-kpc arm. The enormous rolling motions displayed by this feature make it unique among the inner arms. It is also unique in the density-wave theory as the probable site of the inner Lindblad resonance, a region in which energy transported by the spiral waves is expected to pile up. For this reason, the 3-kpc arm will be largely exempted from the following discussion.

Southern Sagittarius and Norma arms. These features present several problems in interpretation. Since we cannot unambiguously resolve these problems, we have not made graphs for these features; they can, however, be followed in the appropriate table.

FIGURE 11

Measured rolling motions for two inner arms. Filled dots: Present measurements; open squares: measurements of Shane; open triangles: measurements of Burton. In comparison with the previous figure, note the smaller magnitude and less consistent signs of the rolling motions.

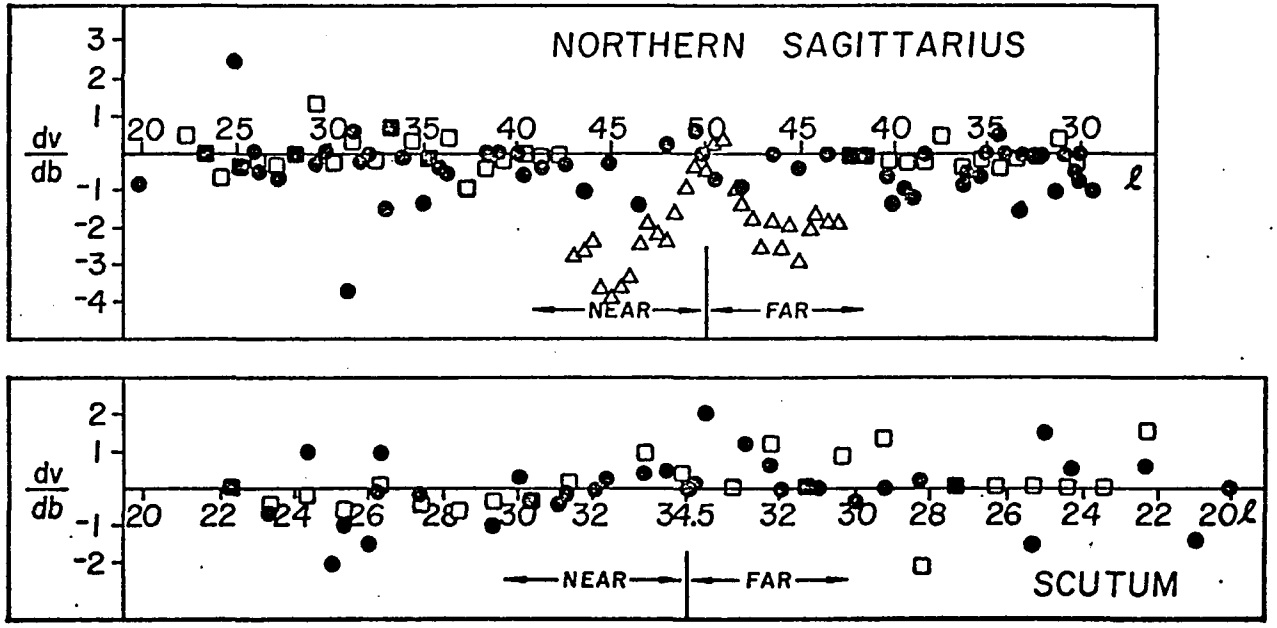
NORTHERN SAGITTARIUS
dv/db
3
2
1
-1
-2
-3
-4
20
25
30
35
40
45
50
45
40
35
30
l
NEAR
FAR
dv/db
2
1
-1
-2
20
22
24
26
28
30
32
34.5
32
30
28
26
24
22
20
l
NEAR
FAR
SCUTUM

To sum up, we must first emphasize that measurements of rolling motion in the inner arms are subject to even more uncertainties than those in the outer arms; but having made that point, we can still arrive at the general conclusion that the rolling motions in the inner arms appear to be decisively smaller in magnitude and more mixed in sign than those in the outer arms.

Geometric Explanation of the Rolling Motion. The observational data just reviewed indicates that the "rolling motion" observed in the outer arms is larger in magnitude and far more uniform in sign than that observed in the inner arms. This suggests that the systematic "rolling motions" may have something to do with the bending of the galactic plane, which so far stands as the most distinctive characteristic for the the outer regions of the Milky Way. In this section, we shall show qualitatively that the distortion of the plane together with ordinary circular differential rotation will lead to apparent rolling motions of the observed magnitude and sign, without any necessity to postulate a true motion of the arm about its own axis. Since the inner arms are displaced in a somewhat random manner above and below the mean galactic plane, the same geometric mechanism may also cause an apparent rolling motion to be observed in them; but the magnitude of the gradient generated in this way will be expected to be relatively small, and its sign will depend on whether the arm is above or below the plane as well as whether it is located on the near or far side of the tangent point.

It is well known that the Galaxy bends up in the northern sky and down in the southern sky. The amount of bending was described by Gum, Kerr, and Westerhout (1960), Kerr and Westerhout (1965), in more detail by Henderson (1967), and again by Kerr in a review article (1969). This kind of distortion

has also been found in external galaxies (Roberts 1970). Toomre and Hunter have suggested that a close encounter with the Magellanic Clouds several hundred million years ago may have excited the galactic plane into oscillating in the observed mode. What is the effect, as displayed in a velocity-latitude diagram, of viewing a spiral arm located in a region of considerable deformation?

Imagine an outer arm located where the distortion of th galactic plane lifts it considerably above the central plane of the Galaxy. Equidensity contours of the arm's cross-section will look roughly like the diagram (Fig. 12), forming ellipses of considerable eccentricity. (The major axis may be of the order of one kilpparsec, while the minor axis will be 200 pcs in length.) If the axis of the arm follows the general slope of the plane, the ellipses will be slanted with respect to the sun, as shown. Two lines of sight drawn to be tangent to a particular density contour will touch it at different distances from the sun. (Points T_1 and T_2 in the diagram.) Because of differential rotation, the velocities of these points differ. As the entire contour is mapped onto the latitude-velocity diagram in this manner, the corresponding equal-brightness temperature contour will appear tilted as shown in the lower part of Fig. 12. The value of dV/db, as read from this diagram, will be negative in sign. The corresponding case for the southern sky, where the arm is below the plane, is also shown. Again the value of dV/db turns out to be negative. Thus the sign of the rolling

FIGURE 12

(Top) Plan view showing an outer spiral arm in both the Northern and Southern Skies. (Middle) Cross-section of the Galaxy showing the bending of the plane and the equidensity contours of the two spiral arms. Points T_1 and T_2 mark the points of tangency to a given density contour in the northern arm. Located at different distances from the sun, and therefore from the galactic center, the gas associated with these points will have different apparent velocities with respect to the sun. (Bottom) The two resulting b-v diagrams. Note that dv/db is negative in both cases.

" ROLLING MOTION " IN THE OUTER ARMS : A GEOMETRIC EXPLANATION

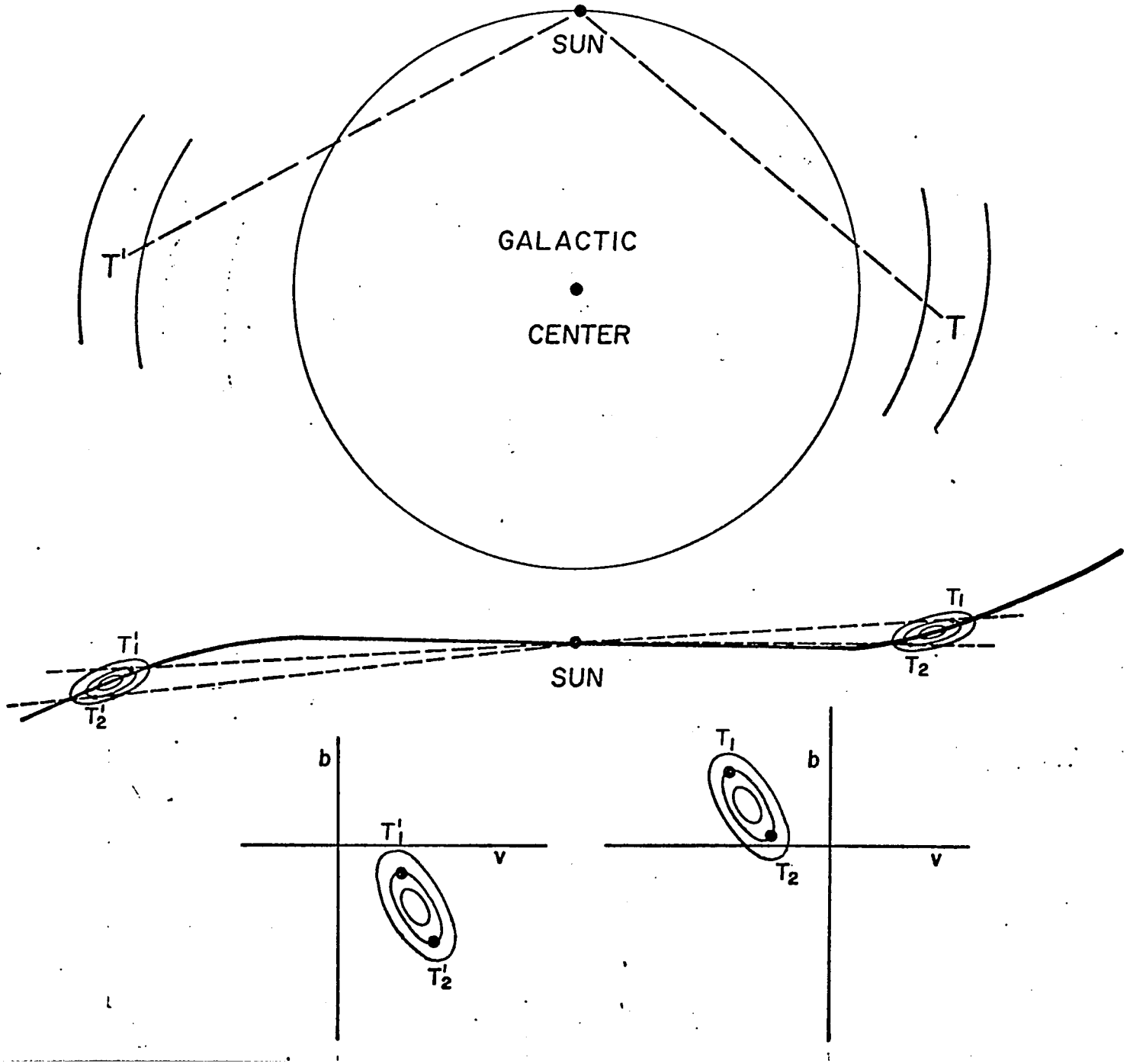

motion in the outer arms is predicted to be consistently negative, as observed.

It is equally important that the magnitude of the gradient dV/db also agree with the observations. The magnitude of the gradient is essentially determined by two quantities:

(1) the difference in velocity between the points at which the line of sight is tangent to the density contour under consideration (i.e. points T_1 and T_2 in the diagram); and

(2) the angle between these two tangent lines.

As an order-of-magnitude estimate, we consider the case of the Outer Arm at a longitude of 45°. The Outer Arm width is taken to be 1.6 kpc and its thickness in the vertical direction as 400 pcs. For the bending of the galactic plane in that direction, we use an approximation derived from Henderson's 1967 observations. The two tangents are separated by a distance of about 300 pcs in the line-of-sight direction, and the angle subtended by them is about 1.4°. (See Fig. 13 for a scale representation.) Using the 1965 Schmidt rotation curve results in a velocity difference between these two points of 3.5 km/sec, which, in turn, yields a value of dV/db equal to -2.4 km/sec/deg. In fact, this is close to the typical value observed in almost all directions.

Essentially the same geometric mechanism as described above seems sufficient to explain the rolling motion of the inner arms as well. Fig. 14 shows how a slight displacement of an arm from the galactic plane (10-30 pcs, as observed by Henderson and others) is sufficient to cause significant differences in the radial distances to the upper and lower

FIGURE 13

A scale drawing using accurate representations of the galactic distortion and the spiral arm location and thickness to determine the distance between the points of tangency. The distance between the upper and lower tangent points turns out to be about 300 pcs, corresponding to a difference in measured radial velocity of about 3.5 km/sec. Since the angle subtended by the two points is about 1.4°, the value of the "rolling motion" (dv/db) will be about -2.4 km/sec/degree. Thus this quantitative determination of the effect of the galactic distortion on the magnitude of the apparent "rolling motion" confirms the qualitative estimate of the effect illustrated in the previous diagram.

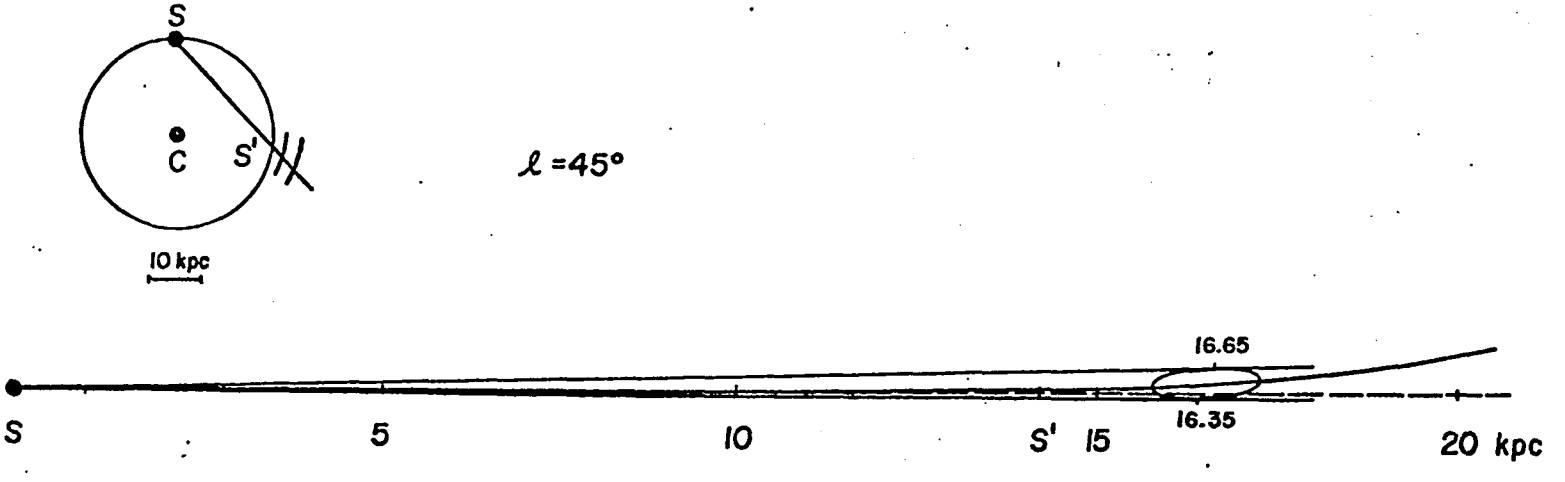
S
C
S'
10 kpc
ℓ =45°
16.65
16.35
S
5
10
S'
15
20 kpc

FIGURE 14

Essentially the same geometric effect invoked to explain the "rolling motions" in the outer arms will explain the "rolling motions" in the inner arms too, provided we allow for the observed displacement of the inner arms from the plane by small distances of 10-30 pcs. Shown is a scale drawing of an inner arm as it would look if displaced by 30 pcs above the plane. Even this small displacement results in a considerable separation of the tangent points, as shown. For example, at $l = 30^{\circ}$, the tangent points to the half-density contours of the near portion of the Sagittarius arm will be about 250 pcs apart, leading to an apparent rolling motion of about -0.5 km/sec/degree. For inner arms that are further away, the distance between the tangent points is lessened; however, the latitude subtended by the arm also decreases, so that dv/db is not much affected.

" ROLLING MOTION " IN THE INNER ARMS : A GEOMETRIC EXPLANATION

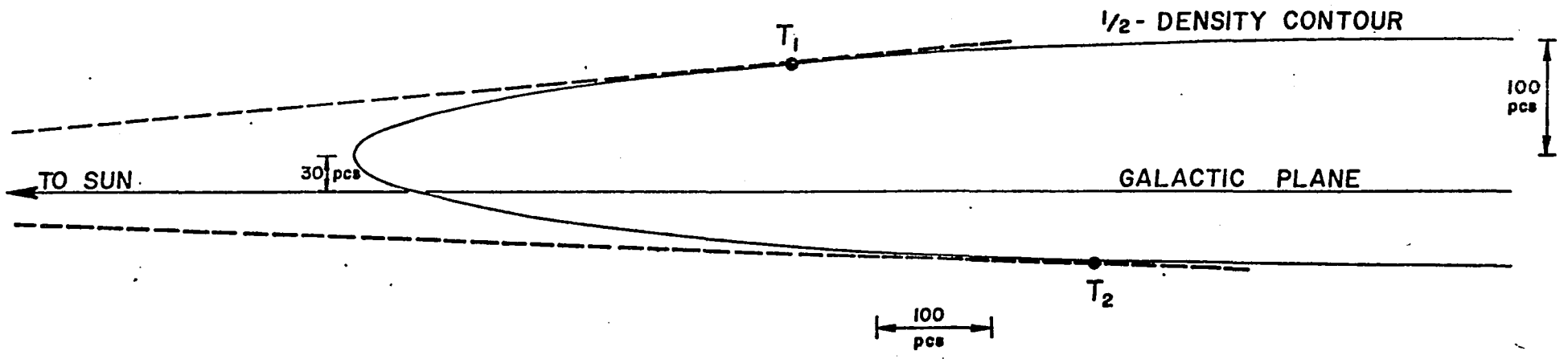

tangent points. For example, at $l = 30^{o}$, allowing the Sagittarius and Scutum arms to be displaced 30 pcs from the plane, we estimate the absolute values of the gradient from this effect to be 0.5, 0.8, and 0.3 km/sec/deg for the Sagittarius near and far arms and the Scutum near arm, respectively.

The main difference to be expected in the case of the inner arms is that, unless an inner arm is consistently above or below the plane, the sign and magnitude of the gradient associated with it cannot be expected to show the systematic behavior of the outer arms. The sign of the gradient depend basically on two things: whether the line of sight velocity is increasing or decreasing with distance across an arm, and whether the axis of symmetry of the cross-section of the spiral arm passes above or below the sun. Once these are specified, the sign is determined. For example, if the Northern Sagittarius near arm is displaced above the plane uniformly, we would expect a consistently negative gradient. However, if the arm is not consistently above or below the plane, but rather passes sometimes through the plane, we cannot expect uniform behavior of the gradients.

Of course, the situation is not so simple as described above. First, the brightness-temperature contours are not a direct mapping of the density contours. Brightness temperature T_b is a monotonic function of optical depth τ, which depends not only on the density but is also modified by a Gaussian factor centered on the velocity of observation:

$$\tau \sim \rho e^{-(v-v_o)^2/2\sigma_v^2}$$

where v is the velocity of the gas, v_o is the velocity that the telescope is "tuned to", and σ_v is the velocity dispersion. The effect of the Gaussian factor containing the velocity dispersion is to restrict the region contributing to the optical depth to a small portion of the path centered around the velocity under consideration. For a value of σ_v of about 8 km/sec, the region of greatest contribution to the optical depth will be on the order of a kiloparsec in length for most longitudes. This "smearing" effect of the velocity dispersion makes it impossible to predict with confidence the exact value of dV/db to be expected from a given situation. Therefore, to prove the viability of the mechanism proposed above, it is necessary to perform the full calculation, attempting to take into effect all the relevant variables such as height of the arm above the plane, slope of the arm with respect to the sun, density variation with vertical distance from the plane, velocity dispersion of the gas, and so on. In the next section, we describe the numerical model set up to allow these calculations and we compare them directly with the observations.

COMPUTER SIMULATION OF LARGE-SCALE GALACTIC STRUCTURE AND DYNAMICS

Here the basic idea is to use our knowledge of the three-dimensional structure of the Galaxy gained in the first section of this paper to obtain theoretical latitude-velocity diagrams which can then be compared with the observations. In principle it is identical to the construction of theoretical 21-cm line profiles or theoretical longitude-velocity diagrams (Yuan 1970; Burton and Shane 1970; Burton 1971; Shane 1971), except that in the present case the structure and motions of the gas perpendicular to the plane must be included. For simplicity, we shall use the turbulent-cloud model of the interstellar gas (Roberts 1969) and again assume constant spin temperature for neutral hydrogen throughout the Galaxy. From the relation

$$d\tau = K_\nu \, ds$$

and using the standard value for K_ν we find that the optical depth τ is related to the gas density and velocity as follows:

$$\tau = \int_0^\infty \rho \, e^{-(v-V)^2/2\sigma_v^2} \, dr$$

where σ_v is the dispersion velocity, v is the velocity at which the optical depth is being measured, r is the distance along the line of sight, and ρ is the density. V is the velocity of the gas along the line of sight, and is made up of contributions from the mean galactic rotation and also the systematic motions predicted by density-wave theory.

Spiral Pattern. The spiral structure of the Milky Way is involved in the present calculations through its implicit functional relation to the gas density ρ and the mean velocity V. Clearly, for the purpose of merely testing the mechanism proposed for the "rolling motion" phenomenon, the choice of a particular spiral pattern is not crucial. But the correct location of a spiral arm will certainly make a direct comparison with observations much easier. Unfortunately, no overall spiral pattern has yet emerged that everyone can agree on. Radio and optical observations (Bok 1970) reveal an extremely complex picture of the spiral structure. For the present calculations, therefore, we simply adopt the spiral pattern due to Yuan and displayed in Fig. 9. In this pattern, spiral arms intersect the sun-center line at distances of 5.5, 8.3, 12.5, and 14.5 kpc. The so-called "Orion arm" is treated not as a true arm but as a spur or local concentration. A four-armed pattern, involving the introduction of two additional arms starting at about 10.5 kpc, is included, according to the results of observations and theoretical work by Yuan. (The two additional arms, in this view, are the Carina and Outer arms.)

Density. The density of the gas in the plane is taken as about 0.5-1.0 atoms/cc, agreeing with the observations of Kerr. It reaches a maximum somewhere between 9 and 11 kpc and goes down rapidly to less than 0.1 atom/cc at 16 kpc, which is the radius chosen as the cutoff point for the Galaxy. The density outside the plane is taken to vary as $\operatorname{sech} \beta^2 \frac{z}{\Delta}$ where β^2, as described previously, is the ratio of the stellar velocity dispersion in the z-direction to the effective turbulent velocity of the gas: $\beta^2 = 2\langle v_z^2 \rangle / a^2$

Here Δ, the stellar thickness, lies somewhere between 300 and 388 pcs (both values were used in the calculations).

Density Contrast. This quantity is determined by the choices of several other parameters as described previously. The most important of these parameters is the strength of the spiral field, which is taken as 5% of the mean field in agreement with the work of Yuan. This value, together with the values for the other parameters, leads to an arm-interarm density contrast of between 3:1 and 5:1, as measured in the plane; the variation with height is determined by the equations involving $\rho^{(1)}$ and γ_z discussed and solved previously.

Velocity Dispersion. Since the velocity dispersion of the gas is not well-known, this was treated as a parameter and varied widely throughout a number of runs. Constant values of 5, 6, 7, 8, and 10 km/sec were employed, as were the possibly more realistic values of $9.0 - 0.4\varpi$ advocated by Burton for the inner regions and a somewhat larger value of $80/\varpi$ suggested by Yuan. If the thickness of the disk is constant in the inner regions, a velocity dispersion decreasing with distance, as given by the formulas of Yuan and Burton, is probably preferable for these regions. However, the considerably larger thicknesses encountered beyond 10 kpc make an extension of these formulae to the outer regions questionable. A compromise solution of using the Yuan or Burton formulas out to ϖ = 10 kpc and then a constant value thereafter, was sometimes employed.

Systematic Motion. The amplitudes of the radial and azimuthal motions predicted by density-wave theory are taken to be consistent with the 5% spiral field strength. Both values are set equal to 8 km/sec near the sun and slightly reduced towards the outer regions. At times, runs were made with these values set equal to zero (corresponding to pure circular rotation) with results that will be discussed later. The value of the z-motion of the gas, as determined by the first section of this paper, is too small to affect the radial velocity with respect to the sun determined from these low-latitude studies.

Bending of the Plane. Since this is one of the most important quantities for the purpose of testing the proposed mechanism for the "rolling motion" phenomenon, it is discussed in more detail in the section entitled "Bending and Corrugation of the Plane." Here it will be enough to state that for the outer regions, the bending of the plane was approximated by a curve of the form $f(\varpi)$ sin $(L - L_0)$, where L is galactocentric longitude and L_0 is a small angle on the order of 20°. A single second-order polynomial for $f(\varpi)$ fits the observed values well enough for $10 < \varpi < 14$ kpc, but for $\varpi > 14$, a higher rate of increase was necessary. This is quite a good approximation for $20^\circ < l \lesssim 105^\circ$, but breaks down for the steep dip in the plane that Henderson found for the region about 8 kpc from the sun lying between $l = 120^\circ$ and 160°.

In the inner regions, Henderson found evidence for a spiral "corrugation", with alternate spiral arms lying either wholly above or wholly below the plane, their centers lying between 10 and 30 pcs away from the plane. Although other observers have not supported this finding, they do agree that the centers of the arms are often displaced from the plane. Therefore we have made runs with a perfectly flat plane inside the 10-kpc circle; a "corrugated" plane according to Henderson, with alternate spiral arms above and below the plane; and a "radially corrugated" plane, such that individual arms are sometimes above and sometimes below the plane, depending only on their distance from the center.

RESULTS OF THE NUMERICAL ANALYSIS

More than 100 individual latitude-velocity diagrams (each of which takes roughly one minute of computer time on the 360-95 to produce) were prepared, covering all longitudes in both northern and southern skies and including a range of values of essential parameters. Comparisons with observations are presented in Figs. 15 + 16. In Fig. 17, the calculated values of dV/db for the Outer arm in the northern sky are plotted against our measurements from the observations. The general trend agrees well, considering the unavoidable scatter in the measurements.

General concludions may be summarized as follows:

(1) The apparent "rolling motions" due to the proposed geometric mechanism always appear at longitudes where the plane is considerably distorted--i.e., for $20^{\circ} \lesssim l \lesssim 140^{\circ}$ and for $220^{\circ} \lesssim l \lesssim 330^{\circ}$. The magnitudes of the gradient appear to be largest in the region where the combined effects of the slope of the plane and the slope of the Schmidt rotation curve are largest.

(2) The sign of the gradient for the outer arms in both northern and southern skies is negative.

(3) The magnitude for the outer arms varies between -1 and -3 km/sec/deg.

FIGURE 15

Model b-v diagram at $l = 40^{\circ}$ compared to observations by Henderson at the same longitude. The dashed line at negative velocity shows the apparent "rolling motion" produced in the Outer Arm by the geometric mechanism discussed in the text. The dashed lines at positive velocities show the apparent "rolling motion" displayed by different density contours of the Northern Sagittarius Arm as a result of a slight displacement from the plane. The value of dv/db in the Outer Arm is 2 or 3 times that in the inner arm, in general agreement with the observations.

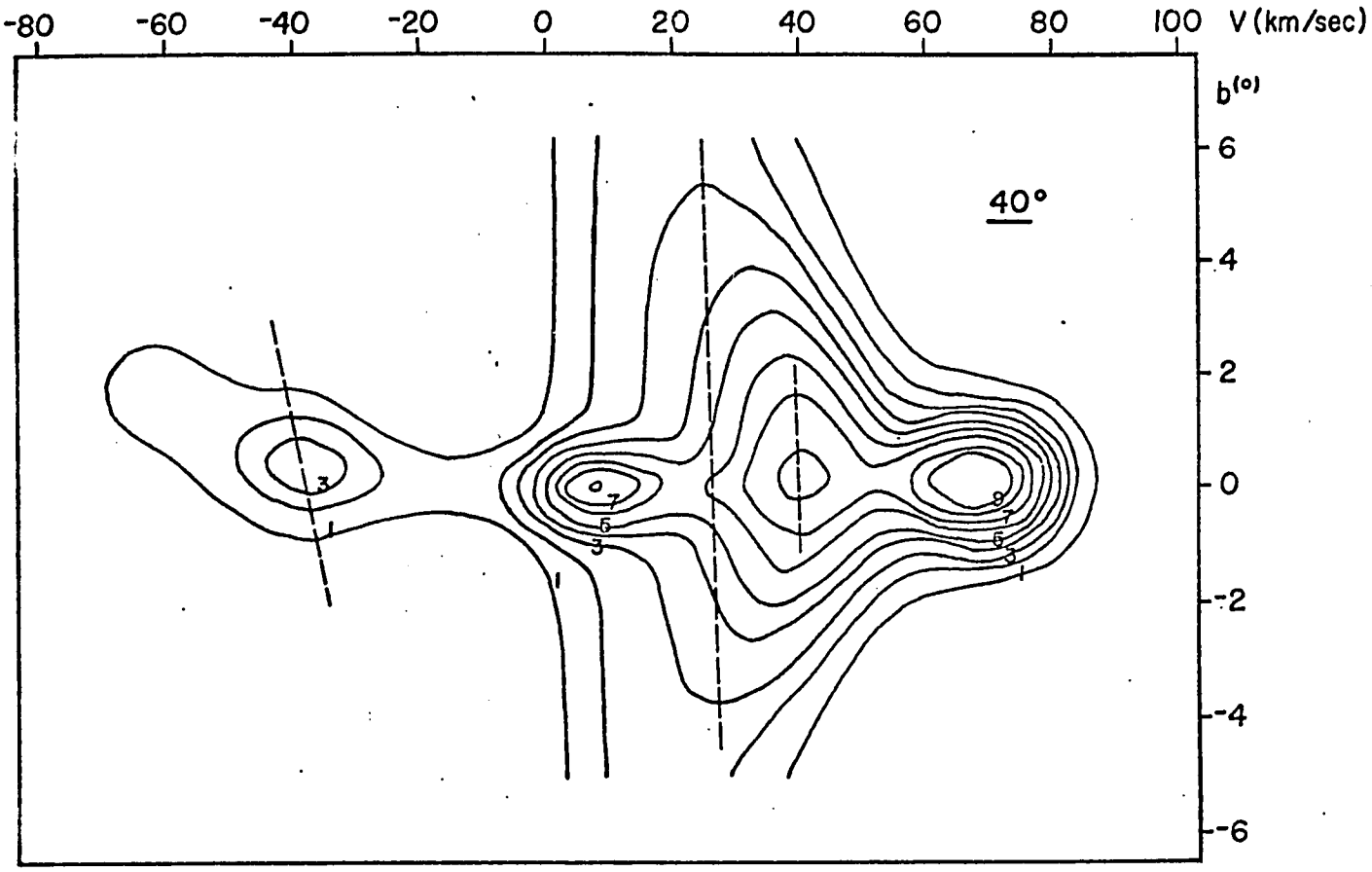
-80 -60 -40 -20 0 20 40 60 80 100 V (km/sec)
b(°)
6
4
2
0
-2
-4
-6
40°
3
1
7
6
3
1
8
7
6
3
1

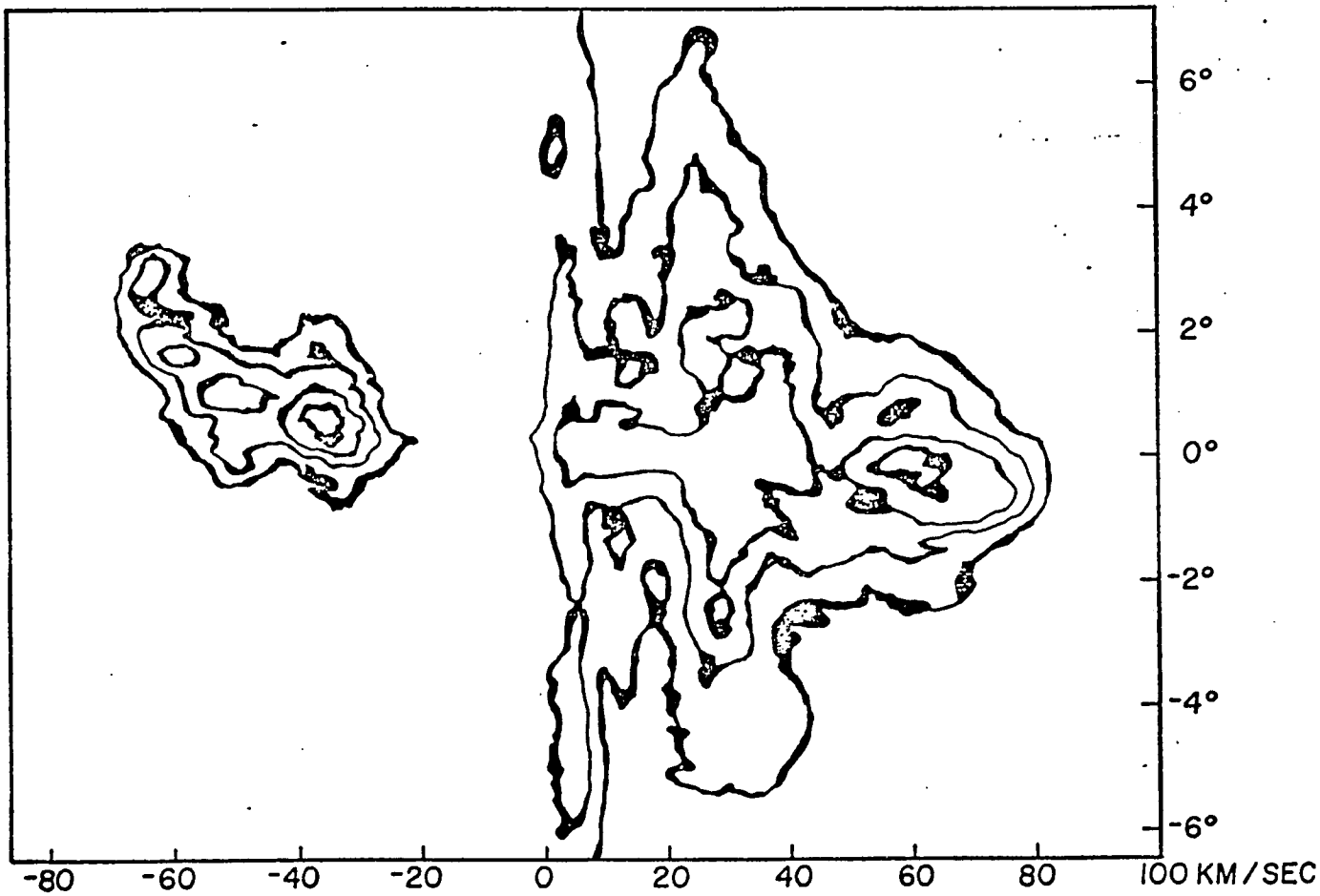
6°
4°
2°
0°
-2°
-4°
-6°
-80 -60 -40 -20 0 20 40 60 80 100 KM/SEC

FIGURE 16

Model b-v diagram at $l = 324^{\circ}$ compared to observations by Kerr at the same longitude. The dashed line at $v = +30$ indicates the apparent "rolling motion" produced in the Carina Arm by the mechanism discussed in the text. Note that an inner arm at about $v = -80$ which was centered on the plane shows no rolling motion, as expected.

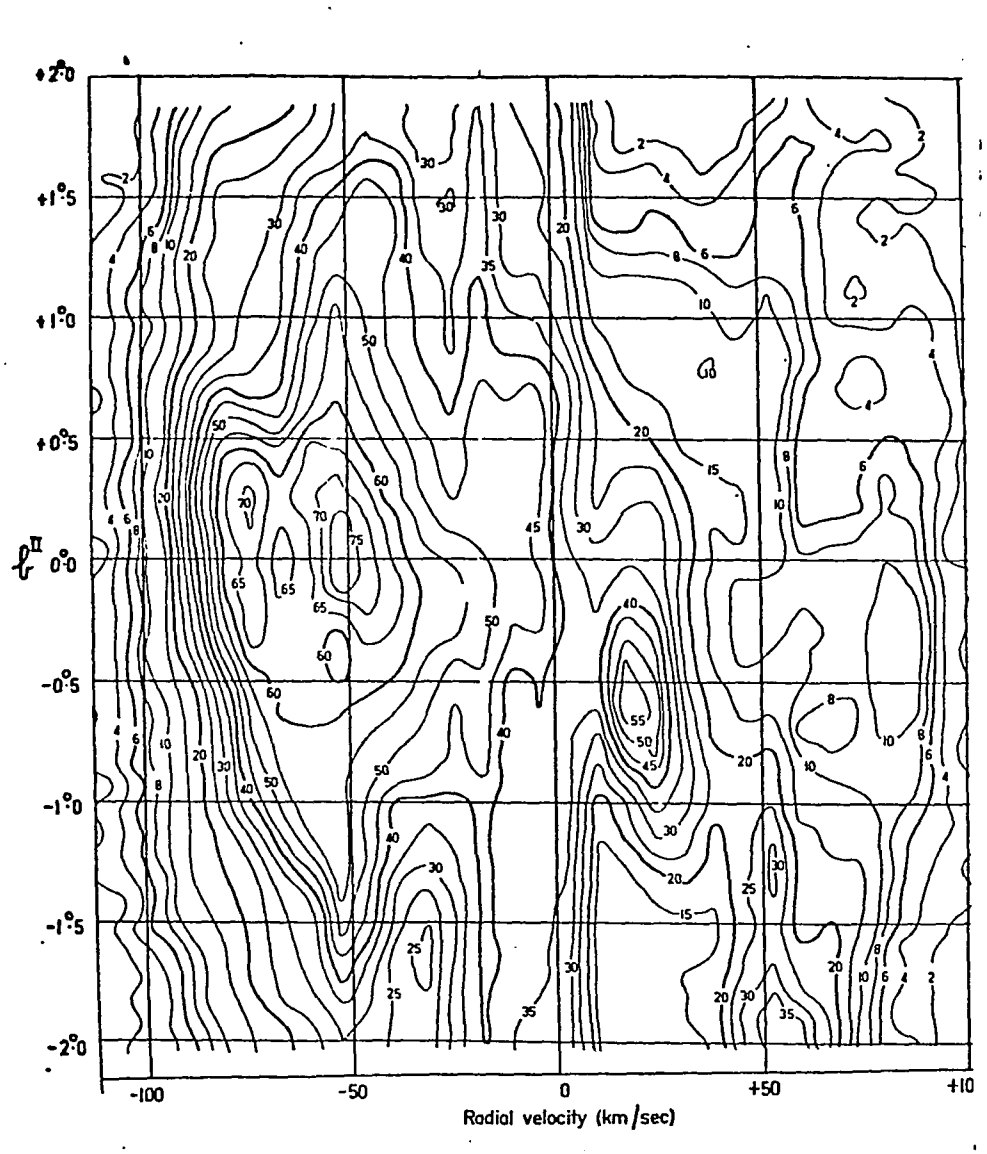
+2°0
+1°5
+1°0
+0°5
0°0
-0°5
-1°0
-1°5
-2°0
b^II
-100
-50
0
+50
+10
Radial velocity (km/sec)

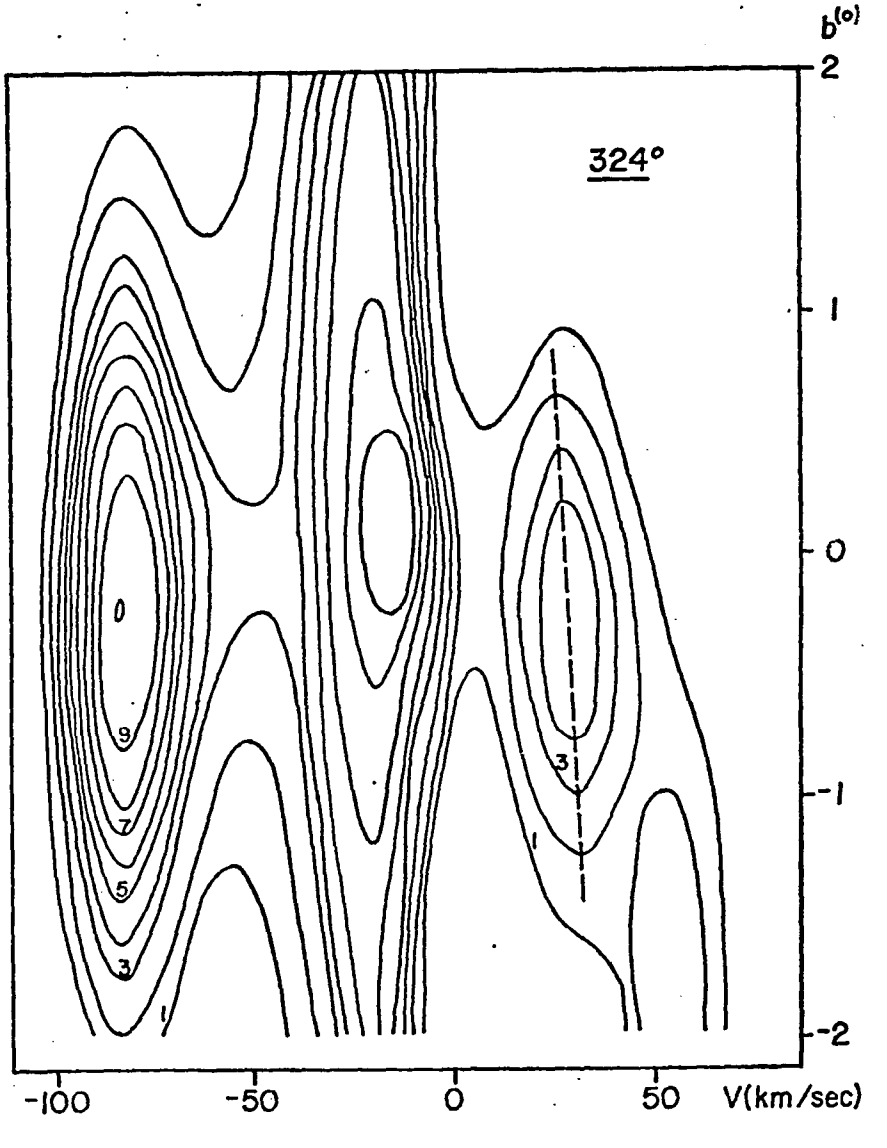
b(°)
2
1
0
-1
-2
324°
-100
-50
0
50
V(km/sec)

91

FIGURE 17

Values of the "rolling motion" obtained from numerical experiments plotted against observed values for the outer arms. It is important to note that a single set of global galactic parameters was used to obtain the three curves, not a different set for each arm. These parameters included a systematic motion of about 8 km/sec magnitude, as predicted by the density-wave theory and observed by various investigators. Using smaller values or no systematic motion at all gave increased values of dv/db and worse fits to the data.

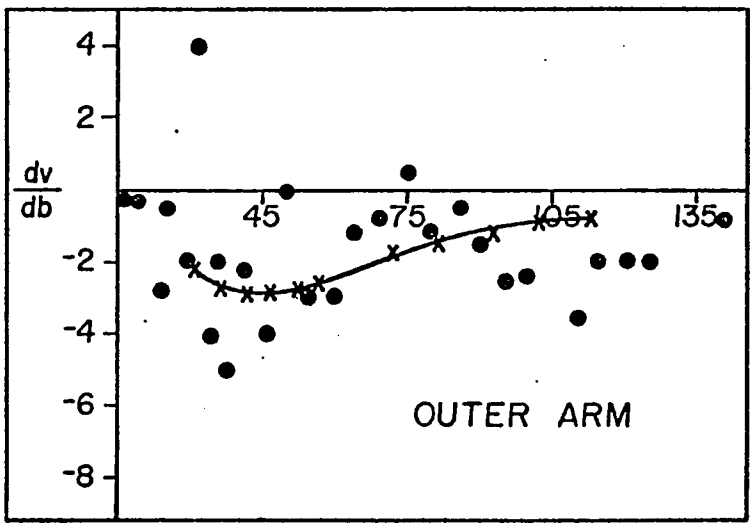
4
2
dv
db
-2
-4
-6
-8
45
75
105
135
OUTER ARM

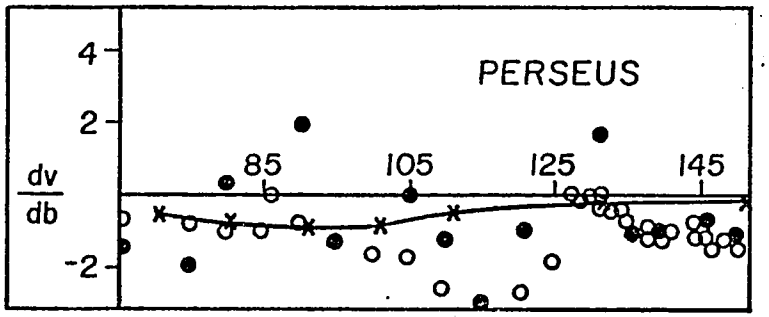
4
2
dv
db
-2
PERSEUS
85
105
125
145

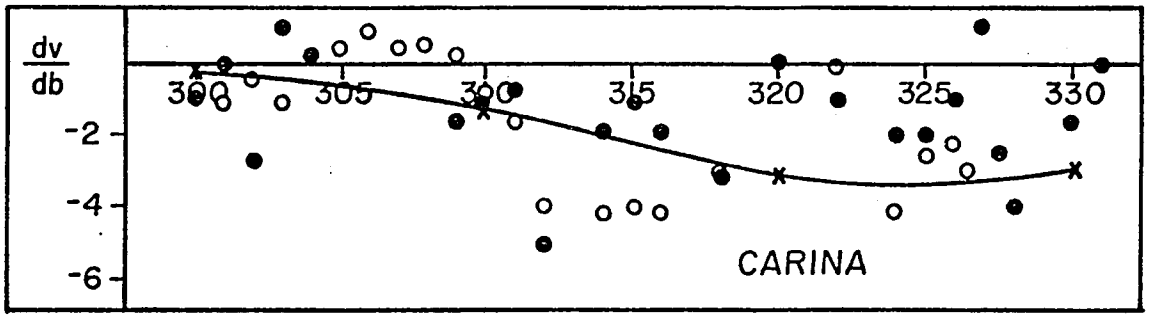
dv
db
-2
-4
-6
300
305
310
315
320
325
330
CARINA

(4) When the inner arms are located exactly on the galactic plane, no apparent "rolling motion" exists. However, if the arms are given displacements of as little as 10 kpc, (typical displacements observed by Henderson, Kerr, and others), the apparent "rolling motion" appears. If the arms are displaced by a "spiral corrugation" of the type suggested by Henderson, the "rolling motions" are small but consistently of one sign. If the arms are displaced by a "radial corrugation" the "rolling motions" are larger but variable in sign.

(5) The magnitude of the gradient dV/db remains roughly the same for the near and the far branches of a spiral arm. This means that the values of dV/dz would be drastically higher for the near branches of the arms, as observed by Burton, Shane, and Harten. Thus these observations of high values of dV/dz in the near branches of the inner arms, which were among the most puzzling aspects of the "rolling motion" phenomenon, are explained in a natural way by the present mechanism.

By varying one parameter while holding the others fixed it was possible to determine those quantities that most affect the magnitude and sign of the apparent "rolling motion" produced by the proposed mechanism. The two essential parameters, that is, those that affected most strongly the calculated behavior of dV/db, were the systematic motion of the gas and the velocity dispersion of the clouds. We shall examine the effects of these parameters in detail.

Systematic Motion. The magnitude of the radial and azimuthal systematic motions predicted by the density-wave theory has a strong effect on the observed magnitude of the rolling motion, in the sense that increases in the value of the systematic velocity lead to decreases in the size of the measured rolling motion. The effect can be explained easily by the diagram provided (Fig. 18). The line-of-sight velocity corresponding to the Schmidt circular rotation curve will be monotonically decreasing with distance, as shown. But the systematic motion will modify this variation, so that the velocity varies less rapidly near a spiral arm, and more rapidly in the interarm regions, creating "velocity plateaus" in regions where the arm is located. The greater the magnitude of the systematic velocity, the more nearly horizontal becomes the plateau. Since the gradient dV/db depends on the difference in velocity between two points located in the plateau region, this flattened portion of the velocity curve will lead to a reduction in the magnitude of the velocity gradient from what it would be in the case of no systematic motion.

FIGURE 18

Effect of density-wave streaming velocities on the Schmidt rotation curve. Near the positions of the spiral arms, the velocity levels off, so that two points in the arm at different distances from the sun will have nearly the same velocity. Thus the apparent "rolling motion" of the arm is smaller with density-wave streaming velocities than it would be with pure circular differential rotation.

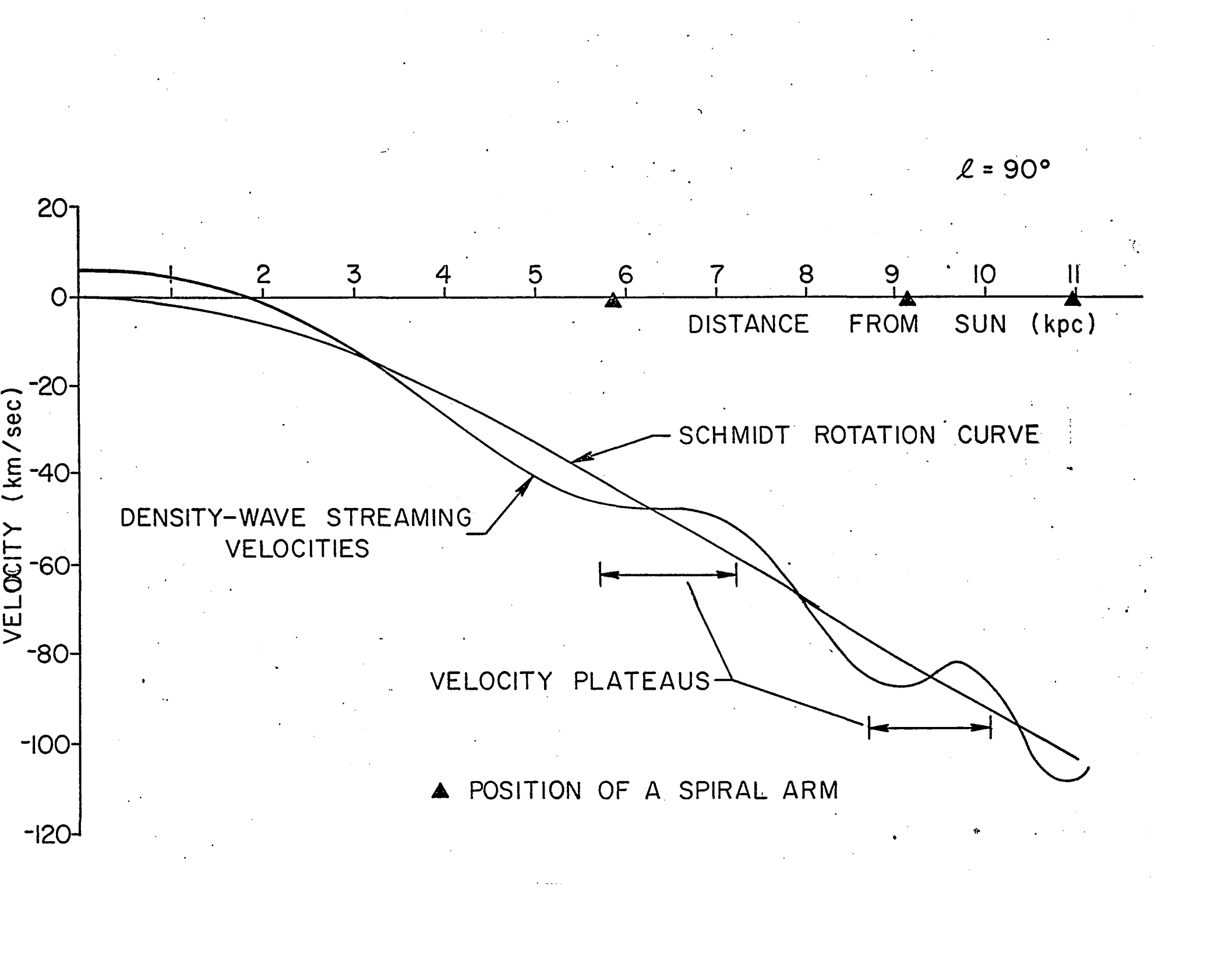
ℓ = 90°
20
0
-20
-40
-60
-80
-100
-120
VELOCITY (km/sec)
1
2
3
4
5
6
7
8
9
10
11
DISTANCE FROM SUN (kpc)
SCHMIDT ROTATION CURVE
DENSITY-WAVE STREAMING VELOCITIES
VELOCITY PLATEAUS
▲ POSITION OF A SPIRAL ARM

Since the systematic motion affects the measured values of the "rolling motions" so strongly, we may turn the problem around somewhat and use the observed values of dV/db to check on the most likely values for the magnitude of the systematic motion. For example, a series of about 10 runs using the 1965 Schmidt circular rotation curve alone (no systematic motion whatever) yielded an average value for the rolling motion of about -5 to -7 km/sec/degree. Such enormous values are hardly observed anywhere in the Galaxy in any extended region. Other runs, using values of 4, 8, and 12 km/sec for the magnitudes of the systematic motion, yielded values for the rolling motion of about -4, -2, and 0 km/sec/deg, respectively. The value of -2 km/sec/deg fits the observed values best, so that it is possible to say that the observed rolling motion indicates that a value of the systematic motion on the order of 6-10 km/sec agrees best with observations. As it happens, this value is in almost perfect agreement with the observed values of the systematic motion (see Roberts and Yuan 1970, Humphreys 1970).

Dispersion Velocity. The second parameter affecting the magnitude of the "rolling motion" is the velocity dispersion of the gas. Increasing the velocity dispersion of the gas results in an increase in the magnitude of the "rolling motion." For example, a series of calculations of dV/db for an outer arm at $l = 330^{\circ}$ using values for the velocity dispersion of 4, 6, 8, and 10 km/sec (with the systematic motion fixed at 8 km/sec) gave values of dV/db equal to -0.3, -1.2, -1.5, and -2.3 km/sec/deg, respectively. I t is clear from these

figures that the effect of the dispersion velocity, while considerable, is quite a bit less than the effect of the systematic motion.

BENDING AND CORRUGATION OF THE GALACTIC PLANE

One of the major parameters in constructing a model of the Galaxy is the observed distortion of the outer parts of the Galaxy: the "hatbrim" effect, with the Southern sky the leading edge (brim turned downward), the Northern sky the trailing part (upward), and the Sun situated over the right ear. A large-scale survey by Oort, Kerr, and Westerhout (1958) first established the sense and magnitude of the bending. A finer-resolution study of the Northern Sky by Henderson (1967) provided more precise figures for the distortion in the outer regions, and also provided evidence for the first time of large connected regions in the inner parts of the Galaxy that deviate by slight amounts (10-30 pcs) from the established Galactic plane. (See Fig. 19, which is taken from Henderson's Fig. 7.) Since this latter result is of the highest importance for the proposed mechanism for the inner-arm rolling motions, we include Henderson's diagram as evidence for the reality of displacement of inner spiral arms.

Bending of the Outer Regions. Henderson's results were given in the form of diagrams of z_0 (position of the centroid of the galactic hydrogen) vs. R (distance from the sun) for a given longitude. These data were converted into functions of ϖ (galactic radius) and L (galactocentric longitude, measured clockwise from the the sun-center line). The data for $\varpi \gtrsim 10$ kpc was then fitted by a curve of the form

$$f(\varpi) \sin (L - L_0)$$

FIGURE 19

Henderson's map of the deformation of the plane in the Northern Sky. Hatched areas are regions below the plane. The "corrugation" of the inner disk is clearly evident.

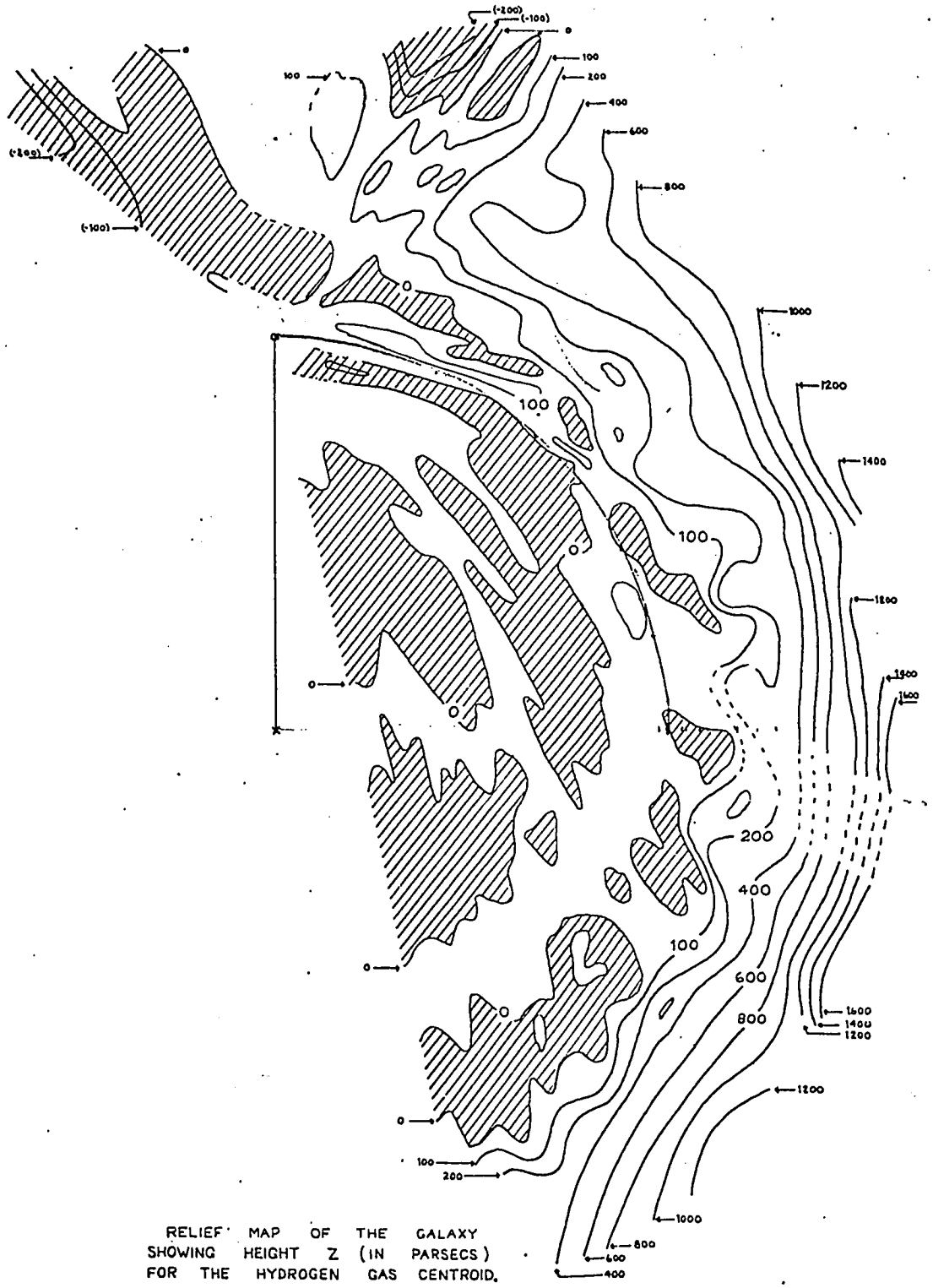

RELIEF MAP OF THE GALAXY SHOWING HEIGHT Z (IN PARSECS) FOR THE HYDROGEN GAS CENTROID.

where $f(\varpi) = 50(\varpi - 10)^2 - 50(\varpi - 10)$ pcs. (ϖ in kpc)
and L_o appears to lie somewhere between -20 and +20°.

To check the closeness of the fit, the curve was then replotted into the form given by Henderson (z_o vs R for fixed longitude l) and the results appear as Fig. 20. It is clear that from $l = 20^\circ$ to $l = 135^\circ$, the fit is very good. For higher values of l, the hydrogen appears to undergo an additional oscillation starting at values of R~5-6 kpc (ϖ~14 kpc) which takes the centroid below the plane at R~8kpc for $135^\circ < l < 185^\circ$, and correspondingly above the plane at about R ~ 7 kpc for $191^\circ < l < 220^\circ$. Since this effect is only important for $\varpi \gtrsim 14$ kpc, and since our model galaxy cuts off not much beyond that point, it was unnecessary for our purposes to seek any better fit. However, any future model galaxies which seek to explain phenomena occurring beyond ϖ~14kpc must take this complication into account.

Henderson's graphs were not themselves raw data; they depended on the Schmidt model rotation curve of 1965. If this curve should be modified, the coefficients in the function would have to be adjusted.

Corrugation of the Inner Parts of the Plane. Henderson's Fig. 7 (our Fig. 19) also indicates that the inner part of the plane has a wavy or corrugated look, going through about two oscillations of about 10-40 pcs magnitude and several kpc wavelength. Henderson has attempted to correlate these fluctuations in height with the inner spiral arms: his findings are reproduced in Fig. 21 (Henderson's Fig. 8.)

FIGURE 20

The match to Henderson's observations on the distortion of the galactic plane by a simple function of the form

$$f(\varpi) \sin(\theta - \theta_0)$$

where θ is galactocentric longitude and θ_0 marks the line of nodes. From $l = 30^\circ$ to 105°, this function is a good approximation. It breaks down near the complicated region around $l = 140^\circ$.

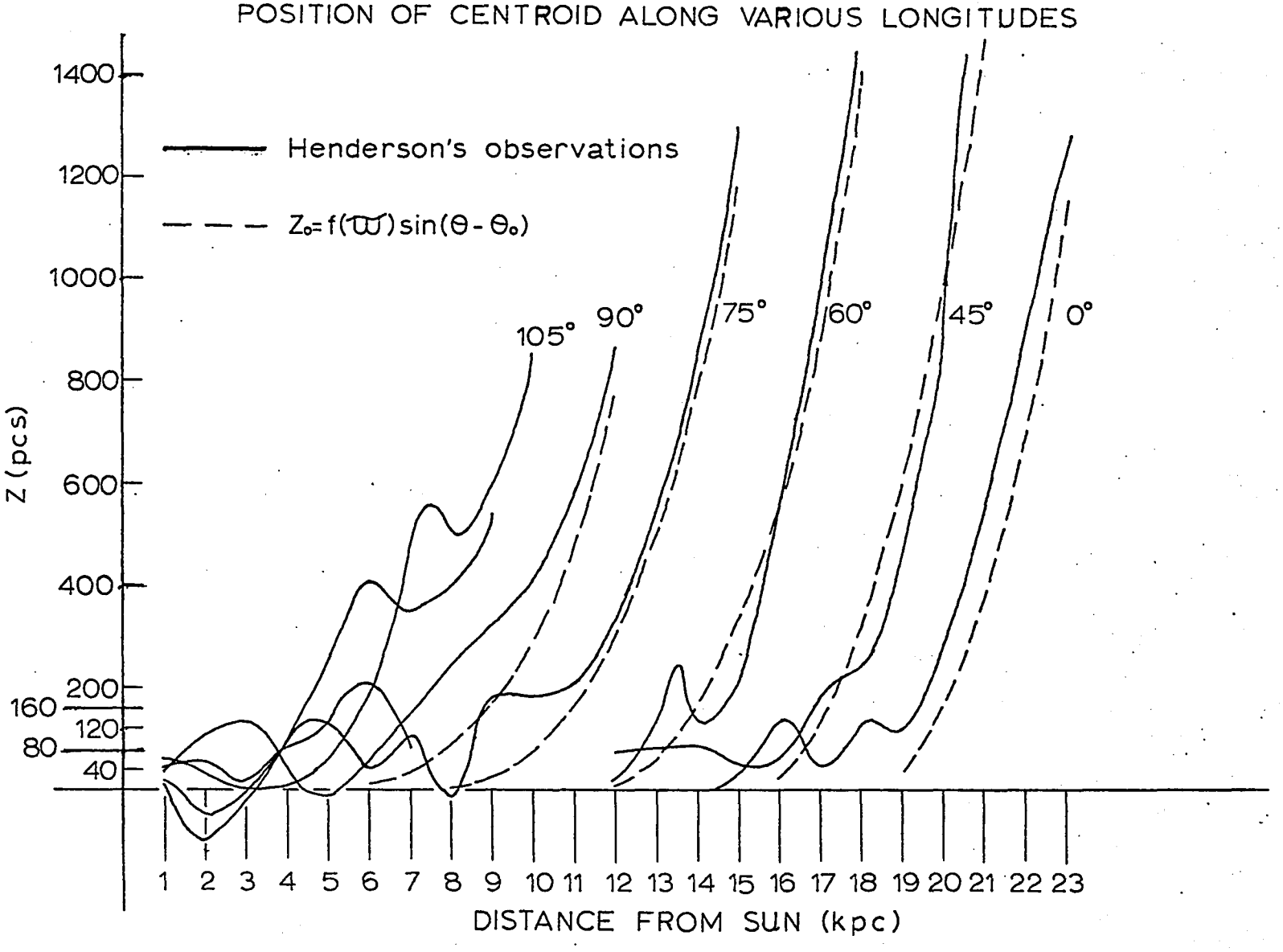
POSITION OF CENTROID ALONG VARIOUS LONGITUDES
Henderson's observations
$Z_o = f(\varpi)\sin(\theta - \theta_o)$
105°
90°
75°
60°
45°
0°
Z (pcs)
1400
1200
1000
800
600
400
200
160
120
80
40
1 2 3 4 5 6 7 8 9 10 11 12 13 14 15 16 17 18 19 20 21 22 23
DISTANCE FROM SUN (kpc)

FIGURE 21

Henderson's superposition of the spiral arms onto his map of the deformation of the galaxy. From this map, he suggested that the inner region may be represented as a "spiral corrugation," with successive spiral arms alternately above and below the plane.

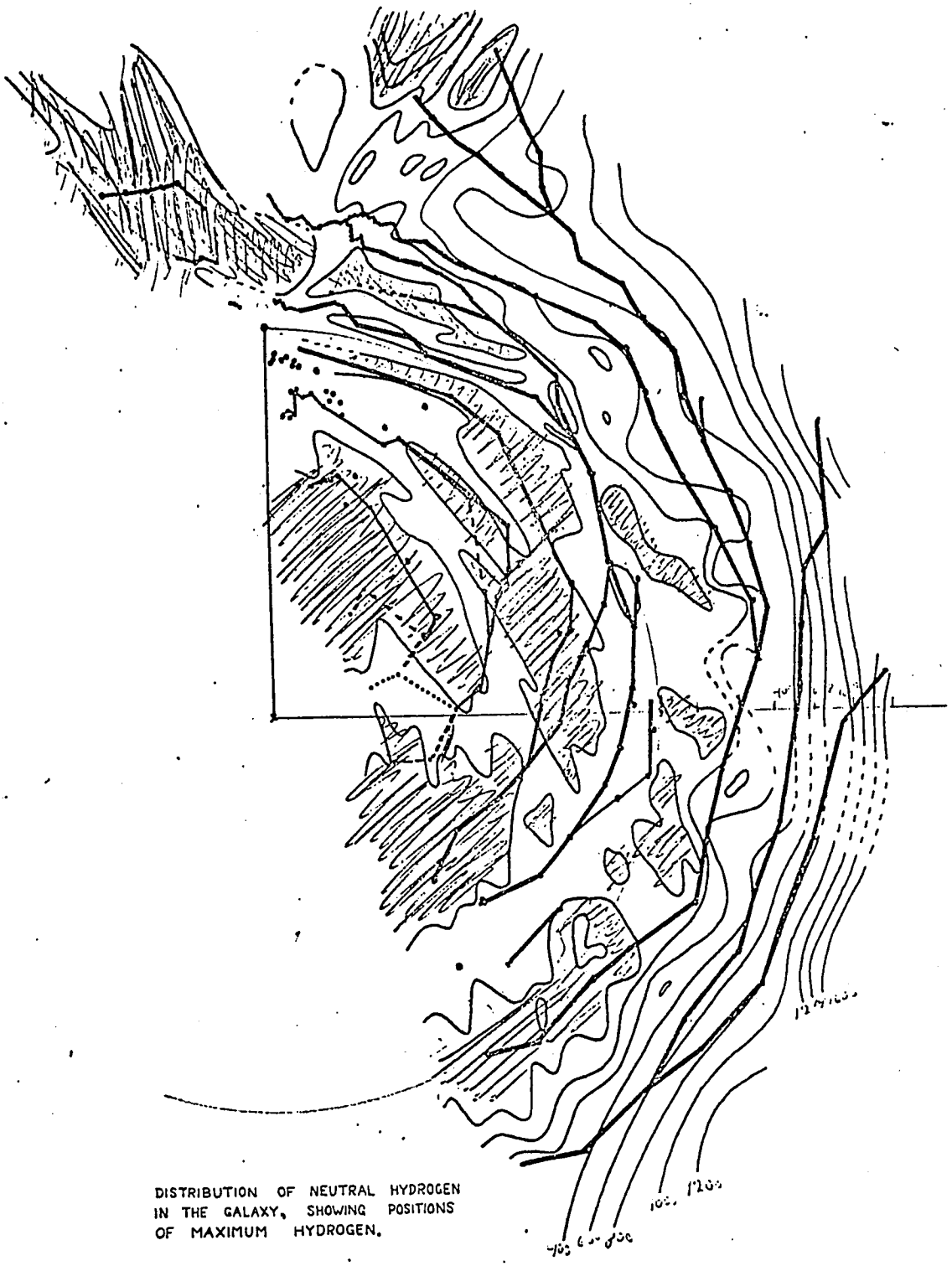

DISTRIBUTION OF NEUTRAL HYDROGEN IN THE GALAXY, SHOWING POSITIONS OF MAXIMUM HYDROGEN.

His inner arms 1 and 3, for example, appear to stay largely below the plane while arm 4 is usually found above the plane. Other investigators, however, appear to have conflicting ideas about the placement of the centroids of the arms. (See Burton 1969) Shane (1971) Even Henderson's own data do not present compelling evidence for the existence of a spiral corrugation.

Nonetheless, whatever the exact form of the fluctuation it is incontestable that the neutral hydrogen in the inner parts of the Galaxy fluctuates in height by some tens of pcs from the central plane. For many purposes, this small fluctuation may be unimportant; however, it turns out to be the essential feature in our proposed geometric mechanism for producing the appearance of "rolling motion" in the inner arms. Without such a fluctuation, there will be no apparent rolling motion in the inner arms, as predicted by our simplified explanation of the mechanism and confirmed by numerical studies; with such a fluctuation, rolling motions of approximately the magnitude actually observed appear at once in our computer model of the Galaxy.

Therefore two possible "corrugations" have been introduced into our model galaxy:

(1) a spiral corrugation such that alternate spiral arms are consistently above and below the plane, as explicitly suggested by Henderson, and

(2) a circular corrugation such that the inner arms pass through the galactic plane as they wind outward from the center.

The main results of the two models follow:

(1) With the spiral corrugation, the inner arms are found to have consistent and predicable rolling motions; i.e., they can be classed in a 3-fold scheme, depending on whether they are Northern or Southern sky arms, Above or Below the plane, and Near or Far regions with respect to the tangent point. For example the near portion of N. Sagittarius would be classed as Northern Near Above (NNA), and we could predict from the model that it would have a negative rolling motion. Any single switch of the classifying letters (say from NNA to NNB) would change the sign. These predictions have been tested by a number of numerical calculations and found to be verified, with the single exception of far arms at certain longitudes, which sometimes fail to produce consistent signs for the gradient dV/db. Therefore, if Henderson's suggestion can be proved to be the case, the present hypothesis of a geometric mechanism for the inner arms can be given an immediate test: check the sign of the observed rolling motion against the sign predicted from the 3-fold classification scheme outlined above.

(2) The circular corrugation produces rolling motions that are variable in sign and somewhat larger in magnitude than those computed from the spiral corrugation. This is to be expected, since the sense of the rolling motion depends basically on whether the axis of the cross-section of the arm passes above or below the sun, and this is affected in a complicated manner by the form of the variation in the shape of the inner regions of the galactic plane.

PROBLEMS MET IN VIEWING THE ROLLING MOTION AS REAL

Theories postulating an actual rolling motion meet with two fundamental physical difficulties and several less fundamental but still disturbing problems in explaining the observations. The fundamental problems are the origin of the rolling motions and their maintenance through several galactic years. The two may be related to some extent, but the problem of the origin is definitely more troublesome. Since the energy involved is of the supernovae magnitude, no ordinary physical phenomena will suffice. Superexplosions of the type advocated by Rickard to explain his observations of Perseus do not seem to be based on any reasonable physical grounds. It is also difficult to imagine that a large-scale disturbance such as the bending of the galactic plane could induce a small-scale motion along the spiral arms in the Galaxy.

The second fundamental problem may be less troublesome. Here what is necessary is to find asymmetrical forces capable of driving the rolling motion. However, gravitation does not supply such forces. The next most likely candidate is the galactic magnetic field. (As Woltjer has remarked, the magnetic field is always popular as an explanation of observed phenomena, since we know so little about it.) The rather meager knowledge of the magnetic field may be summarized as follows: the field in the solar vicinity is parallel to the galactic plane, lies roughly along the direction of the local spiral arm (or the Orion Spur) at

with some evidence that the lines of force may reverse their direction by 180° across the galactic plane; and, finally, with a strength of 2-3 microgauss. (See Van de Hulst 1967 for extensive references.) This observed topology of the magnetic field is consistent with the suggestion by Roberts and Yuan (1970) that the galactic magnetic field is parallel to the velocity field in the frame rotating at the pattern speed of the spiral density wave. The most remarkable feature about this model is that it is completely free from the difficulty of the winding up of the magnetic field lines. Here we shall make the same assumption: i.e., $\underset{\sim}{H} \sim \rho \underset{\sim}{u}$ where both the magnetic field $\underset{\sim}{H}$ and the velocity field $\underset{\sim}{u}$ are those in the rotating frame.

Without the magnetic field, the interstellar gas is revolving about the galactic center under the influence of three forces: the pressure gradient of the gas, the gravitational force of the axisymmetric potential, and the gravitational force due to the presence of the spiral wave. The plane components of all three forces are always even functions of z, wheras the vertical components are all odd functions of z. With these forcing functions, the flow of interstellar gas naturally settles into a pattern which is symmetrical with respect to the plane of the Galaxy. (See the first section of this paper.) Adding a magnetic field introduces the Lorentz force to the problem: $(\nabla \times \underset{\sim}{H}) \times \underset{\sim}{H}/4\pi$. But for $\underset{\sim}{H} \sim \rho \underset{\sim}{u}$, no mixed term is created in the Lorentz force that will break the initial symmetry.

A complete search of the first-order terms of the Lorentz force fails to turn up any candidates for asymmetric motions of the type needed. Even if the higher terms of the Lorentz force might produce these motions, they will probably not be important in view of the small value of the field strength. Therefore, we conclude that the galactic magnetic field is an unlikely cause of the rolling motions observed in spiral arms.

A less basic but still disturbing question confronting theories postulating an actual rolling motion is the explanation of the following interesting observation: Virtually all observers agree that the value of dV/dz is considerably higher for the near portions of an inner arm than fro the far portions. For example, Shane finds that for the Scutum arm, dV/dz for the near portion oscillates between +10 and -40 km/sec/kpc, while for the far portion, it remains between the much narrower limits of +5 and -2 km/sec/kpc. Similarly, Harten (1971) finds that the average value for dV/dz for the near portions of Norma and Southern Sagittarius are twice as high as for the far portions: for Norma, his values are -12 and -6 km/sec for the near and far portions; for S. Sagittarius, the values are -15 and -7 km/sec/kpc. Finally, Burton finds an avergge dV/dz of about -28 for the near portion of the Northern Sagittarius arm, while for the far portion the corresponding value is only -9 km/sec/kpc.

If the rolling motion is actually occurring in the arms, then why should this motion increase in the portions of the arms that are closer to us? Of course, if the rolling motion is only the geometric effect proposed here, the problem does not arise. The greater values of dV/dz are a consequence of the fact that dV/db does not change very much with distance. (This is because both ΔV and Δb decrease with distance from the sun. ΔV decreases because the tangent points move closer together in the more distant arms; Δb decreases because the more distant arm subtends a smaller angle.)

We conclude that theories postulating true rolling motions in the arms raise rather more questions than they answer; Time would perhaps be better spent on proving or disproving the geometric mechanism presented here.

STUDIES ON THE THICKNESS OF THE GASEOUS LAYER: OUTER ARMS

I have located only three studies specifically concerned with the thickness of the gaseous disk outside the 10-kpc circle. Using the data published in each study, it is possible to show that the thickness of the disk appears to increase with distance from the sun. We shall determine the magnitude of this effect, and try to determine its cause.

Lozinskaya and Kardashev (1963) used an 18 x 8-meter radio telescope with a beam width of 47' by 113' to study the thickness of the outer regions of the Galaxy at 20° intervals in longitude between $l = 20^{\circ}$ and 240°. They made about 140 measurements of the latitude difference between half-intensity points. Their major conclusion was that the thickness of the outer region of the disc increased rapidly with increasing galactic radius. In addition, they found a suggestion that the increase was associated with the deformation of the disk, being largest where the disk was most distorted (galactocentric longitude $L \sim 90^{\circ}$, heliocentric longitude l between 45° and 60°). Their data is plotted as a function of distance from the sun in Fig. 22. It seems clear that there are two interpretations of the data. There does indeed appear to be a slight maximum in the R = 11-13-kpc range, which corresponds approximately with the region of greatest deformation. However, the behavior on both sides of this maximum is far from symmetric with regard to L, as we might expect if it were associated with the deformation of the disk, which can be well represented by a sin L law. In every case, the points symmetric about the region of greatest deformation have differing values of measured thickness, with the higher values corresponding to the more distant regions. We conclude that there is a strong

FIGURE 22

Thickness of the hydrogen layer as determined by Lozinskaya and Kardashev (1963), averaged over successive rings of 1 kpc width. The general increase in thickness with distance is clearly evident here, although there is a suggestion of a maximum occurring at about 12-15 kpc from the sun, which corresponds roughly to the region of greatest deformation of the Galaxy.

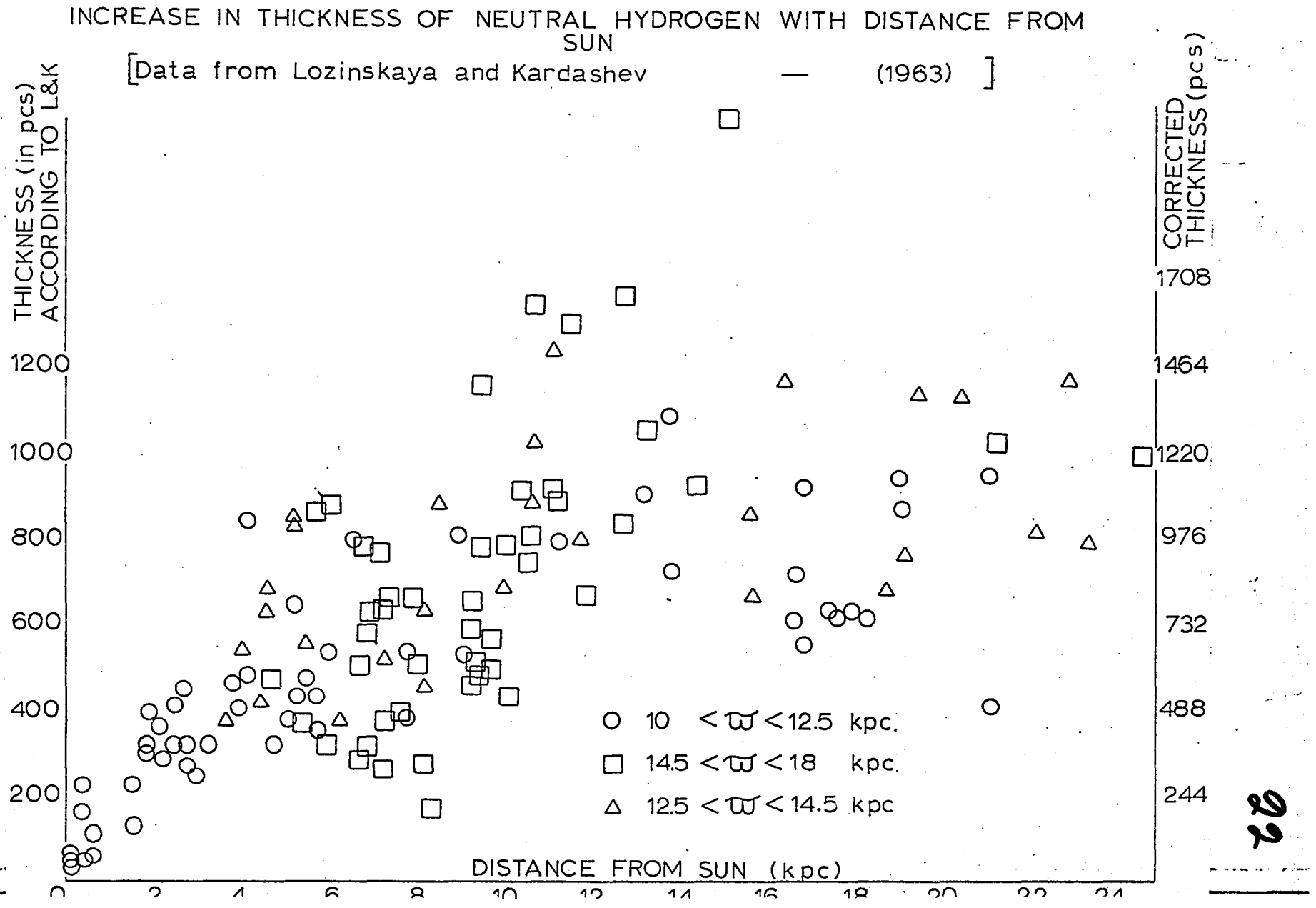
INCREASE IN THICKNESS OF NEUTRAL HYDROGEN WITH DISTANCE FROM SUN
[Data from Lozinskaya and Kardashev — (1963)]
THICKNESS (in pcs) ACCORDING TO L&K
CORRECTED THICKNESS (pcs)
1200
1000
800
600
400
200
1708
1464
1220
976
732
488
244
10 < ϖ < 12.5 kpc.
14.5 < ϖ < 18 kpc.
12.5 < ϖ < 14.5 kpc
DISTANCE FROM SUN (kpc)
0
2
4
6
8
10
12
14
16
18
20
22
24

indication of a distance effect in L&K's data, although they did not call attention to it.

In the same year, Milton and McGee (M&M) studied the thicknesses of concentrations of neutral hydrogen between longitudes 212°-325° and 25°-75°. They too found that the thickness increases markedly with increasing galactic radius. Because of information due to J. V. Hindman, who said he had noticed the great increase in thickness also but had disregarded it because the distribution appeared heliocentric, M&M plotted their data on thickness versus the distance from the sun, finding that "no heliocentric tendency is seen." Yet on Fig. 29A their data is plotted exactly as they give it in their published table and a clear distance effect is seen, in both the Northern Sky and Southern Sky portions of their study. I am unable to explain their statement. A least-squares program using their data shows a thickness increase with distance on the order of 40 pcs/kpc.

Finally Henderson in his unpublished thesis (1967) used the 300-foot telescope at Green Bank to study the thickness of the hydrogen in the Galaxy at 5-degree intervals of longitude between $l = 16^{\circ}$ and 230°. Henderson's theoretical resolution of 11' was between 5 and 10 times better than L&K's, and several times better than M&M's. Since one angular degree (L&K's approximate resolution) at 20 kpc corresponds to a linear dimension of about 350 pcs, this is clearly a crucial point. Moreover, rather than measure the latitude difference between half-intensity points, Henderson used an "equal-area" method in which he integrated the brightness temperature over latitude and determined the rectangle of equal area whose height corresponded to the peak brightness temperature and whose width he then

called the thickness of the gas layer. (If the brightness temperature is Gaussian, this method gives a thickness 4% larger than the half-intensity method.) The advantage of this method is that isolated clouds that happen to be situated just where they can push up the half-intensity contour by a degree or more will hardly affect the thickness as determined from Henderson's integration technique. Henderson's results agree qualitatively with those of the previous investigators; however, he is the first of the three to notice the distance effect. He states ("In the scans from $l = 70^{\circ}$ to 230° the thickness increases monotonically such that at the edge (15 kpc) it is approximately double that of the average inner region. If the value at the solar neighborhood is taken to be 250 pc, it becomes 500 pc at the edge. Between $l = 16^{\circ}$ and 70° the value for the thickness at the edge becomes much larger, from three to four times the value at $R_{\odot}$. This would be in general agreement with Lozinskaya and Kardashev (1963) but we do not believe the effect to be as large as measured, only another optical depth effect." Henderson goes on to explain that the peak brightness temperature at 16° is lower than that at 230°, which may result in a larger measured width. He concludes, "In all probability the thickness near the edge between $l = 16^{\circ}$ and 70° is also of the order of 500 pc." However, he shows some awareness of the unsatisfactory nature of this explanation (Why should the temperature of the hydrogen be lower on the opposite side of the Galaxy?) in his very next paragraph, in which he

states "The above paragraph brings up some interesting problems, for in effect it is saying that the opacity is a function of distance from the sun, or the excitation temperature of the hydrogen is lower on the opposite sides of the Galaxy or the distance-velocity scale is in error such that the density determinations were wrong. All these require putting the sun at a favored position. Perhaps there is a measureable extinction of radio frequency radiation in the Galaxy. Such a proposal would be in agreement with the recent work of Hoyle and Wickramasinghe (1967). The mechanism proposed is the oscillation of dislocations within the interstellar grains (10^{10} c/s and lower.)"

Thus we have the following situation: Three separate investigators agree that the thickness of the gas layer increases with galactic radius beyond the position of the Sun. The data of all three display a distance effect, although one group (L&K) interpret it as related to the distortion of the Galaxy and the other group (M&M) denies that it is there. The third investigator, noting the distance effect, confines his remarks on the quantitative increase of the thickness to the statement that the thickness approximately doubles between the position of the Sun and the "edge" of the Galaxy.

Two problems suggest themselves at this point: (1) Can we somehow remove the distance effect from the data and find the true thickness of the gas layer? (2) What is the cause of the distance effect?

A close examination of Henderson's data gives us hope that the first question can be answered successfully. Fig. 23 shows the thicknesses of the outer regions replotted as functions of radius at constant longitudes. There appears to be enough internal consistency in the points to justify connecting those at constant longitude with straight lines. Then a particular value of ϖ can be chosen, and its intersections with the line corresponding to each longitude plotted in a graph of thickness versus distance from the sun for a constant radius. (See Fig. 24) (Alternatively, the actual observed points may be used, by selecting, say, all points between 10.5 and 11.5 kpc from the center, and plotting them against distance rather than the (unobserved) intersections of the ϖ = constant line with the line of constant longitude. Because of the regularity of the data, it is doubtful that the two methods would give significantly different results.) Finally, if the points display sufficiently small scatter, we may extrapolate them backward to where R (distance from the sun) = 0, thus finding a "true" value for the thickness corresponding to each value of the radius ϖ.

The results were clearly quite regular, and a least-squares fit to the data for each selected value of ϖ gave the following results for the thickness T of the gas layer and for the increase of the thickness with increasing distance from the sun $\left(\frac{\partial T}{\partial R}\right)$

ϖ (kpc)	T (pcs)	$\frac{\partial T}{\partial R}\left(\frac{\text{pcs}}{\text{kpc}}\right)$
11	190	25
12	230	34
13	280	39
14	330	40

FIGURE 23

Thickness of the gas layer as determined by the integration technique of Henderson. Note the remarkably uniform decrease of the thickness from low longitudes (large distances) to high longitudes (small distances).

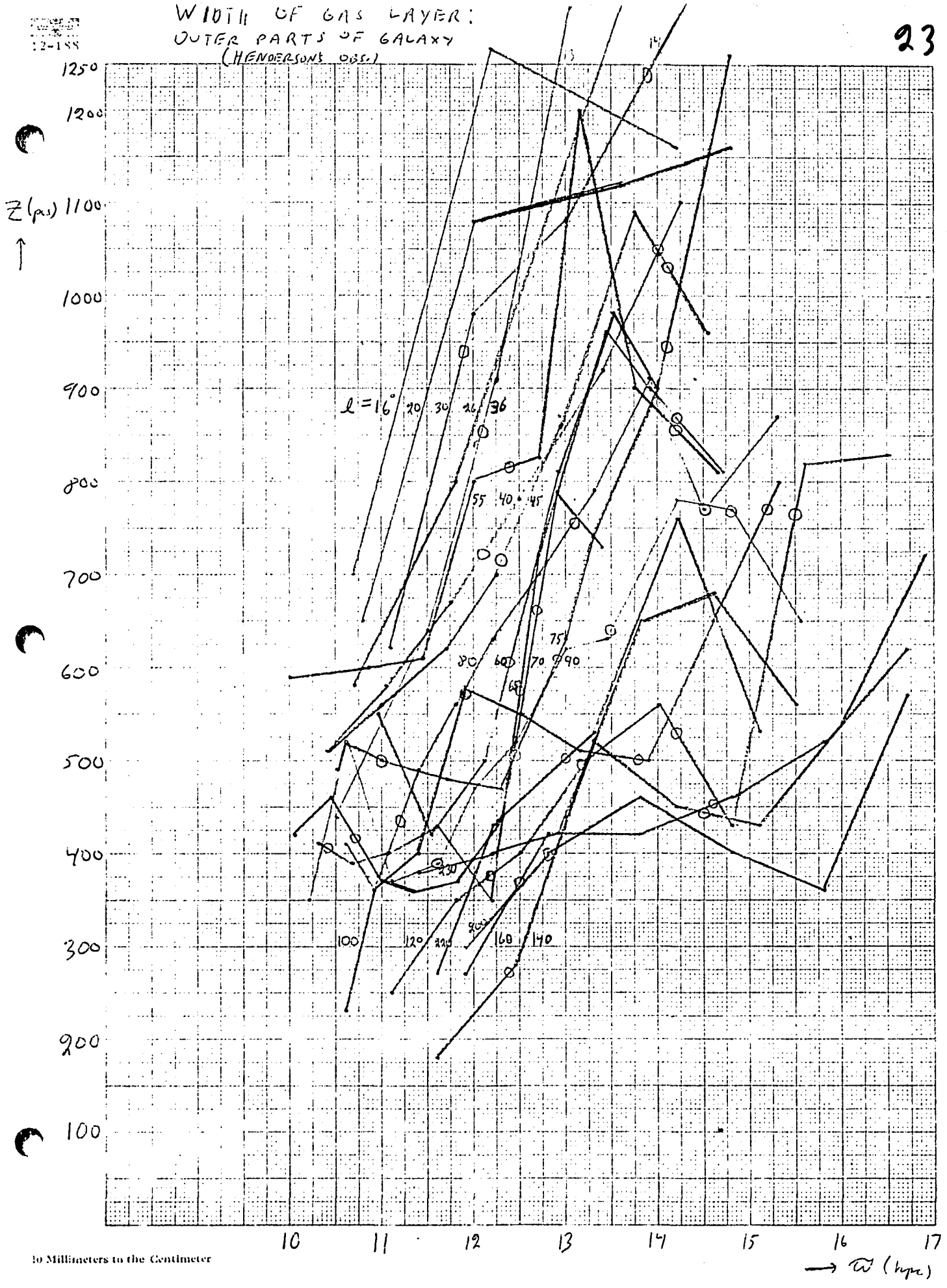
WIDTH OF GAS LAYER:
OUTER PARTS OF GALAXY
(HENDERSONS OBS.)
Z (pc)
1250
1200
1100
1000
900
800
700
600
500
400
300
200
100
10
11
12
13
14
15
16
17
→ ω (type)
l = 16°
20
30
26
36
55
40
45
75
80
60
70
90
65
230
100
120
220
160
140
240

FIGURE 24

The previous diagram transformed to lines of constant galactocentric radius. By extrapolating backwards to R = 0, we remove the "distance effect" consisting of a roughly linear increase in the measured thickness of the gas with increasing distance from the sun. Provided that the "distance effect" is an illusion of some sort, and is linear, the intercepts with R = 0 correspond to the "true" thickness of the Galaxy. Note that the values of the thickness at R = 0 (ranging from 190 pcs at ϖ = 11 kpc to 330 pcs at ϖ = 14 kpc) are considerably smaller than all previous estimates made from 21-cm line surveys.

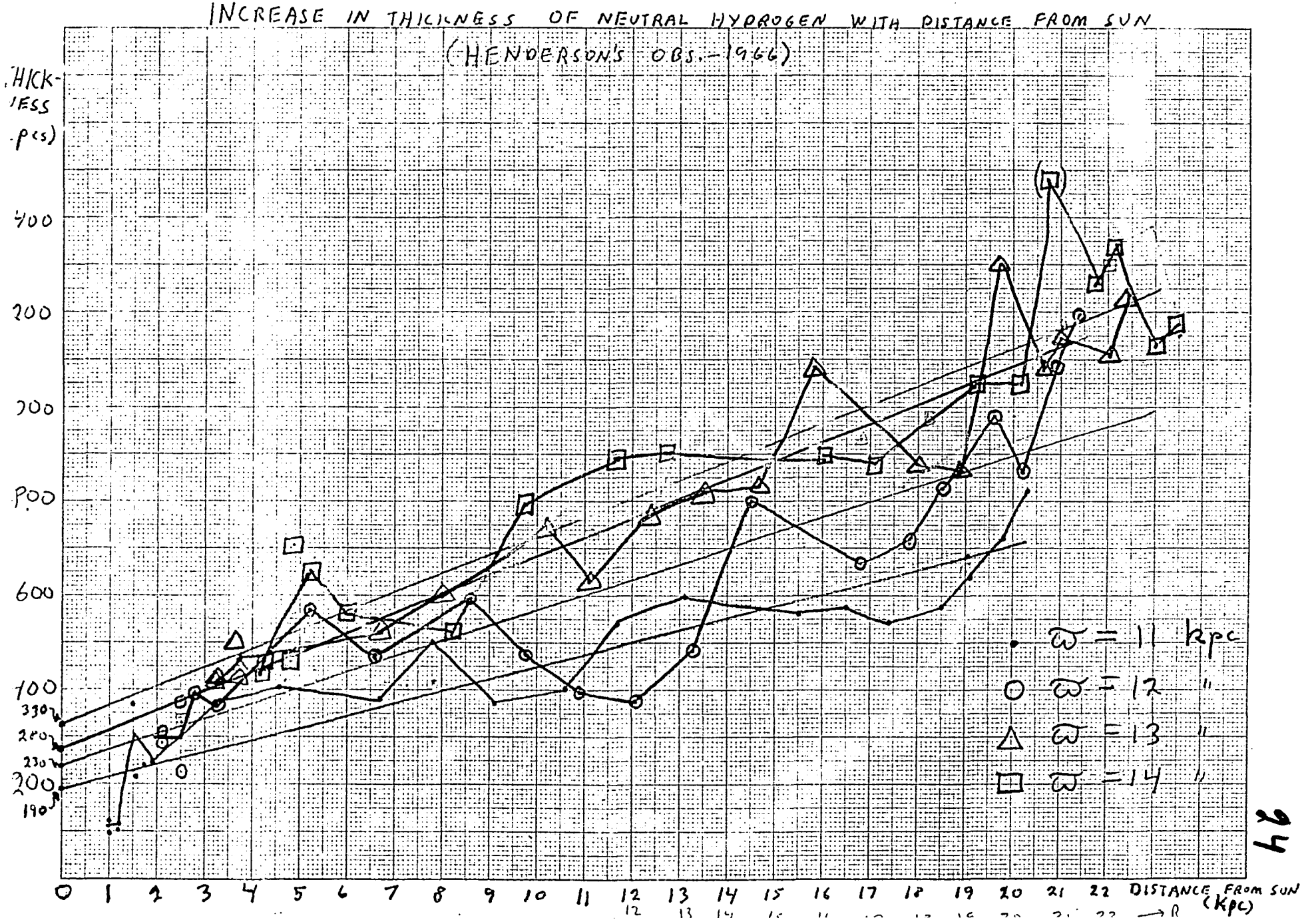
INCREASE IN THICKNESS OF NEUTRAL HYDROGEN WITH DISTANCE FROM SUN
(HENDERSON'S OBS.-1966)
THICK-
NESS
(pcs)
400
300
200
100
330
280
230
200
190
0 1 2 3 4 5 6 7 8 9 10 11 12 13 14 15 16 17 18 19 20 21 22
DISTANCE FROM SUN
(Kpc)
ω = 11 kpc
ω = 12 "
ω = 13 "
ω = 14 "

The data indicates that the true value of the thickness ranges from about 200 pcs at ϖ = 11 kpc to about 330 pcs at ϖ = 14 kpc, with an indication that it then begins to fall off somewhat, although the last interpretation is based on only a few points. These values are considerably lower than the values obtained by L&K, M&M, and even Henderson himself, from whose data they are obtained, because of the removal of the distance effect, which added from 25-40 pcs per kpc to the measured thickness in all four least-squares determinations of the best fits to the data of Fig. 24.

Since these results depend on Henderson's observations, which were restricted to the 16°-230° longitude range, we may ask if a similar procedure may be adopted for observations in the Southern Sky in order to remove the distance effect. However, since L&K cover the same longitude range as Henderson, only M&M's points are available. But since M&M have only 23 data points in the Southern Sky (compared with L&K's 137 and Henderson's 144) we do not have enough points for a statistically reliable sample. Accordingly, I have made my own measurements from the S. Sky observations available to me: Hindman and Kerr (H&K) (1969), who observed at 5° intervals between longitudes 190° and 299°, and Kerr (K) (1969), who treats longitudes from 300° to 60° at one-degree and five-degree intervals. Because of Kerr's restricted latitude range of $+2^{\circ}$ to -2°, only the nearby arm (Carina) can be utilized; the more distant regions lie below the -2° cutoff line because of the distortion of the galactic plane. From the H&K and K surveys, we have made 83 measurements of the gas thickness in spiral arms in the Southern Sky to add to M&M's 23. We have also made 124 measurements of half-intensity points from Henderson's N. Sky data to compare with his equal-area values as a check on the accuracy of the method.

The results from our own series of measurements may be summarized as follows: 1) There is no systematic difference between the values for the thickness obtained from measuring half-intensity points and those achieved by Henderson in his equal-area integration method. However, as expected, a far larger scatter exists in the half-intensity method, with the

average deviation from Henderson's corresponding measurement being $\pm$ 25%.

2) No difference was observed in the thickness of the arm and interarm regions, both according to Henderson's equal-area measurements and my half-intensity measurements. We should recall that we are probably measuring basically the cold component of the hydrogen gas, so that the theoretically expected greater thicknessss of the hot interarm region might not be observable in 21-cm line studies. (However, Weaver has reported finding that the scale height of the interarm regions increases by a factor of two or more over that of the arm regions.)

3) The distance effect appears very prominently once again in our own measurements. There is no indication whatever of a connection with the deformation of the Galaxy; rather, there is a monotonic and approximately linear increase in the measured thickness with distance from the sun, whose magnitude is roughly 30 pcs/kpc.

4) Because of the large scatter in these measurements, it seems no longer justified to attempt to extrapolate backward to $R = 0$ along different values of ω, thus determining the "true" value of the thickness at various radii.

With the recent publication of the results of the galactic survey undertaken at Hat Creek Observatory (Weaver 1973), another independent check of the "distance effect" has become possible. Although published in the inconvenient form of profiles rather than contour maps, the data was utilized to provide about 75 measurements of thickness which agreed remarkably well with the data of Henderson. (See Fig. 25.) The increase in thickness according to Weaver's data was 36 pcs/kpc, compared to the Henderson values of 25, 34, 39, and 40 pcs/kpc.

In summary, I have shown that four separate investigations of the gas disk beyond the position of the sun have indicated not only an increasing thickness of the gas layer with increasing radius from the galactic center; but also a distance effect such that the thickness appears to increase with distance from the sun, in both the Northern and Southern Skies. In addition, I have shown that the distance effect can be removed from the best series of observations to give an improved estimate of the "true" thickness, showing that this true thickness is considerably smaller than all previous estimates; and that the behavior of the distance effect is approximately linear, with a slope of about 35 ± 5 pcs/kpc. It remains to investigate the cause of the distance effect.

FIGURE 25

Increase in galactic thickness with distance from the sun as measured from the Hat Creek survey (Weaver and 1973). The results of this recent survey, utilizing a telescope of 28' beam width, agree very well with earlier surveys. Once again the apparent increase in thickness is linear with a magnitude of 36 pcs/kpc.

INCREASE IN THICKNESS OF NEUTRAL HYDROGEN WITH DISTANCE FROM SUN

[Measurements From Data of Weaver —— (1973)]

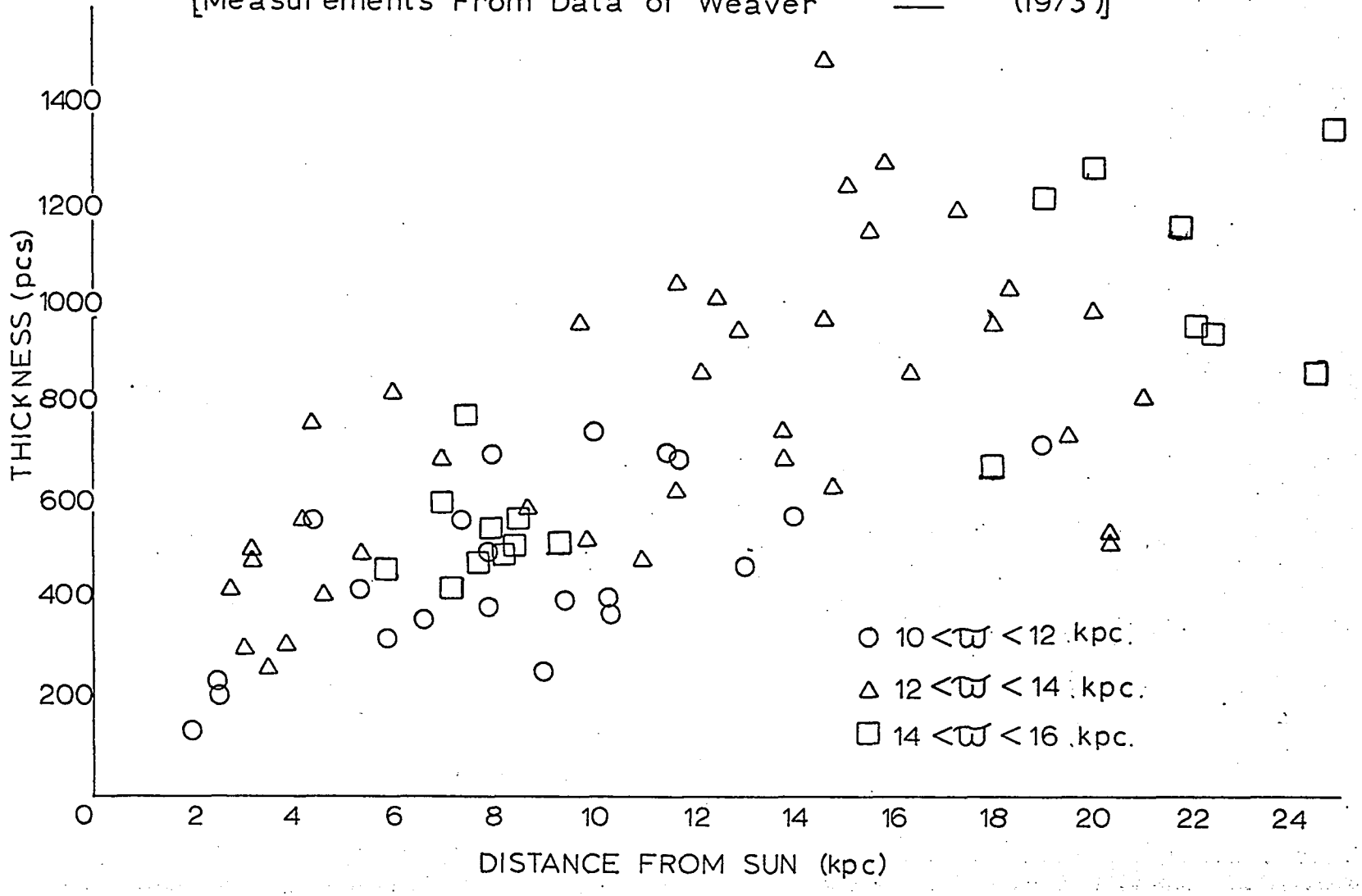

FIGURE 26

The increase in thickness of neutral hydrogen with distance from the sun, according to Henderson's integrated measurements. If this diagram is compared with the similar diagrams prepared from the data of Lozinskaya and Kardashev and that of Weaver, the large reduction in scatter made possible by using Henderson's integration technique rather than direct measurements of the half-intensity points is evident: there is virtually no overlap in measured thicknesses at points inside and outside the 12.5-kpc circle.

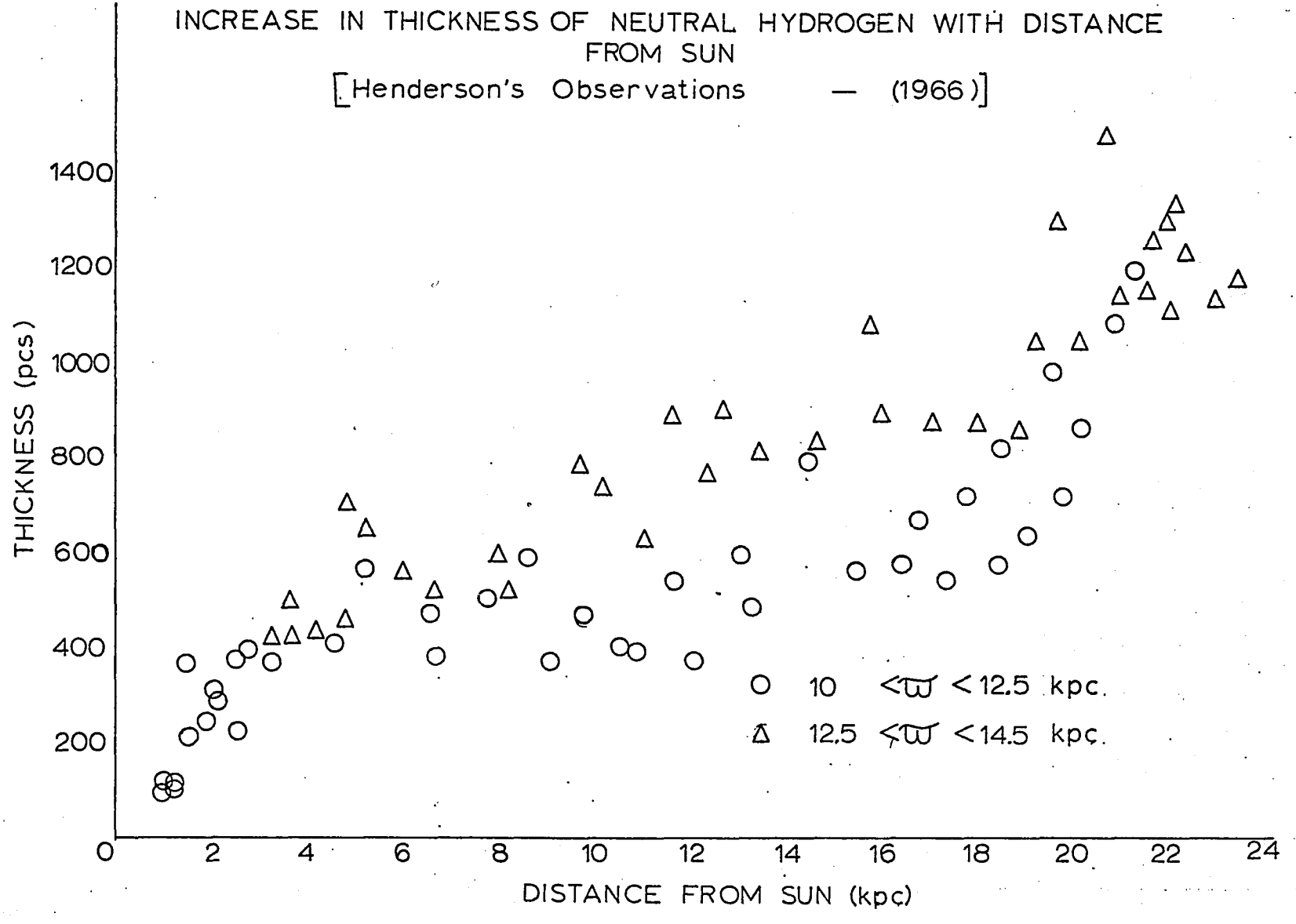
INCREASE IN THICKNESS OF NEUTRAL HYDROGEN WITH DISTANCE FROM SUN
[Henderson's Observations — (1966)]
THICKNESS (pcs)
1400
1200
1000
800
600
400
200
0
2
4
6
8
10
12
14
16
18
20
22
24
DISTANCE FROM SUN (kpc)
10 < w < 12.5 kpc.
12.5 < w < 14.5 kpc.

FIGURE 27A

Direct measurements of the full half-intensity thickness of the Galaxy as read directly from Henderson's 1966 observations. These measurements agreed with Henderson's integrated values almost exactly in their mean values, but the much larger scatter makes it impractical to attempt to find the "true" galactic thickness by means of extrapolation backward to $R = 0$ along lines of constant galactocentric radius. The average increase in thickness with distance from the sun is about 30 pcs/kpc. This leads to an increase of at least 200% by the time we reach a distance of 20 kpc from the sun.

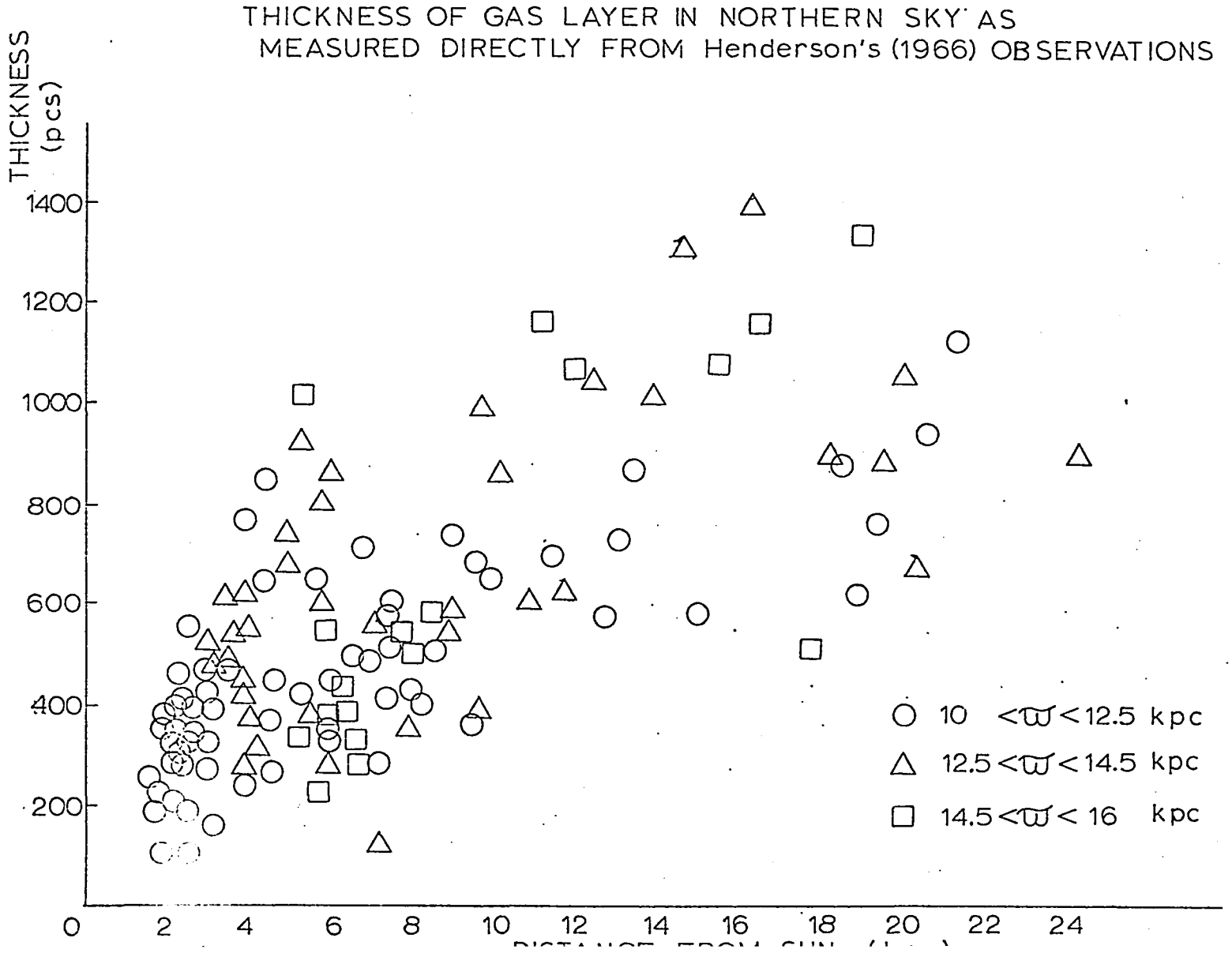
THICKNESS OF GAS LAYER IN NORTHERN SKY AS
MEASURED DIRECTLY FROM Henderson's (1966) OBSERVATIONS
THICKNESS
(pcs)
1400
1200
1000
800
600
400
200
0
2
4
6
8
10
12
14
16
18
20
22
24
10 <ϖ< 12.5 kpc
12.5 <ϖ< 14.5 kpc
14.5 <ϖ< 16 kpc

FIGURE 27B

More direct measurements of galactic thickness, this time from the Southern Sky observations of Kerr and Hindman & Kerr. Once again the enormous increase in thickness with distance from the sun is evident.

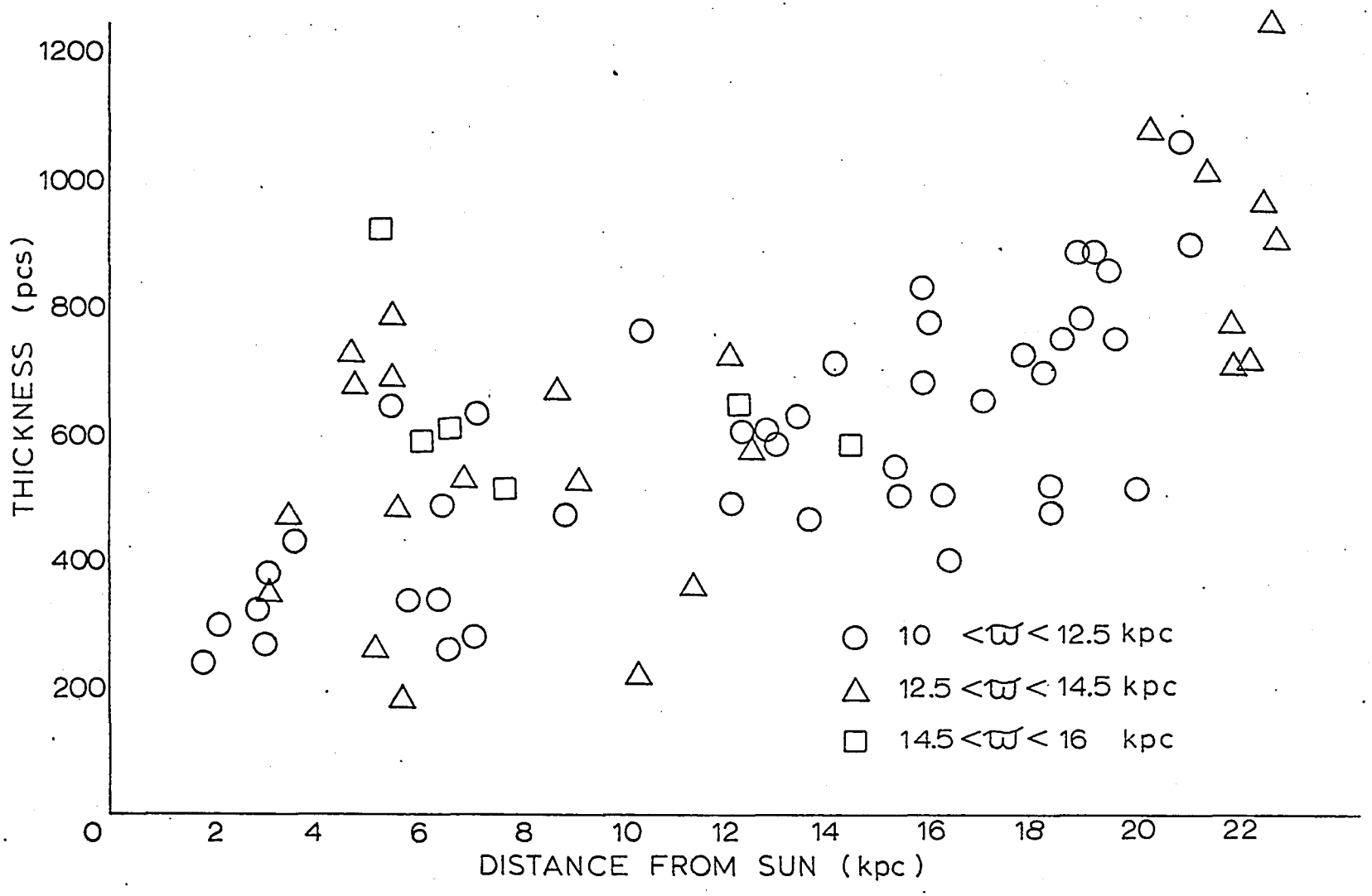
THICKNESS OF GAS LAYER IN S, SKY AS MEASURED DIRECTLY FROM:
Kerr (ℓ= 300°→343°)
Hindman and Kerr (ℓ= 190°→299°)
THICKNESS (pcs)
1200
1000
800
600
400
200
0
2
4
6
8
10
12
14
16
18
20
22
DISTANCE FROM SUN (kpc)
10 <ϖ< 12.5 kpc
12.5 <ϖ< 14.5 kpc
14.5 <ϖ< 16 kpc

FIGURE 28A

The huge increase in apparent thickness of the neutral hydrogen in the Galaxy is apparent in this contour-line diagram obtained from Henderson's integrated measurements of the thickness. Note that on the far side of the Galaxy, the thickness of the region between approximate galactic radii 10 and 14 kpc varies between 600 and 1200 pcs; but close to the sun the same region varies between about 200 and 400 pcs in thickness. Thus the increase in thickness between the near side and far side of the Galaxy is about threefold.

APPARENT THICKNESS OF GAS ACCORDING TO
MEASUREMENTS FROM DATA OF Henderson (1967)

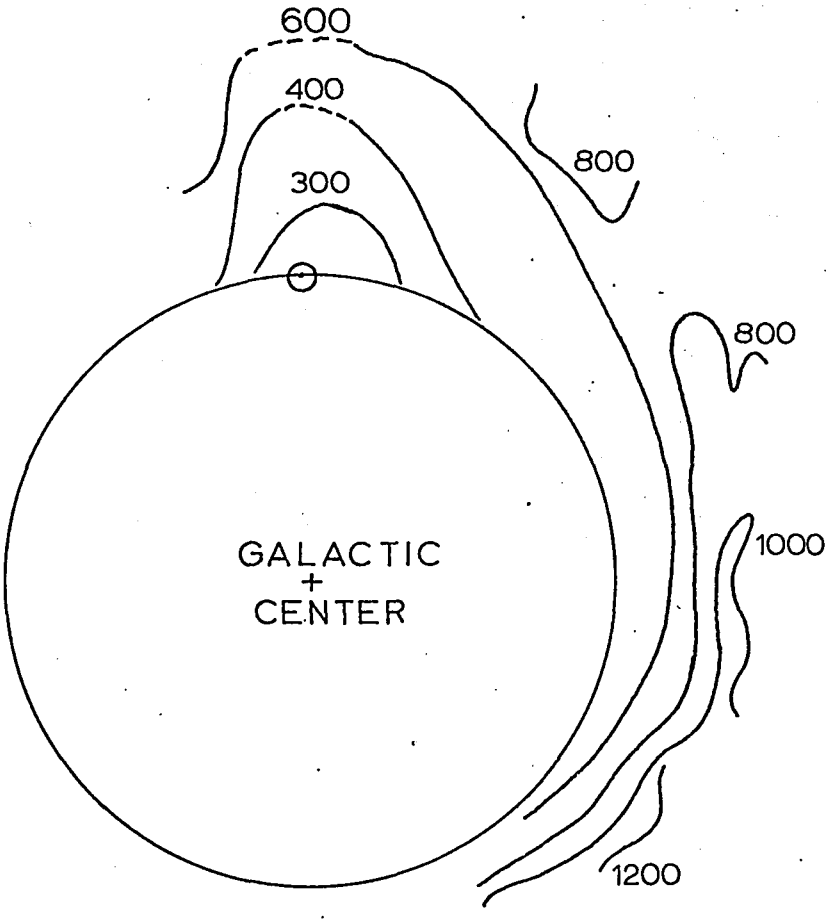

FIGURE 28B

The same diagram as the previous one, using least-square fits to Henderson's data.

APPARENT THICKNESS OF GAS ACCORDING TO LEAST-SQUARES FITS TO Henderson's INTEGRATED MEASUREMENTS (1967)

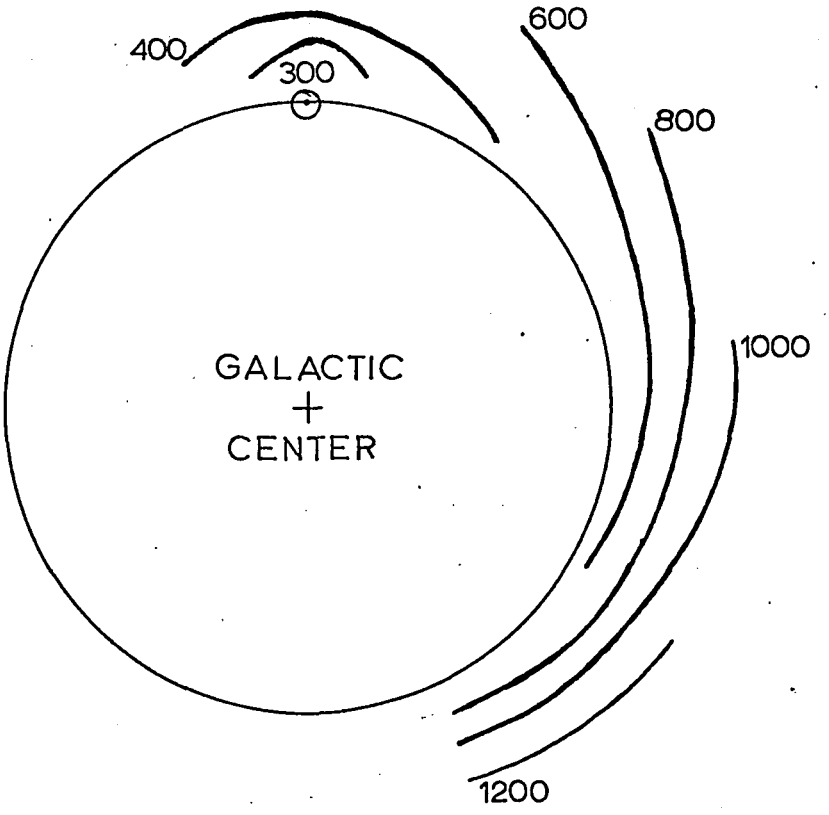

FIGURE 29A,B,C

The following three diagrams are sample least-square fits to the data on the thickness of the galaxy gathered by the studies of Lozinskaya and Kardashev (L&K), Milton and McGee (M&M), and Henderson (H). The measurements from the L&K and H studies were made on gas between 11.5 and 12.5 kpc from the center of the Galaxy; but because of the small number of points in the M&M study, all their measurements, made on gas between 11 and 17 kpc from the center, are included. Each study finds a linear increase in the thickness of between 20 and 40 pc/kpc. The thickness extrapolated to R = 0 is much larger (about 360 pcs) in the L&K and M&M studies than it is in the Henderson thesis (about 240 pcs). This is a consequence of the fact that Henderson's beam width was several times smaller than that available to the other investigators.

```
DD 10 DUMMY(60)
DD 11 DUMMY(133)
EXEC

EXECUTION
HERE ARE THE COEFFICIENTS OF THE DISCRETE LEAST SQUARES POLYNOMIAL OF DEGREE N= 1

388.821533

41.826050

LEAST SQUARES FIT TO MCGEE'S DATA ON THICKNESS OF GALACTIC NEUTRAL HYDROGEN

    Y   POLY1      Z       F    ERROR
  0.0   388.82
  0.50  409.73
  1.00  430.65
  1.50  451.56
  2.00  472.47
  2.50  493.39
  3.00  514.30   3.20  370.00  152.46
  3.50  535.21
  4.00  556.13
  4.50  577.04   4.60  680.00  -58.78
  5.00  597.95
  5.50  618.86   5.60  600.00  -23.05
                 5.90  673.00  234.41
  6.00  639.76
  6.50  660.69   6.60  570.00   94.87
  7.00  681.60
  7.50  702.52
                 7.80 1145.00  429.94
  8.00  723.43
  8.50  744.34   8.60  930.00  181.47
  9.00  765.26
                 9.40  560.00  201.99
  9.50  786.17
 10.00  807.08  10.20  620.00  155.45
 10.50  827.99
 11.00  848.91
 11.50  869.82  11.60 1250.00  370.00
 12.00  890.73  12.00 1075.00  179.27
                12.40  870.00  -37.40
 12.50  911.65
 13.00  932.56
                13.40  700.00 -249.25
 13.50  953.47
                13.60  850.00 -120.20
 14.00  974.39
 14.50  995.30
                14.90  910.00  162.03
 15.00 1016.21
 15.50 1037.13  15.50  810.00  247.13
 16.00 1058.04
 16.50 1078.95  16.70  500.00  587.32
 17.00 1099.86
 17.50 1120.78  17.70 1230.00  100.86
 18.00 1141.69
                18.30  950.00 -204.24
 18.50 1162.60
                18.60 1310.00  134.85
 19.00 1183.52  19.10 1340.00  152.30
 19.50 1204.43
 20.00 1225.34
 20.50 1246.26
 21.00 1267.17  21.00 1470.00  202.33
                21.40 1500.00  210.10
 21.50 1288.08  21.70 1310.00  106.45
 22.00 1308.99
 22.50 1329.91
 23.00 1350.82
 23.50 1371.73
 24.00 1392.65
 24.50 1413.56
 25.00 1434.47
STEP TIME WAS 000.13 SECONDS
```

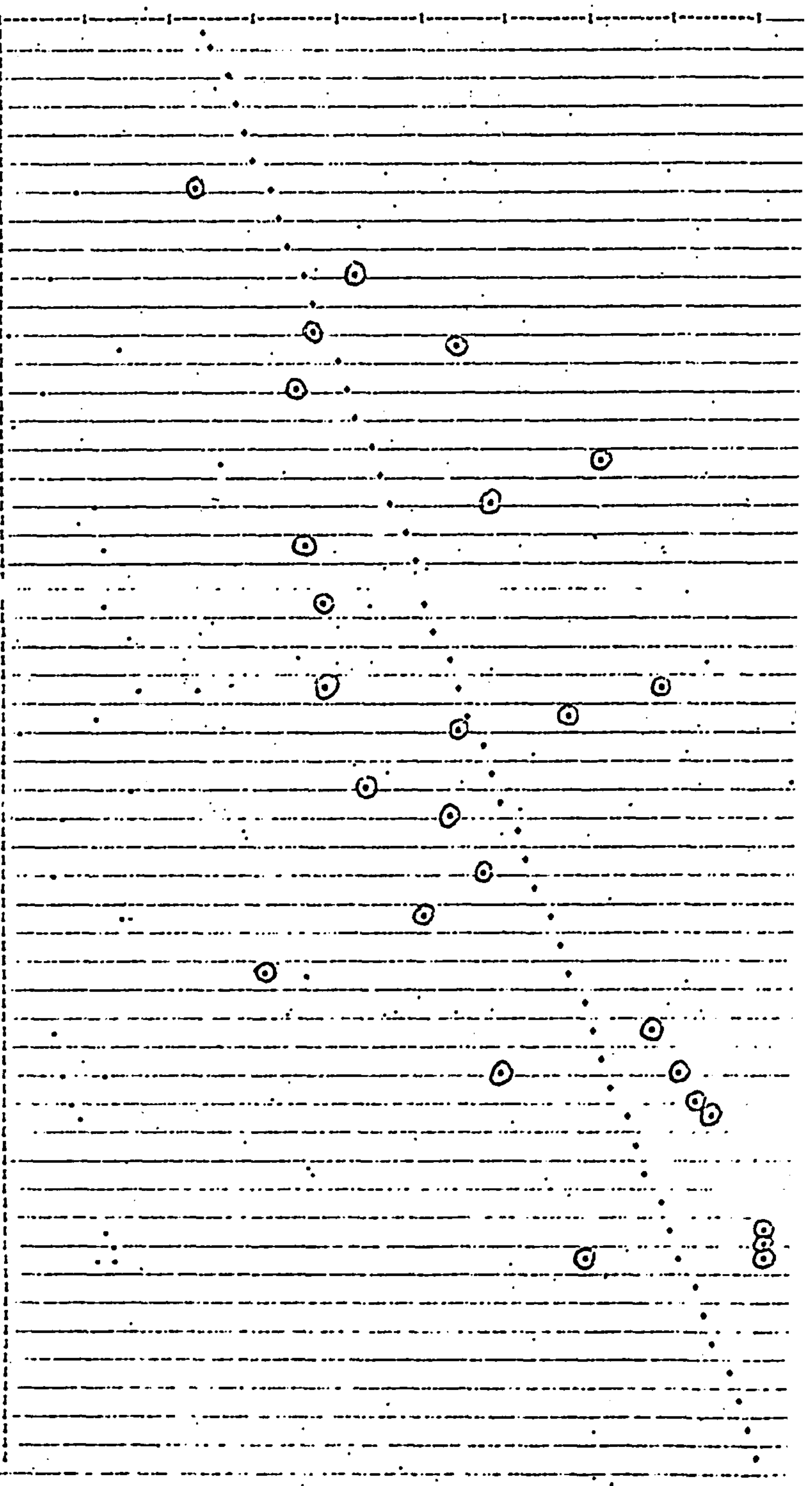

```
DO 16 CUMPY(6U)
DO 11 CUMPY(133)
CALC *
      EXECUTION
HERE ARE THE COEFFICIENTS OF THE DISCRETE LEAST SQUARES POLYNOMIAL OF DEGREE N= 1

 236.297656

 34.114487
```

LEAST SQUARES FIT TO HENDERSON'S DATA ON THICKNESS OF GALACTIC NEUTRAL HYDROGEN

X	PCLY1	Z	F	ERROR
0.0	236.30			
0.50	247.35			
1.00	264.41			
1.50	281.47			
2.00	298.53	2.47	227.00	87.561
2.50	315.58	2.75	395.00	70.891
3.00	332.64	3.26	363.00	21.491
3.50	349.70			
4.00	366.75			
4.50	383.81			
5.00	400.87	5.20	573.00	165.331
5.50	417.93			
6.00	434.98			
6.50	452.04	6.60	470.00	14.551
7.00	469.10			
7.50	486.15	7.00	707.00	210.611
8.00	503.21			
8.50	520.27	8.60	595.00	71.321
9.00	537.33			
9.50	554.38	9.80	475.00	89.621
10.00	571.44			
10.50	588.50	10.90	365.00	207.141
11.00	605.56			
11.50	622.61			
12.00	639.67			
12.50	656.73	12.80	375.00	262.961
13.00	673.79			
13.50	690.84	13.30	485.00	159.021
14.00	707.90			
14.50	724.96	14.50	800.00	75.041
15.00	742.01			
15.50	759.07			
16.00	776.13			
16.50	793.19	16.80	665.00	130.421
17.00	810.24			
17.50	827.30			
18.00	844.36			
18.50	861.41	18.50	820.00	41.411
19.00	878.47			
19.50	895.53	19.60	960.00	81.061
20.00	912.59	20.20	855.00	44.411
20.50	929.64			
21.00	946.70	20.90	1080.00	136.711
21.50	963.76	21.40	1195.00	234.651
22.00	980.82			
22.50	997.87			
23.00	1014.93			
23.50	1031.99			
24.00	1049.04			
24.50	1066.10			
25.00	1083.16			

```
STEP TIME 045 0000.13 SECONDS.
```

DD 10 DUMMY(8C)
DD 11 DUMMY(133)
ERRC -- 0

EXECUTION

HERE ARE THE COEFFICIENTS OF THE DISCRETE LEAST SQUARES POLYNOMIAL OF DEGREE N= 1

342.883789

20.762665

LEAST SQUARES FIT TO LOZINSKAYA DATA ON THICKNESS OF GALACTIC NEUTRAL HYDROGEN

X	POLY1	Z	F	ERROR
0.0	342.88			
0.50	353.46			
1.00	363.65			
1.50	374.03			
		1.90	310.00	72.333
2.00	384.41	2.10	360.00	-26.491
2.50	394.79	2.50	410.00	-15.211
		2.60	270.00	131.022
3.00	405.17			
3.50	415.55			
		3.90	460.00	30.149
4.00	425.93	4.20	840.00	409.611
4.50	436.32			
		4.80	320.00	122.561
5.00	446.70	5.10	370.00	-76.771
		5.30	430.00	22.931
5.50	457.08	5.50	470.00	12.921
		5.80	340.00	123.311
6.00	467.46			
6.50	477.84			
7.00	488.22			
7.50	498.60			
		7.80	530.00	25.171
8.00	508.99			
8.50	519.37			
9.00	529.75	9.10	520.00	11.821
9.50	540.13			
10.00	550.51			
11.00	571.27			
11.50	581.65			
12.00	592.04			
12.50	602.42			
13.00	612.80			
		13.30	900.00	280.971
13.50	623.18	13.50	1080.00	448.521
14.00	633.56			
14.50	643.94			
15.00	654.32			
15.50	664.71			
16.00	675.09			
16.50	685.47			
17.00	695.85			
17.50	706.23	17.70	810.00	106.381
18.00	716.61	18.00	620.00	96.611
		18.30	810.00	112.841
18.50	726.99			
19.00	737.37			
19.50	747.76			
20.00	758.14			
20.50	768.52			
21.00	778.90	21.20	400.00	383.651
21.50	789.28			
22.00	799.66			
22.50	810.04			
23.00	820.43			
23.50	830.81			
24.00	841.19			
24.50	851.57			
25.00	861.95			

STEP TIME WAS 0000.13 SECONDS.

CAUSES OF THE DISTANCE EFFECT

A number of candidates for the most probable cause of the distance effect can be enumerated. We shall list them briefly and then describe each in further detail.

1) Local high-velocity gas.
2) Excitation temperature lower on the opposite side of the galaxy.
3) Distance-velocity scale in error.
4) Measurable extinction of radio frequency radiation.
5) Connection with the deformation of the Galaxy.
6) Instrumental effects due to finite beam-widths or side-lobe radiation.
7) Multiplicity of sources of different half-widths.

Suggestion number 1) was made by Hindman, according to Milton and McGee (1963), numbers 2-4 are due to Henderson, number 5 to Lozinskaya and Kardashev, and numbers 6 and 7 to the present investigators.

1) Local high-velocity gas.

Local high-velocity gas would add a wide-latitude component to the distant gas observed at the same velocity and thus lead to a higher derived value of the thickness. Yet the observed linear increase of thickness over every longitude and a wide range of distances from the Sun leads to the requirement that there be carefully-graded amounts of local gas at almost every velocity! We may thus reject this possiblity.

2) Temperature lower on the far side of the Galaxy

It is apparent from all large-scale surveys of neutral hydrogen in the Galaxy that the antenna temperature decreases with increasing distance. The famous Dutch map of the density of hydrogen in the Galaxy (density is often determined directly from brightness temperature) shows this effect clearly. The temperature of the Perseus arm in Henderson's observations drops from 85°K to 40°K as the distance changes from 4 kpc to about 10 kpc. Such a decrease in peak temperature could lead to increased apparent thicknesses if the peaks were affected more than the wings of the profile. However, it is important to note that such a decrease in temperature and increase in measured thickness would also be expected from instrumental effects of the types to be discussed in sections 6) and 7) below. Moreover, it is difficult, if not impossible, to imagine a mechanism that would provide such an asymmetric and heliocentric temperature variation. Therefore we reject this explanation for the observed distance effect.

FIGURE 30

Four of the five spiral features shown here exhibit a decrease in brightness temperature with increasing distance from the sun. If the features are of approximately constant density for most of their lengths, the decrease in measured brightness temperature expected from beam-smoothing effects is not large enough to explain the observed decrease.

VARIATION OF MEASURED BRIGHTNESS TEMP. WITH DISTANCE FROM SUN

[From surveys by Henderson —(1966), Kerr-(1969), and Hindman and Kerr —(1969)]

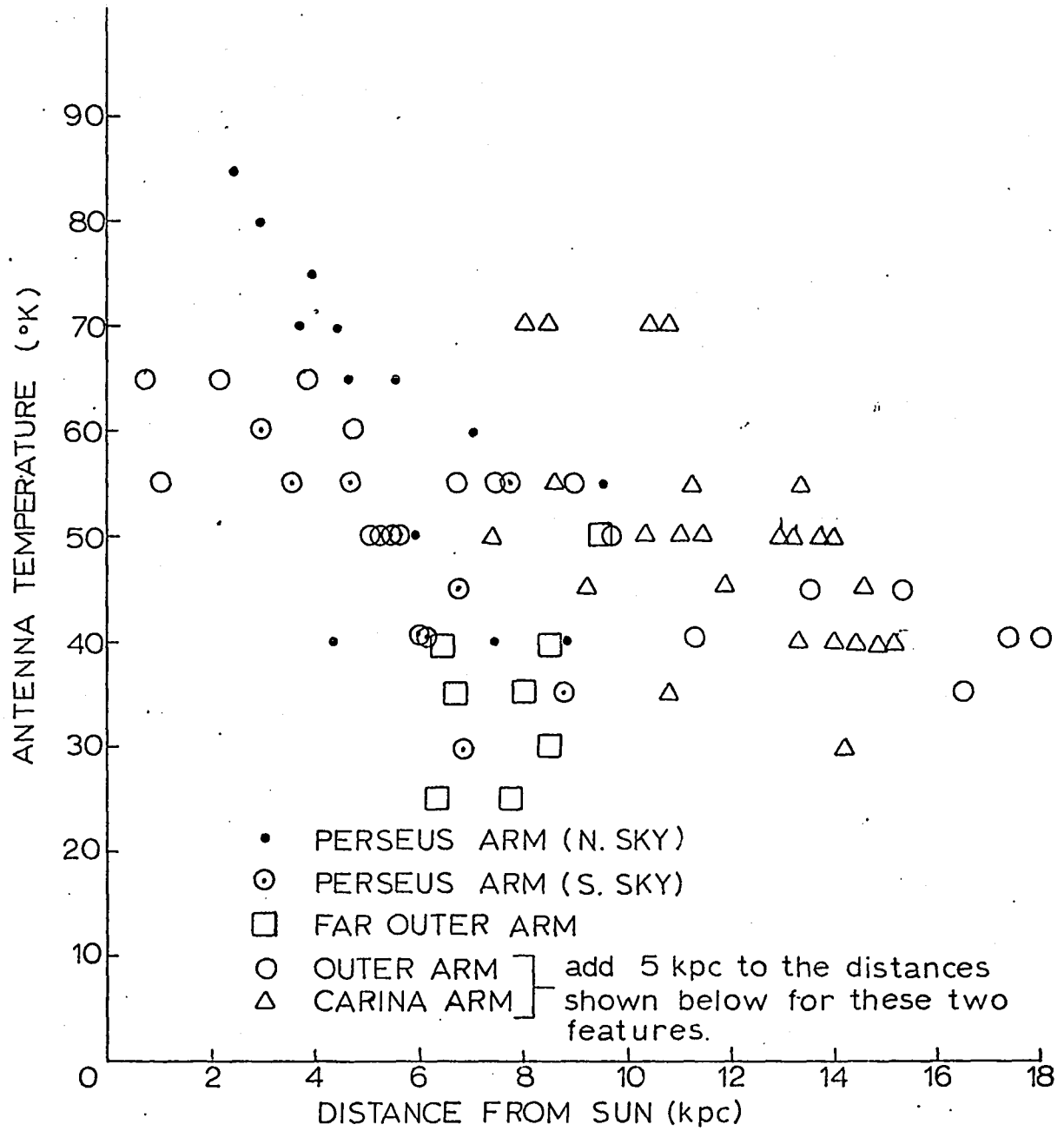

3) Distance-velocity scale in error

At first glance, this explanation seems quite attractive: since the thicknesses are based on estimated distances away from us, if the distances were too large, the thicknesses would be too large also. But the magnitude of the observed effect is far too large to be accounted for by this mechanism. To bring the value of 1500 pcs found for distant arms at low longitudes down to a more reasonable 500 pcs, the distance would have to be reduced from the presently-accepted value of about 20-25 kpc down to 7-8 kpc. This corresponds to a sun-center distance of about 3 kpc, which is ridiculous.

This qualitative argument was checked by a computer program which recalculated the thicknesses of the hydrogen on the basis of a sun-center distance of 8.2 kpc instead of the presently-accepted 10 kpc. The effect on a trailing outer spiral arm in the Northern Sky was to have its distance from the sun decreased at low longitudes and increased at higher ones, which is in the right general direction. But at still higher longitudes (greater than 90°) the effect was reversed. And in no case was the thickness increased by more than a few percent of the required amounts. Therefore we rule out this explanation.

4) Measurable extinction of radio frequency radiation

This suggestion, due to Henderson, is intriguing in that it is highly unexpected; it would represent a real challenge to theorists to determine the basis for such extinction. It provides an attractive way of explaining both the observed decrease in peak temperatures and the increase in thickness with increasing distance, since the extinction would act mainly on the peak temperatures of the profile and not affect the wings very much. There is even a nice parallel with the discovery of optical extinction by Trumpler, who found it by observing systematic increases in the diameters of star clusters with increasing distance.

However, a theoretical basis is lacking. The optical extinction curves show a steep decrease with increasing wavelength, such that radiation of radio wavelengths would show extinction capabilities many orders of magnitude below those shown by visible radiation. The mechanism suggested by Hoyle and Wickramasinghe--oscillations of dislocations in dust grains--appears to have been a one-sentence throwaway that has not received any further attention. Therefore, this explanation should be returned to only in time of greatest need; that is, upon the failure of all other explanations.

5) Connection with the deformation of the Galaxy

It appears that only in the data of Lozinskaya and Kardashev, the originators of this proposal, can information be found to support it. The measurements of Henderson, Milton and McGee, and the present investigators all show a definite connection with distance from the sun, and no correlation with the observed "flapping" mode of the Galaxy; these conclusions were originally obtained by eye estimate and checked by least-squares analysis of the variation of thickness with galactocentric longitude. Even L&K's data, as mentioned previously, show a considerable asymmetry with respect to the maximum deformation, points at equidistant longitudes on both sides having different values of thickness with the more distant point invariably the larger thickness. Thus it appears that this explanation can be rejected as unsupported by the data.

6 & 7) The effects of finite beam widths, error beams, and multiplicity of sources on measured brightness temperatures

We consider here whether the observed increase in thickness of the spiral arms with distance from the sun can be explained in terms of errors introduced by 1) the finite beam width of the telescope, (which produces a decrease of the peak temperature and an increase of the temperature near the wings of the profile and thus an increase in apparent half-width), 2) an "error beam" such as may be produced by irregularities in the surface of the dish, (which will also lead to smoothing and widening of the profile in most cases), and 3) blending of Gaussian components by the telescope, so that the half-width of the combined profile may be considerably different from the half-width of one of the components.

Finite Beam Width. Let the sky brightness temperature near (l_o, b_o) vary as

$$T_b(l,b) = T_{bo}\, g(l-l_o)\, h(b-b_o)$$

Then the temperature measured by the telescope will be

$$T_A = T_{bo} \frac{\iint g(l-l_o)\, h(b-b_o)\, f(l-l_1, b-b_1)\, d\Omega}{\iint f(l-l_1, b-b_1)\, d\Omega}$$

where $f(l-l_1, b-b_1)$ is the antenna distribution pattern when the telescope is pointed in the direction (l_1, b_1). In many cases, $f(l-l_1, b-b_1)$ is a Gaussian:

$$f(l-l_1, b-b_1) = e^{\frac{-\left[(l-l_1)^2 + (b-b_1)^2\right]}{2\sigma_{Tel}^2}}$$

where σ_{Tel} is related to the half-power beam width (HPBW) as

$$\sigma_{Tel} = \frac{HPBW}{2\sqrt{2\ln 2}}$$

follows:

$$\sigma_{Tel} = \frac{HPBW}{2\sqrt{2\ln 2}}$$

Let us further suppose that the sky brightness temperature is Gaussian:

$$T_b(l,b) = T_{b_0}\, e^{\frac{-(b-b_0)^2}{2\sigma_b^2}}\, e^{\frac{-(l-l_0)^2}{2\sigma_l^2}}$$

where σ_b and σ_l represent the variations in latitude and longitude, respectively, of the source. (For example, for a spherical cloud, $\sigma_b = \sigma_l$; but for a spiral arm, which varies much more slowly in longitude than in latitude, $\sigma_b \ll \sigma_l$.)

Carrying out the indicated integration, we arrive at the expression for the measured brightness temperature T_A of a Gaussian source centered at (l_o, b_o):

$$T_A(l,b) = T_{b_0}\, f_b\, f_l\, e^{\frac{-(b-b_0)^2}{2(\sigma_b^2+\sigma_{Tel}^2)}}\, e^{\frac{-(l-l_0)^2}{2(\sigma_l^2+\sigma_{Tel}^2)}}$$

where

$$f_b = \left[1 + \frac{\sigma_{Tel}^2}{\sigma_b^2}\right]^{-1/2}, \quad f_l = \left[1 + \frac{\sigma_{Tel}^2}{\sigma_l^2}\right]^{-1/2}$$

Setting $(l,b) = (l_o, b_o)$, we see that the measured brightness temperature at maximum is less than the true temperature by the factor $f_b \cdot f_l$. For example, in the case of a spiral arm which is nearly uniform in longitude $(\sigma_l \gg \sigma_{Tel})$ the measured temperature will be low by a factor of 2 when the arm is far enough away so that its angular size equals the beam width of the telescope. We might pause here to point out that the angular size of a typical spiral arm at a distance of 10 kpc is roughly 1.5°, which is already comparable with the HPBW of a 25-meter telescope--so the effect is certainly not insignificant.

The thickness of the source as measured by the telescope is $W_M = 2(b_o - b_{\frac{1}{2}})$, where $b_{\frac{1}{2}}$ is given by:

$$\exp\left[-\frac{(b_o - b_{1/2})^2}{2(\sigma_b^2 + \sigma_{Tel}^2)}\right] = \frac{1}{2}$$

Solving this equation, we find that the measured thickness W_M exceeds the true thickness W ($\equiv 2\sqrt{2\log 2}\,\sigma_b$) by the factor f_b:

$$W_m = \frac{W}{f_b} = 2\sqrt{2\log 2}\,\sigma_b \sqrt{1 + \frac{\sigma_{Tel}^2}{\sigma_b^2}}$$

To see what these equations mean in terms of telescopes operating today, we tabulate the ratio of the measured thickness W_M to the true thickness W as a function of the ratio of the telescope beam width σ_{Tel} to the source width σ_b. (We are here ignoring the variation in longitude, which may be permissible when considering spiral arms but is less defensible if the source considered were a single cloud.) Choosing a value of the thickness of the gas layer of 236 pcs (corresponding to σ_b = 100 pcs) allows us to calculate the distances R at which a telescope of given beamwidth will overestimate the true thickness by a specified amount. In columns 3 and 4 of Table XIII we calculate R for the case of two telescopes, one with beam width 12' (corresponding to the Green Bank 300-foot telescope) and the other with beam width 2° (roughly the beam width of the telescopes at Leiden, the Crimea, and Australia.) The table makes it clear that the beam-smoothing effect alone could account for an error of over 300% in the measured thickness of an arm 21 kpc away, in the case of a telescope of 2° beam width. This effect, if not properly taken into account, could

explain a large portion of the tremendous increase in thickness (300-500%) found by Lozinskaya and Kardashev (1963) and Milton and McGee (1963).

However, the 300-foot telescope is another matter. Given our assumptions--that the arm can be represented as a single Gaussian and that the true beam width is the theoretical one of 10'--then the maximum overestimate for the thickness of a distant arm would be less than 5%.

Therefore, for the present idealized case, we come to the conclusion that the observed increase in thickness of the galactic disk with distance from the sun cannot be explained as the result of beam-smoothing alone, although the error from this effect may be sizable in the surveys done by the smaller radio telescopes.

Error beam. The previous discussion applies in the idealized case of a telescope with a single perfect Gaussian beam. In fact, however, the observations taken with the 300-foot telescope in the period 1966-1970 were seriously affected by widespread irregularities in its surface caused by workmen continually traversing the dish. The actual antenna pattern has been discussed by Harten (1969), who finds that it can be well represented by an 11-minute main beam and two error beams of 2° and 6° widths. About half the total power received by the antenna is due to the error beam. What effect will this have on the measurement of the thickness of a spiral arm,

Harten states that the power level response of the antenna to the 2° and 6° beams is 24 and 33 decibels, respectively. This is sufficient information to allow us to write down the complete antenna pattern:

$$f(\theta,\varphi) = \sum_{i=1}^{3} A_i \, e^{\frac{-(\theta^2+\varphi^2)}{2\sigma_i^2}}$$

where θ and φ are measured away from the direction in which the antenna is facing. The σ_i's are proportional to the HPBW's of the main beam and the two error beams; and the A_i's obey the following relations:

$$\sum A_i = 1 \qquad A_2 = 10^{-2.4} \qquad A_3 = 10^{-3.3}$$

Once again the antenna temperature is given by the convolution of the actual brightness temperature distribution by the antenna pattern:

$$T_A = \frac{\int_{4\pi} T_b(\theta,\varphi) f(\theta,\varphi)\, d\Omega}{\int_{4\pi} f(\theta,\varphi)\, d\Omega}$$

Since the error beams are circularly Gaussian, we can without loss of generality make the transformation

$$(\theta, \phi) \longrightarrow (l - l_1, b - b_1)$$

where (l_1, b_1) are the coordinates giving the direction in which the antenna is facing.

Finally, we can let the actual brightness temperature distribution be represented by a sum of products of Gaussians:

$$T_b(l,b) = \sum_j T_j \, e^{-\frac{(l-l_{oj})^2}{2\sigma_{lj}^2}} \, e^{-\frac{(b-b_{oj})^2}{2\sigma_{bj}^2}}$$

where l_{oj} and b_{oj} represent the location of the source; and σ_{lj} and σ_{bj} determine its angular extent.

At least three major classes of sources can be recognized: single clouds, of radius 5-30 pcs; spiral arms, of thickness 200-300 pcs and considerably greater extension in longitude; and an "envelope" component, which may account for the extensions to high latitudes of the spiral arms noticed by Schmidt, Kepner, Oort, and Shane, and whose thickness may be taken as 600-700 pcs, following Shane and Falgarone and Lequeux (1973). This last component is characterized by high dispersion velocities and may be tentatively identified with the hot intercloud medium. (See Takakubo, (1967)) In the case of the nearly spherical clouds, $\sigma_b \sim \sigma_l$; but in the other two cases, $\sigma_b \ll \sigma_l$. The relative contribution of each of these components to the observed brightness temperature is uncertain. Shane suggests a density in the plane of his "envelope" of about 0.05 atoms/cm^3, or about 5-10% the density of the main gaseous component. On the other hand, Falgarone and Lequeux suggest 0.15 atoms/cm^3 for their thick component, and only 0.29 for the main component; a ratio of 50% or almost an order of magnitude larger than Shane's estimate. The clouds

are at lower temperatures and higher optical depths, and may contribute half of the observed brightness temperature within a spiral arm. Both the arms and the envelope may be considered centered on the plane, while the clouds are concentrated in a region probably less than 200 pcs thick.

With this short discussion of the physical characteristics of the sources of interest, we can try to determine what the antenna temperature will be for a telescope of the characteristics described above and a medium made up of the three classes of sources described. Since the arms and envelope are centered on the plane, and the clouds are concentrated toward that same plane, we may consider the case in which all three components are centered at (l_o, b_o). In this case, the antenna temperature will be

$$T_A = \frac{\sum_i \sum_j A_i T_j \int e^{-\frac{(b-b_i)^2}{2\sigma_i^2}} e^{-\frac{(b-b_o)^2}{2\sigma_{bj}^2}} db \int e^{\frac{-(l-l_i)^2}{2\sigma_i^2}} e^{\frac{-(l-l_o)^2}{2\sigma_{lj}^2}}}{2\pi \sum_i A_i \sigma_i^2}$$

$$= \frac{\sum_i \sum_j A_i \sigma_i^2 T_j (1+g_{ij}^2)^{-\frac{1}{2}} (1+h_{ij}^2)^{-\frac{1}{2}} e^{\frac{-(l_i-l_o)^2}{2(\sigma_i^2+\sigma_{lj}^2)}} e^{\frac{-(b_i-b_o)^2}{2(\sigma_i^2+\sigma_{bj}^2)}}}{\sum A_i \sigma_i^2}$$

where g_{ij} and h_{ij} are the ratios of the telescope beam widths to the source widths in latitude and longitude, respectively:

$$g_{ij} = \frac{\sigma_i}{\sigma_{bj}} \quad , \quad h_{ij} = \frac{\sigma_i}{\sigma_{lj}}$$

Since we are interested in the half-width in latitude at constant longitude, the exponential variation in l can be ignored. Then T_{Amax} will be proportional to

$$\sum_i \sum_j A_i T_j \sigma_i^2 (1+g_{ij}^2)^{-\frac{1}{2}} (1+h_{ij}^2)^{-\frac{1}{2}}$$

and the half-width in latitude $b_{\frac{1}{2}}$ will be the solution to

$$\frac{1}{2} = \frac{\sum_i \sum_j A_i \sigma_i^2 T_j (1+g_{ij}^2)^{-1/2} (1+h_{ij}^2)^{-\frac{1}{2}} e^{\frac{-(b_{1/2}-b_0)^2}{2(\sigma_i^2+\sigma_{bj}^2)}}}{\sum_i \sum_j A_i \sigma_i^2 (1+g_{ij}^2)^{-1/2} (1+h_{ij}^2)^{-1/2}}$$

Effects of the error beam: single source. We first consider how the thickness measurements of the telescope are affected by the error beam in the case of a siggle source; e.g., a spiral arm of about 300 pcs thickness. Fig. 31 displays the variation with distance of the measured thickness of such a source, as it would be found by telescopes of beamwidth 2^o (corresponding to the instrument used by Milton and McGee); 80' (the average beamwidth of the instrument used by Lozinskaya and Kardashev); 11' (the theoretical beam width of the 300-foot telescope); and finally, a model of the actual 300-foot telescope as described by Harten, with an 11' main beam collecting about half the total power and a 2^o and 6^o error beam.
It is interesting to note that the effect of the error beam was not simply to increase the error in a roughly monotonic way; rather, the error wazs increased rapidly for the smaller distances, ($R < 10$kpc) but then was actually reduced for the larger distances ($R < 25$kpc). The amount of the error (10-20%), while five or six times the error of a few percent expected from the theoretical 11' beam, still falls far short of the 100-200% error that seems to be demanded by the observations.

FIGURE 31

The error due to finite beamwidths in measuring the thickness of a single Gaussian source. The curves marked 10' and 6° correspond to the errors (in measuring thickness of a 300-pc source at the distances from the sun displayed on the horizontal axis) made by perfect telescopes of those beamwidths. The curve marked $2^{\circ} + 6^{\circ} + 10'$ corresponds to the actual pattern of the 300' telescope, according to the description of Harten and co-workers. The effect of the error beam is to vastly increase the error associated with distances of less than 10 kpc, but then to level off. The error throughout most of the region of interest ($R < 25$ kpc) lies between eight and twelve percent.

% ERRORS (DUE TO ANTENNA SMOOTHING) IN MEASURING THICKNESS OF GALACTIC NEUTRAL HYDROGEN FOR A TELESCOPE WITH A HPBW OF 10' AND AN "ERROR BEAM" HPBW OF 6° AS A FUNCTION OF DISTANCE

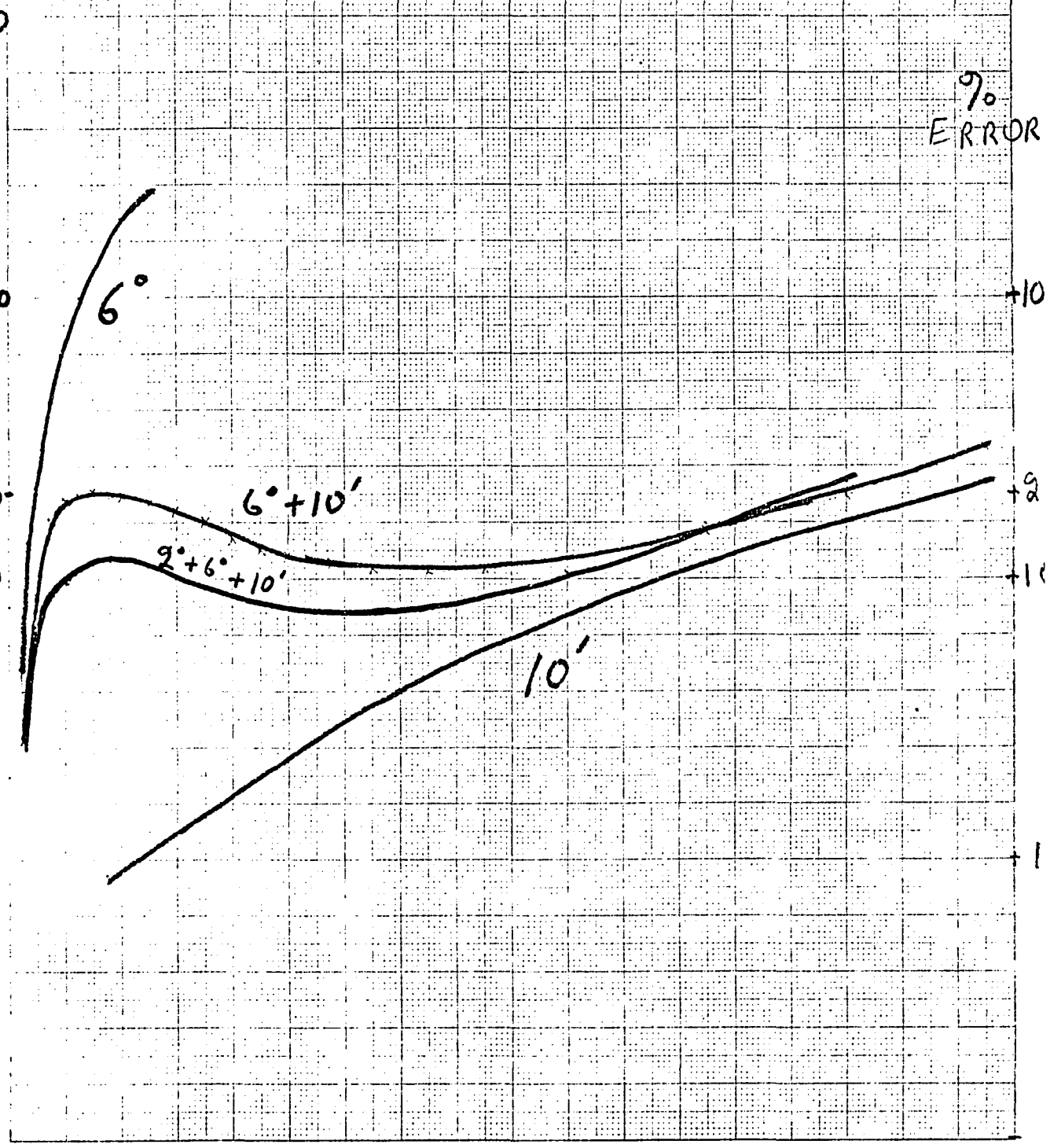

FIGURE 31A

The curve represents the error due to beam-smoothing effects for a radio telescope with the antenna characteristics of the 300-foot radio telescope at Green Bank (i.e., a 10-minute beam with a 2-degree and 6-degree error beam as described by Harten) for a spiral arm located at various distances from the sun, and having its brightness temperature distributed in the vertical direction as a perfect Gaussian in the latitude b. The crosses represent measurements of the thickness of a more realistic (non-Gaussian) spiral arm density distribution, taken from a map produced by a computer program that imitated the reception characteristics of the 300-foot telscope. Different crosses at the same distance from the sun represent different choices of the following parameters: no systematic motion versus a systematic motion of 8 km/sec, and a flat versus a distorted galactic plane. Results indicate that the thickness error due to beam-smoothing effects is insensitive to the non-Gaussian distribution of brightness temperature due to these parameters; therefore the observed thickness overestimate of several hundred percent cannot be due to these factors.

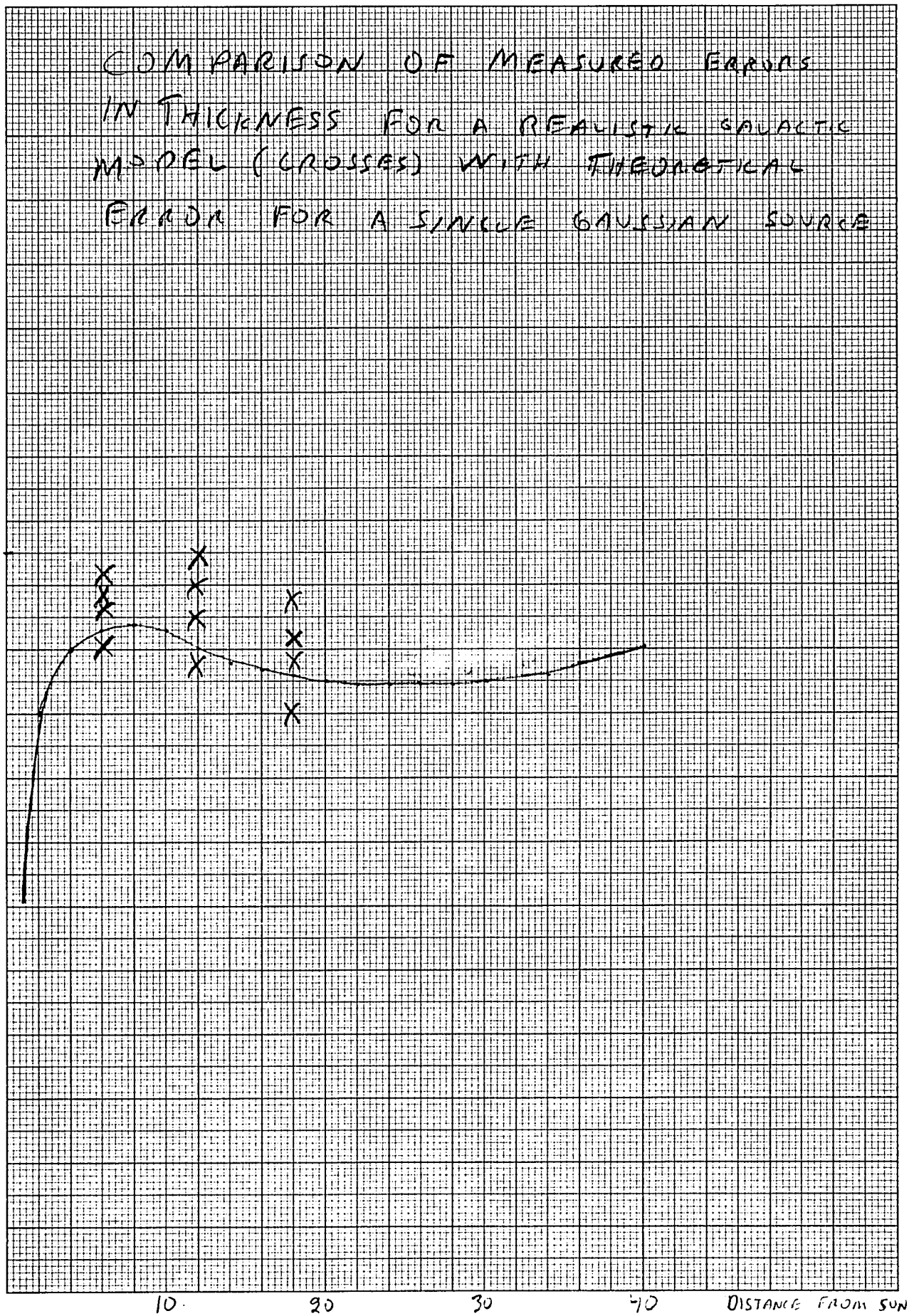

FIGURE 32

The curve shows the theoretical overestimates of the galactic thickness caused by measuring the half-intensity width in brightness temperature T_b rather than in optical depth τ, assuming that τ behaves as a Gaussian in the latitude b. Individual points mark the overestimates of the thickness made from actual measurements of brightness-temperature contour maps prepared by a computer in a numerical simulation of the galactic distribution of hydrogen.

OVERESTIMATE IN THICKNESS CAUSED BY USING T_b INSTEAD OF τ

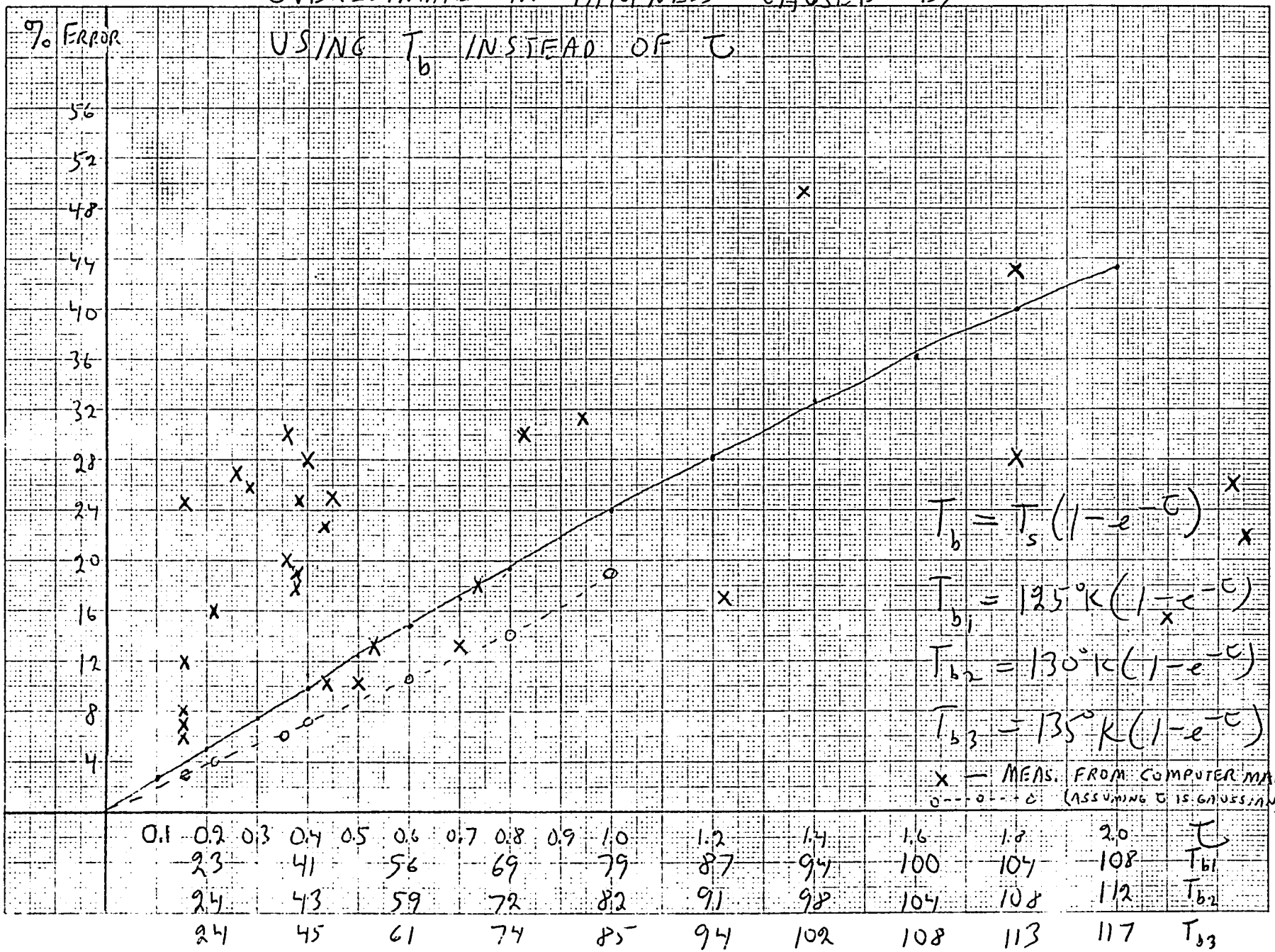

τ	0.1	0.2	0.3	0.4	0.5	0.6	0.7	0.8	0.9	1.0	1.2	1.4	1.6	1.8	2.0
T_{b1}		23		41		56		69		79	87	94	100	104	108
T_{b2}		24		43		59		72		82	91	98	104	108	112
T_{b3}		24		45		61		74		85	94	102	108	113	117

We conclude that the observed distance effect cannot be explained as simply due to the error beam of the 300-foot telescope, at least as long as we represent the spiral arm as a single Gaussian source.

Effects of Multiple Sources. However, as mentioned above, the choice of a single Gaussian source to represent the spiral arm is a poor approximation to reality. Every observer has emphasized the rather discrete, cloudy, patchy nature of the interstellar medium. Henderson's observations of nearby spiral arms show that a given spiral arm normally has several peaks, as though clouds of about 1/10 the thickness of the spiral arm were stacked vertically. What effect would such small, possibly quite intense, sources as superimposed on a more smoothly-varying background have on the measured thickness of the arm?

Simplifying the situation somewhat, we can ask what effect a single cloud of 20pc diameter and located at the center of a smoothly-varying component of 200pc thickness would have on the measured thickness of the arm? (Here we speak of the arm as the sum of the small intense cloud and the other component, which may be a blend of other clouds and the intercloud medium.)

Since we are not sure of the relative proportions of the intensity contributed by the cloud and by the arm, other component, we treat this as a parameter and study the effect of increasing the relative contribution of cloud from 0 to 1 in steps of 0.1. The results are given in Fig. 33. Once again it seems clear that the error is insufficient to explain the observations.

But one more ingredient remains to be added to the pot: the observed "envelope" of two or three times the thickness of the arm. Adding this in the proportions suggested by Falgarone and Lequeux (i.e., the width being 2-3 times that of the arm, with a central density at the plane of about $\frac{1}{2}$ that of the arm) and again treating the contribution of the cloud to the brightness temperature as a parameter, we arrive at the results summarized in Fig. 33.

The three top curves correspond to a two-component medium (no single clouds), with one component of thickness 200 pcs and the other of thickness 600 pcs, and the relative strengths varying from 5:5 (equal densities in the plane) to 7:3. (Thus straddling the value suggested by Falgarone and Lequeux of 2:1.) Although some rather large overestimates (nearly 100%) of the thickness of the thin component can be achieved, the variation with distance is not as it should be (dashed line).

The three bottom curves correspond to a three-component medium, with the arm-envelope ratio constant at 2:1 and with the proportion of the brightness temperature contributed by the single cloud ranging from 0.1 to 0.4. The behavior is qualitatively similar.

FIGURE 33

Effect of multiple sources and of a telescope with an error beam on measuring thicknesses of the sources.
Top three lines: Thickness overestimate caused by a source of 600 pcs thickness combined with a source of about 300 pcs thickness. The ratio shows the strength of the 300-pc source compared to that of the 600-pc source. The ratio suggested by Falgarone and Lequeux (about 6.6:3.4) would lie between the second and third lines from the top.
Bottom three lines: The effect of adding a small intense source of about 20-30 pc radius, such as a cloud.

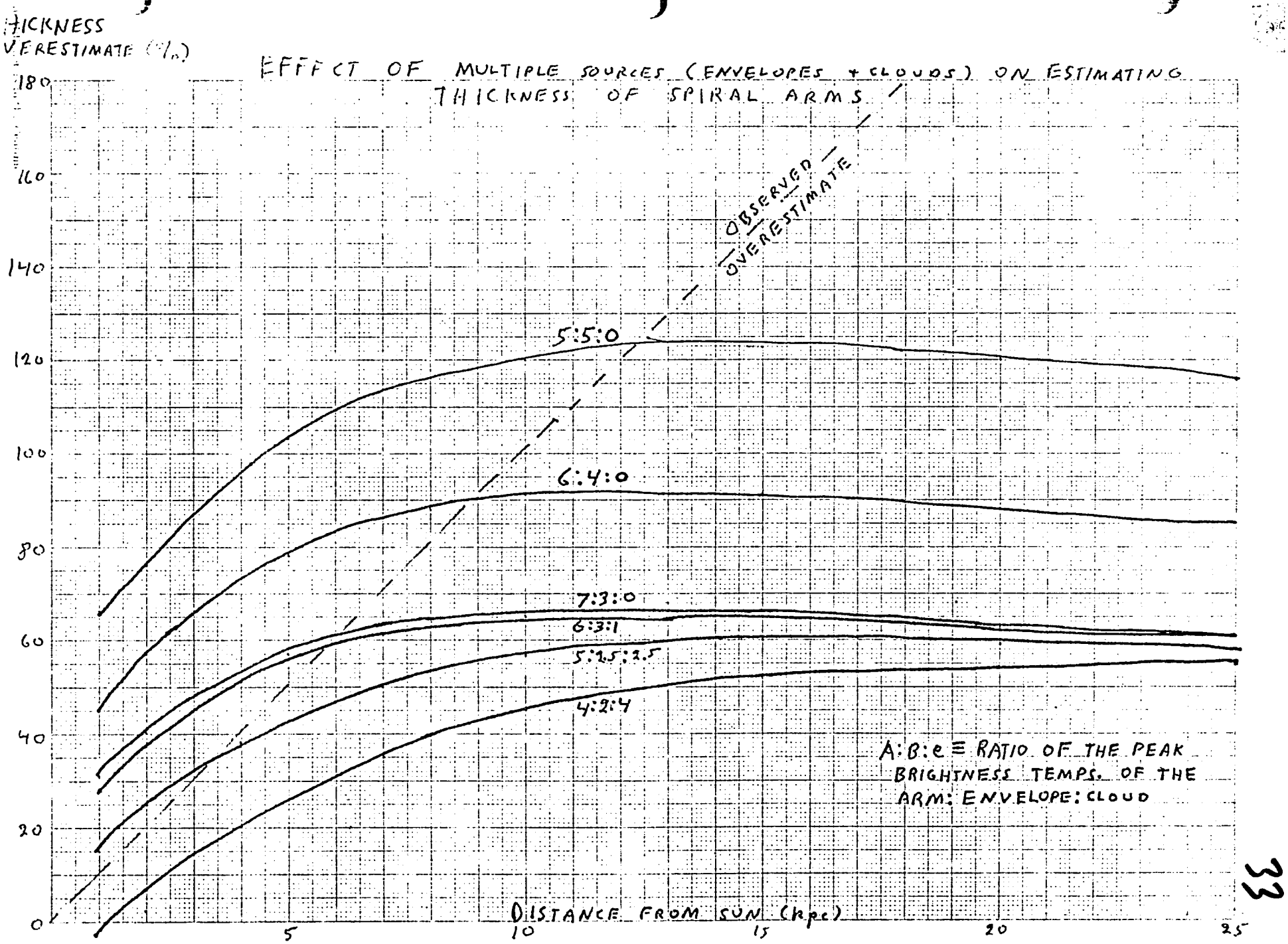
THICKNESS OVERESTIMATE (%)
EFFECT OF MULTIPLE SOURCES (ENVELOPES + CLOUDS) ON ESTIMATING THICKNESS OF SPIRAL ARMS
OBSERVED / OVERESTIMATE
5:5:0
6:4:0
7:3:0
6:3:1
5:2.5:2.5
4:2:4
A:B:e ≡ RATIO OF THE PEAK BRIGHTNESS TEMPS. OF THE ARM: ENVELOPE: CLOUD
DISTANCE FROM SUN (kpc)
180
160
140
120
100
80
60
40
20
0
5
10
15
20
25

We conclude that the present model of the interstellar medium is incapable of reproducing the observed distance effect, although the actual amounts of the overestimates in thickness produced by multiple sources are larger by far than the amounts produced by alternative proposals.

STUDIES ON THE THICKNESS OF THE GASEOUS LAYER: INNER DISK

A study of the thickness of the region interior to the Sun could be useful in eliminating some of the explanations advanced above for the existence of the distance effect observed in the outer parts of the Galaxy. For example, if we could show conclusively that no distance effect is observable in the inner regions, this would be strong prima facie evidence against many of those explanations that depend on a true physical distance effect (extinction) or on the arguments from instrumental limitations (finite beamwidths, error beams, inadequate correction for multiplicity of sources). On the other hand, if the distance effect is also observable in the inner regions, then the arguments connecting it with the deformation of the Galaxy or with different physical conditions at different longitudes can be discarded. In either case, the number of possibilities is reduced.

However, the thickness of the hydrogen layer in the inner regions is far more difficult to determine unambiguously than that in the outer part, for two reasons. The first is the distance ambiguity: the brightness temperature observed at any given velocity has been built up by contributions from two more or less widely separated regions (the "near" and "far" regions) along the line of sight. Unless one region has contributed a negligible amount of the total optical depth, the "thickness" determined from measuring the half-intensity width will be completely meaningless. Secondly, the optical depth is much larger in the inner regions; brightness temper-

atures of 100-125°K are common, as opposed to the 50-80°K temperatures normally encountered in the outer regions. Thus the practice of using T_b instead of the optical depth τ to determine the thickness leads to considerable errors, on the order of 25-100%. Moreover, the errors cannot be reliably corrected by using the relationship

$$T_b = T_s (1 - e^{-\tau})$$

since the spin temperature T_s of the hydrogen is not known suffieiently well to allow us to solve for τ!

Several ways out of these difficulties have been proposed: In his now-classic series of papers outlining the spiral structure of the Galaxy for the first time, Schmidt proposed avoiding the difficulty of separating the near and far components of the gas by measuring the thickness only at tangent points. That is, he measured the thickness only at points of maximum velocity; if the velocity is perfectly circular, this corresponds to the point of closest approach to the center of the Galaxy along the particular longitude chosen. The distance of this point is simply $\varpi_\odot \cos l$, where $\varpi_\odot$ is the distance from the Sun to the galactic center. This distance does not depend on any assumed velocity model (except that the velocity must be circular.) Using the then-accepted value of 8.2 kpc for $\varpi_\odot$, Schmidt found quite constant values for the thickness averaging 220 pcs. (The current value of 10kpc for $\varpi_\odot$ gives a thickness of 276pcs.)

(We note parenthetically that Schmidt was not able to avoid the second of the two difficulties mentioned above: in

fact, he has chosen the worst possible regions on this account, because the tangent points are precisely the points at which the highest optical depths and brightness temperatures are obtained. This is beaause the telescope is integrating the contributions of hydrogen at a particular velocity over a very long path. Thus, determining the precise value of the optical depth τ becomes essential to determine the proper correction to make in order to achieve the correct thickness. Schmidt chose a value of 125^{o} for the average (harmonic) temperature of the hydrogen. If this value is underestimated, the optical depth will be overestimated and the true thickness will be larger than calculated; and vice versa. Thus the absolute value of Schmidt's value for the thickness cannot be completely trusted. However, we are more concerned here with whether his values show the distance effect observed in the outer regions.)

Fig. 34 shows Schmidt's actual observed points (adjusted to the current value of 10kpc for ω_{o}). We note that they show no indication of a distance effect. However, it is clear from this diagram that Schmidt's points are concentrated in a very small distance range of between 7 and 9.5 kpc--<u>if there were a distance effect in the inner regions, these observations would never reveal it</u>, because the region observed has too small an extent.

FIGURE 34

The thickness of galactic hydrogen interior to the sun. Dashed line: best fit to Henderson's 1967 measurements. The slope is about 20 pcs/kpc. Dash-dot line: best fit to my own measurements from Henderson's 1966 observations. The slope is virtually zero. Dotted circles: Schmidt's 1957 measurements, corrected to present values for the sun-galactic center distance of 10 kpc. Again the slope is zero, although the limited variation of R would make it difficult to see an increase of the modest size indicated by Henderson's measurements.

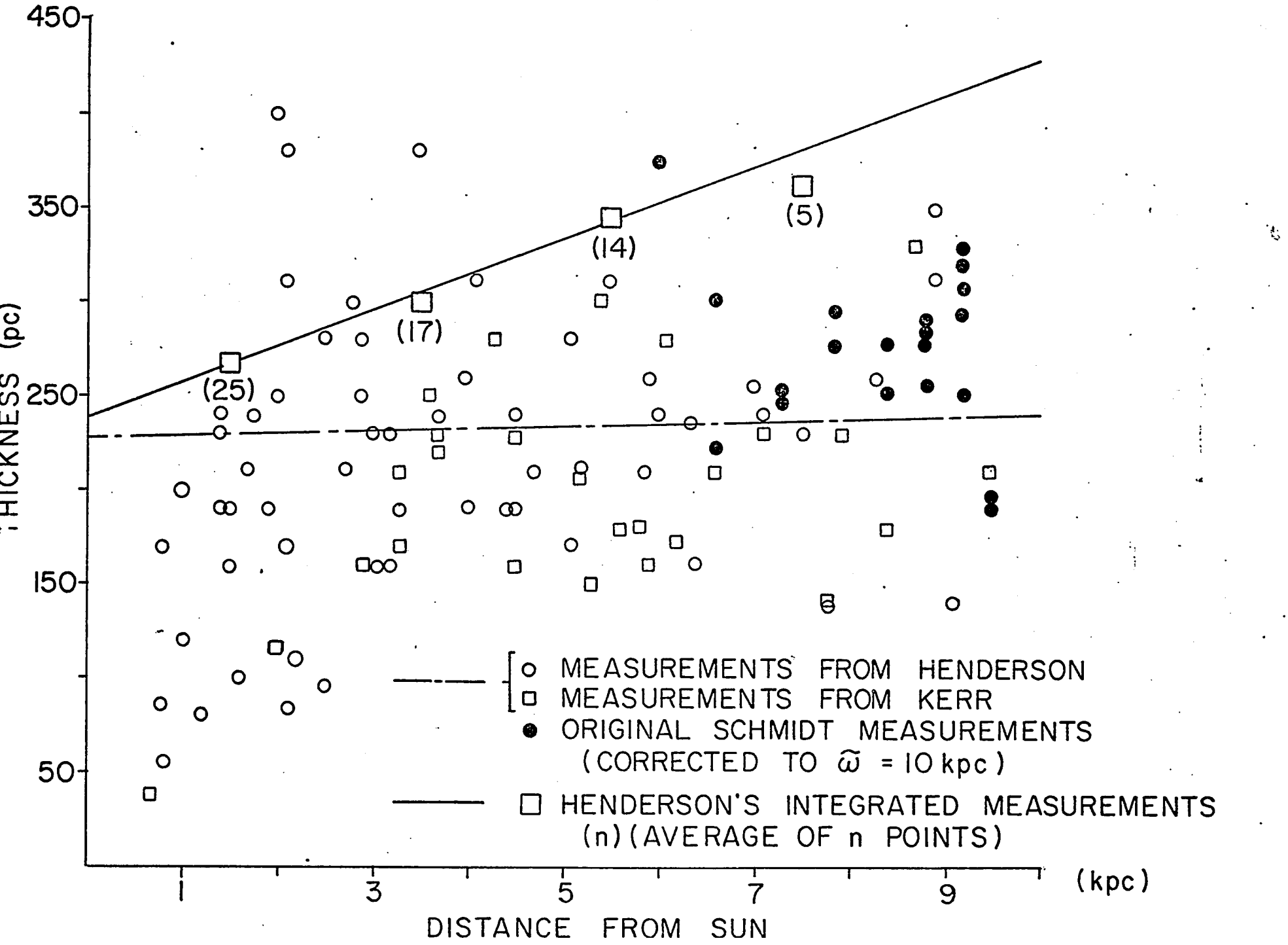
450
350
250
150
50
THICKNESS (pc)
(25)
(17)
(14)
(5)
MEASUREMENTS FROM HENDERSON
MEASUREMENTS FROM KERR
ORIGINAL SCHMIDT MEASUREMENTS
(CORRECTED TO $\tilde{\omega}$ = 10 kpc)
HENDERSON'S INTEGRATED MEASUREMENTS
(n)(AVERAGE OF n POINTS)
1
3
5
7
9
(kpc)
DISTANCE FROM SUN

Another approach was chosen by Henderson (1967). He attempted to separate the contributions of near gas and far gas by the following (admittedly crude) stratagem: Since the contribution of the far arm is confined to small latitude ranges (b usually between $\pm$ 1°K) he measured the thickness of the near gas simply by ignoring the variation of brightness temperature in that interval; i.e., treating it as a constant. This results in an overestimate of the thickness of the near gas, since the true peak temperature is somewhat higher than the temperature at the cutoff point. Also, since the optical depth is not negligible in the inner part of the disk, the use of brightness temperature rather than optical depth to determine the thickness results in a further overestimate of the thickness. Thus, his result of 300 pcs for the average thickness of the near gas regions of the inner disk must be considered a large overestimate. However, since we are concerned here mainly with the change in thickness with distance, this systematic error does not matter. Since Henderson integrated the profile rather than simply taking half-intensity points, his method should produce small scatter. In short, his results concerning the relative variation of thickness with distance should be the most reliable available. A least-squares fit to 60 points in the near regions of the inner portions of the disk shows the following behavior of thickness T with distance from the sun R:

$$T(\text{kpc}) = 240 + 19R$$

where R is in kpc. This is a large variation, with the thickness reaching a value of 400 pcs at R = 8kpc. Yet it is somewhat smaller (about ½ to 2/3) than the increase of 30-35 pcs/kpc observed in the outer regions. Thus it is strong, but not

FIGURES 35A,B

The following two diagrams are sample least-square fits to the integrated data obtained by Henderson concerning the thickness of the inner disk ($\varpi < 10$ kpc) and my own direct measurements made from the same studies. The direct measurements show far greater scatter and are probably not dependable for the reasons discussed in the text. If Henderson's integrated measurements are dependable, they indicate that the "distance effect" is discernible in the inner part of the Galaxy as well as the outer part, although the magnitude of 20 pcs/kpc may be somewhat smaller than the magnitude of about 30 pcs/kpc determined for the outer disk.

```
EXEC   *

   EXECUTION
HERE ARE THE COEFFICIENTS OF THE DISCRETE LEAST SQUARES POLYNOMIAL OF DEGREE N=  1

240.448411

18.801003
```

HENDERSON'S INTEGRATED MEASUREMENTS

THICKNESS OF INNER DISK VS. DISTANCE FROM SUN; ~~GAMMA MEASUREMENTS~~

Y	POLYI	Z	F	ERROR
0.0	240.45			
0.50	249.03			
1.00	259.31	1.00	240.00	19.311
1.50	268.74			
2.00	278.17	2.00	250.00	28.171
2.50	287.60			
3.00	297.03	3.00	290.00	7.031
3.50	306.46			
4.00	315.89	4.00	320.00	4.111
4.50	325.32			
5.00	334.75	5.00	450.00	99.251
5.50	344.17			
6.00	353.62	6.00	290.00	63.621
6.50	363.05			
7.00	372.48	7.00	400.00	27.521
7.50	381.91			
8.00	391.34	8.00	450.00	38.661
8.50	400.77			
9.00	410.20			
9.50	419.63			
10.00	429.06			
10.50	438.49			

EXEC *

EXECUTION
HERE ARE THE COEFFICIENTS OF THE DISCRETE LEAST SQUARES POLYNOMIAL OF DEGREE N= 1

174.546692

10.233587

THICKNESS OF INNER DISK VS. DISTANCE FROM SUN DIRECT MEASUREMENTS

Y	POLYI	Z	F	ERROR
0.0	174.55			
0.50	179.66	0.70	40.00	141.71
		0.80	50.00	126.73
1.00	184.78	1.20	80.00	106.83
		1.40	190.00	1.13
1.50	189.90	1.50	100.00	29.90
		1.80	240.00	47.03
2.00	195.01	2.10	170.00	26.64
2.50	200.13	2.70	210.00	7.82
		2.90	160.00	44.22
3.00	205.25	3.20	160.00	47.29
		3.30	210.00	1.68
3.50	210.36	3.50	300.00	89.64
4.00	215.48	4.00	190.00	25.48
		4.30	260.00	61.45
4.50	220.60	4.50	240.00	19.40
5.00	225.71	5.10	280.00	54.26
		5.40	300.00	74.19
5.50	230.83	5.60	180.00	51.85
		5.80	160.00	53.96
6.00	235.95	6.00	240.00	4.05
		6.40	100.00	80.64
6.50	241.07	6.60	210.00	32.09
7.00	246.18	7.00	260.00	13.82
7.50	251.30	7.50	230.00	21.30
		7.90	230.00	25.39
8.00	256.42			
		8.30	260.00	6.51
8.50	261.53	8.70	330.00	66.42
		8.90	310.00	44.37
9.00	266.65	9.10	140.00	127.67
9.50	271.77	9.50	210.00	61.77
10.00	276.88			
10.50	282.00			
11.00	287.12			

conclusive, evidence for the existence of a distance effect in the inner portions of the disk.

In an attempt to gain further information on the thickness of the inner portions of the Galaxy, I made measurements of half-intensity latitude widths directly from published observations of the Northern Sky by Henderson and the Southern Sky by Kerr (1969). Since the original computer tapes were not in my possession, I could not use the superior method of integrating the profile. Also, since the actual peak temperatures, which included contributions from both near and far regions, were used to determine the half-width, the effect from this factor would be a systematic underestimate of the thickness of the near regions. (However, measuring T_b instead of τ produces an overestimate, so that the two factors tend to cancel.) In any case, since the aim is to determine the variation of thickness with distance from the sun, we are again not too concerned with the magnitudes obtained. The results of a least-squares analysis of 26 measurements of near arm regions from the Henderson observations and 13 measurements of the Southern Sky inner arm regions from Kerr's measurements were as follows:

$$T = 227 \qquad \text{(H)}$$

$$T = 183 + 8R \qquad \text{(K)}$$

$$T = 220 + R \qquad \text{(both)}$$

Essentially no distance effect appears!

Twenty-three more points which could not be assigned definitely to spiral arm regions from both sets of observations gave the following behavior of thickness T with distance R:

$$T = 216 + 7R$$

And, finally, 26 points from what appeared to be interarm regions gave the following results:

$$T = 99 + 23R \qquad (H)$$

$$T = 93 + 15R \qquad (K)$$

$$T = 100 + 19R \qquad (\text{both})$$

However, the last series of values must be given very little weight. The reason is that in interarm regions, a large fraction of the peak optical depth is due to the distant material. This leads to a sharply reduced value for the thickness. More to the point for the present investigation, the change of the thickness with distance is also affected. Since, for any given line of sight, as the distance to a near region is increased the distance to the far region decreases, the apparent half-width in latitude of the far region increases. Since this in turn increases the apparent half-width of the combined temperature profile, we would expect our measured thicknesses to display an apparent increase with distance.

To sum up, we have considered previous investigations of the thickness of the inner regions of the disk by Schmidt (1957) and Henderson (1967) and also made some measurements on published observations ourselves. Schmidt's investigation showed no distance effect but was confined to too small an extent to be useful. Henderson's integrated measurements on 60 points in the near regions showed a linear increase of about 20 pcs/kpc, which, however, is rather smaller than the values found by him, M&M, L&K, and the present investigators in the outer regions of the Galaxy. And, finally, measurements

of about 62 points in regions that were not interarm regions showed essentially no distance effect. We have not found any detailed investigations of the inner regions of the Galaxy and their thicknesses other than those mentioned. On the other hand, the literature abounds in statements to the effect that the inner parts of the Galaxy are extremely flat. It seems possible that the expectation that the Galaxy is flat, derived both from edge-on photographs of external galaxies and theoretical expectations, has inhibited actual examination of the data for possible variations in thickness with distance from the sun.

In conclusion, it appears that the question of whether a distance effect is displayed in the inner parts of the Galaxy is still an open one. The distance ambiguity and uncertainty as to the temperature of the hydrogen make it extremely difficult to determine the magnitude of the thickness, but the variation of the thickness with distance should be relatively easy to determine. Since the "eror beam" of the 300-foot telescope has cast observations made with it in the 1966-70 period under a cloud, perhaps the best procedure would be a remapping of the region, followed by the integration method adopted by Henderson, to give a conclusive answer to the question.

APPENDIX : FORMAL ANALYSIS OF THE 3-D GAS EQUATIONS

After solving the fluid equations for the first-order systematic motions of the gas in the plane--$u_{\varpi}^{(1)}$ and $u_{\theta}^{(1)}$ -- we are left with a system of two first-order inhomogeneous ordinary differential equations in two unknowns--the spiral density perturbation $\rho^{(1)}$ and the vertical gas velocity u_z. If we make the assumption that the negligible density of the gas layer at the height ($\sim$300 pcs) where the Vandervoort stellar potential reaches the limits of its validity justifies our treating this point as suitable for the application of boundary conditions normally applied at infinity, then we have a well-posed mathematical problem and can develop a full analytic solution.

For Case I, in which the perturbation gas density is considered small compared to the axisymmetric density, we have the following complete system of equations:

$$if j_z + \rho^{(0)} a^2 \frac{\partial \mu}{\partial z} = -\rho^{(0)} \frac{\partial \Psi^{(1)}}{\partial z}$$

$$if\mu + \frac{1}{\rho^{(0)}} \frac{\partial}{\partial z} j_z = -\frac{if k^2}{K^2 - f^2} \Psi^{(1)}$$

with the boundary conditions

$$\mu(z) = \mu(-z)$$

$$j_z \Big|_{z \to \pm\infty} = 0$$

where $j_z \equiv \rho^{(0)} u_z$ is the mass flux in the vertical direction, and $\mu \equiv \frac{\rho^{(1)}}{\rho^{(0)}}$ is the ratio of the spiral perturbation density to the axisymmetric density.

Here $\varphi^{(1)} \equiv N_0 \, \mathrm{sech}^{|h|\Delta} z/\Delta$ is the Vandervoort spiral gravitational potential,

$$f = -m(\Omega - \Omega_p)$$

$$\rho^{(0)} = \rho_0 \, \mathrm{sech}^{\beta^2} z/\Delta$$

$$\beta^2 = \frac{2\pi G \sigma_* \Delta}{a^2} = \frac{2\langle v_z \rangle^2}{a^2}$$

We may combine the equations to get a single second-order equation for j_z or for μ:

$$j_z'' + \beta^2 \tanh\xi \, j_z' + \eta^2 j_z = F \, \mathrm{sech}^{|h|\Delta + \beta^2} \xi \tanh\xi$$

$$\mu'' - \beta^2 \tanh\xi \, \mu' + \eta^2 \mu = G \, \mathrm{sech}^{|h|\Delta} \xi + H \, \mathrm{sech}^{|h|\Delta + 2} \xi$$

where the prime denotes $\frac{d}{d\xi}$; $\xi = z/\Delta$

The boundary conditions in the first case are

$$j_z(0) = 0, \quad j_z(\infty) = 0$$

and in the second case are

$$\mu(z) = \mu(-z), \quad \int_{-\infty}^{\infty} \rho^{(0)} \mu \, dz = \frac{-k^2}{\kappa^2 - f^2} \int_{-\infty}^{\infty} \rho^{(0)} \varphi^{(1)} dz$$

Here

$$F = -i \frac{N_0}{a^2} |h| \Delta \rho_0 f \Delta (1 - x)$$

$$x = \frac{k^2 a^2}{\kappa^2 - f^2}$$

$$G = \frac{-N_0}{a^2} \left[\frac{(|h|\Delta)^2}{\frac{\kappa^2}{f^2} - 1} + |h|\Delta(\beta^2 + |h|\Delta) \right]$$

$$H = -\left(\frac{-N_0}{a^2}\right) \left[|h|\Delta(|h|\Delta + \beta^2 + 1) \right]$$

$$\eta = \frac{f\Delta}{a}$$

We can transform the homogenous equation for the mass flux j_z into the hypergeometric equation by making the substitution $u = \cosh^2 \xi$:

$$u(u-1)y'' + \left[\tfrac{1}{2}(\beta^2+2)u - \tfrac{1}{2}(\beta^2+1)\right]y' + \frac{\eta^2}{4}y = 0$$

This is the hypergeometric equation with

$$a + b + 1 = \tfrac{1}{2}(\beta^2+2)$$

$$c = \tfrac{1}{2}(\beta^2+1)$$

$$ab = \frac{\eta^2}{4}$$

Since u varies only between 1 and ∞ , we take the general solution around u = 1:

$$y = A y_1' + B y_2'$$

$$y_1' = F(a, b, \tfrac{1}{2}; 1-u) \qquad y_2' = (1-u)^{1/2} F(c-b, c-a, 3/2; 1-u)$$

But we are allowed only the odd solution for j_z, since we have demanded a plane-symmetric form for the density $\rho^{(1)}$; therefore, since $1-u = -\sinh^2 \xi$, which is even, we must have

$$A = 0.$$

Then the odd solution for the homogeneous part of j_z is

$$y_2' = i \sinh \xi \, F(c-a, c-b, 3/2; -\sinh^2 \xi)$$

To study the behavior around z = 0, we may expand in series form:

$$y_2' = i \sinh \xi \sum_{h=0}^{\infty} a_{2h} (i \sinh \xi)^{2h}$$

$$a_0 = 1$$

$$a_2 = \frac{(c-a)(c-b)}{3/2} = \frac{\beta^2 + 1 + \eta^2}{6}$$

$$a_4 = \frac{(c-a+1)(c-b+1)}{2!\, 5/2} a_2 = \frac{3\beta^2 + 9 + \eta^2}{20} a_2$$

$$a_{2h+2} = \frac{(2h+1)\beta^2 + (2h+1)^2 + \eta^2}{(2h+3)(2h+2)} a_{2h}$$

(This series is identical to that obtained from the original equation by the Frobenius method of series solution.)

We note that the coefficients depend on two dimensionless parameters: β^2, which is a measure of how tightly the gas is held to the plane by gravitational forces, and $\eta^2 \equiv \left(\frac{f\Delta}{a}\right)^2$, which compares a typical "z-velocity" f Δ (the product of the circular frequency f of the gas with respect to the spiral configuration with the scale height Δ of the stellar component) to the "effective sonic speed" a. Both quantities increase as we go inward toward the center of the Galaxy (assuming both a and Δ are constants or slowly varying with radius) so that, for small values of z, the homogeneous solution, which goes as $\sinh \xi (1 - a_2 \sinh^2 \xi)$ tends to be limited more and more sharply as we move to the interior of the Galaxy. The dependence on β^2 is, of course, to be expected, since the more tightly the gas is held to the plane, the less must be the vertical flux. The coefficients above also show that

there is a much stronger dependence on β^2 than on η^2. In fact, since β^2 is normally about ten times as large as η^2, it appears that the homogeneous solution is dependent only weakly on the value of the circular angular velocity f.

The solution around z = ∞ is

$$j_{z\,homog}^{\infty} = \alpha y_1^{\infty} + \beta y_2^{\infty}$$

where α and β are known functions of a, b, and c, and where

$$y_1^{\infty} = u^{-a} F(a, 1-c+a, 1-b+a; \tfrac{1}{u})$$

$$y_2^{\infty} = u^{-b} F(b, 1-c+b, 1-a+b; \tfrac{1}{u})$$

Since $a \equiv \frac{\beta^2}{4} + \sqrt{(\frac{\beta^2}{4})^2 - \frac{\eta^2}{4}}$ and $b \equiv \frac{\beta^2}{4} - \sqrt{(\frac{\beta^2}{4})^2 - \frac{\eta^2}{4}}$ are both greater than 0, the homogeneous solution for j_z satisfies the boundary condition at infinity by going to zero as

$$u^{-b} \equiv (\cosh^2 z/\Delta)^{-b}$$

The general solution to the homogeneous equation for μ may be found in the same way. Letting $u = \cosh^2 \xi$ again, we once again obtain the hypergeometric equation for μ:

$$u(u-1)\mu'' + [(1-\tfrac{\beta^2}{2})u - \tfrac{1-\beta^2}{2}]\mu' + \tfrac{\eta^2}{4}\mu = 0$$

Taking the even solution around u = 1 (z=0), we have

$$\mu_{homog}^{1} = A F(a', b', \tfrac{1}{2}; 1-u)$$

where $a' = -\frac{\beta^2}{4} + \sqrt{(\frac{\beta^2}{4})^2 - \frac{\eta^2}{4}}$ and $b' = -\frac{\beta^2}{4} - \sqrt{(\frac{\beta^2}{4})^2 - \frac{\eta^2}{4}}$

Once again the solution around infinity is

$$\mu_{homog}^{\infty} = \alpha' \mu_1^{\infty} + \beta' \mu_2^{\infty}$$

where α' and β' are fixed in terms of a' and b', and where

$$\mu_1^{\infty} = (-u)^{-a'} F(a', 1-c'+a', 1-b'+a'; 1/u)$$

$$\mu_2^{\infty} = (-u)^{-b'} F(b', 1-c'+b', 1-a'+b'; 1/u)$$

But since both a' and b' are < 0, the homogeneous solution blows up at infinity.

Case II. The above results were obtained for the case in which the perturbation density is small compared to the axisymmetric density. How do these results change when, as is probably the case for our own Galaxy, the spiral density is comparable in size to the axisymmetric density?

The system of equations is now

$$if j_z + \rho^{(0)} a^2 \frac{\partial \mu}{\partial z} = -\rho^{(0)} \frac{\partial \varphi^{(1)}}{\partial z}$$

$$(1+\chi) if \mu + \frac{1}{\rho^{(0)}} \frac{\partial}{\partial z} j_z = \frac{-if h^2}{k^2 - f^2} \varphi^{(1)}$$

where $\chi \equiv \frac{h^2 a^2}{k^2 - f^2}$ is the term measuring the effect of the added pressure produced by the spiral density.

Again combining the equations to get a single second-order differential equation for j_z or for μ :

$$j_z'' + \beta^2 \tanh\xi \, j_z' + (1+\chi)\eta^2 j_z = F_\chi \operatorname{sech}^{|h|\Delta + \beta^2}\xi \tanh\xi$$

$$\mu'' - \beta^2 \tanh\xi \, \mu' + (1+\chi)\eta^2 \mu = G \operatorname{sech}^{|h|\Delta}\xi + H \operatorname{sech}^{|h|\Delta+2}\xi$$

where $F_\chi = \rho_0 a(-\eta)\left(-\frac{N_0}{a^2}\right)|h|\Delta$

and G and H are as before.

It is evident that the previous results for the homogeneous solutions may be applied to this case with the single difference that η^2 is to be replaced with $(1+\chi)\eta^2$.

Particular Solution. With the general solution to the homogeneous equations for both j_z and μ in hand, it is a straightforward matter to derive the particular solution to the inhomogeneous equation. For example, the particular solution for j_z may be written in integral representation:

$$j_p = y_2' V$$

where $$y_2' = (1-u)^{1/2} F(c-b, c-a, 3/2; 1-u)$$

and where $$V = \int_1^u (u-1)^{-1/2} u^{-\left(\frac{1+\beta^2}{2}\right)} (y_2')^{-2} du$$

$$+ \int_1^u (u-1)^{-1/2} u^{-\left(\frac{1+\beta^2}{2}\right)} (y_2')^{-2} \left[\int_1^u \frac{F}{4} u'^{\left(-\frac{h/\Delta - 1}{2}\right)} y_2' du' \right] du$$

But a glance at the above expression makes it abundantly clear that the full analytic solution is too unwieldy to allow information about the functions of interest to be extracted easily. Thus it appears that the analytic approach to this problem must be supplemented by the numerical approach adopted in the main text.

TABLE I: OUTER ARM

ℓ (deg.)	V (km/sec)	b (deg.)	dV/db (km/sec-deg)	Obs	Notes
16	-24		-0.2	H*	
20	-30	+0.6	-0.3	K, H	
25	-32	+0.4	-2.7	K	
26	-36	+0.5	-0.5	H	
30	-32	+1.0	-2	K, H	2**
31	-35	+1.0		K	
32	-36	+1.0	+4	K	
33	-37	+0.9	-8	K	
34	-26	+0.4	-6	K	
35	-27	+0.2		K	1
36	-35	+0.9	-2	H	1
39	-38	+0.6	-6	K	
40	-34	+0.5	-6	K	1
45	-42	+1.1	-9	K, H	
50	-50	+1.6	0	K	
55	-46	+1.6	-1	H, K	1
60	-63	+1.4	-4	H, K	1, 2
65	-68	+0.5	-1.2	H	1
70	-68	+0.5	-0.8	H	1
75	-74	+1.8	+0.5	H	1
80	-67	+1.2	-1.2	H	1
86	-76	+2.2	-0.5	H	1, 4
90	-77	+2.0	-1.5	H	1
95	-72	+1.7	-2.5	H	

OUTER ARM (CONT.)

ℓ	V	b	dV/db	Obs	Notes
100	-62	+1.9	-2.4	H	
105	-65	+2.6	0	H	
110	-67	+3.0	-3.5	H	1
115	-64	+2.4	-2	H	1
121	-67	+3.0	-2	H	1
125	-76	+2.4	-2	H	5
132	-67	+1.9		H	
136					
140	-62	+1.5	-0.8	H	5
146	-56	+2.6	+2.5	H	1
150	-54	+0.8	+1	H	
155	-48	+1.2		H	

* H: Henderson (1966), K: Kerr (1969), HK: Hindman and Kerr (1969), B: Burton (1970), S: Shane (1971).

** number referring to the following comments:

1. Two or more components at different velocities or latitudes.
2. Splitting of ridge lines indicating possible close approach of other features.
3. Nearby low-density patches or absorption.
4. Inner contour lines give different values of dv/db from the outer ones.
5. Identification of spiral arm doubtful.

OUTER ARM (SOUTHERN SKY)

ℓ	V	b	dV/db	Obs	Notes
200	22	-1.0	0	H, HK	
205	32	-0.9	-0.3	H	4
210	42	-1.5	0	H, HK	1
215	49	-1.7	-0.2	H, HK	1
220	58	-0.7	0	H, HK	1
225	63	-2	-0.2	H	1
230	68	-1.4	0	H, HK	
235	70	-1.5		HK	
240	83	-2.0	-2	HK	
245	84	-3	-1	HK	
250	92	-3.3	0	HK	
255					
260	90	-1.4		HK	
265	92	-1.9	+2	HK	
270					
275	105	-3.0		HK	5
280	97	-3.3	+1	HK	
285	92	-3.7	0	HK	
290	93	-2.9	-1	HK	1
295					
299					

TABLE II: PERSEUS ARM

ℓ (deg.)	V (km/sec)	b (deg.)	dV/db (km/sec-deg)	Obs	Notes
65	-12	+0.4	-1.5	H*	
70	-24	+1.6	-?	H	5*
75	-22	+0.7	-2	H	
80	-35	+2.0	+0.3	H	4
86	-42	+0.8	0	H	2
90	-45	-0.1	+2	H	5
95	-46	+0.1	-1.3	H	
100	-53	0.0		H	2
105	-51	+0.8	0	H	1
110	-48	+0.9	-1.2	H	
115	-45	+2.7	-3	H	
121	-50	+2.5	-1	H	2
125	-55	+2	-0.7	H	1
131.5	-48	+1.4	+1.7	H	4
136	-47	+1.9	-1	H	1
140	-40	+1.4	-1.0	H	1
146	-36	+1.1	-0.7	H	
150	-32	-1	-1.1	H	
155	-30	+1	-1	H	
160	-30	+1		H	

* See footnotes on Table I.

PERSEUS (SOUTHERN SKY)

ℓ	V	b	dV/db	Obs	Notes
205	20	-0.6	+0.1	H	1
210	24	-0.4	+0.5	H	1
215	27	-1.6	0	H, HK	
220	31	-1.5	0	H, HK	
225	40	-1	+1	H	5
230	39	-1	-0.1	H	
235	50				
240					
245	61	-0.7	0	HK	
250	70	-0.6	0	HK	
255	68	-0.4	-1.5	HK	
260	61	-0.8	-2	HK	
265	62	-2.3	+5	HK	1
270	67	-0.8		HK	4, 1
275	72	-1.7	+4	HK	
280	73	-1.1		HK	
285	70	-1.8		HK	
290	70	-1.2	-1	HK	1
295	83	-2.2		HK	
299	80	-3		HK	

TABLE III: CARINA FEATURE

ℓ (deg.)	V (km/sec)	b (deg.)	dV/db (km/sec-deg)	Obs.	Notes
295	23	-0.3	-1	HK*	
299	25	0.0		HK	
300	30	-0.1	-1	K	
301	30	<-0.5	0	K	3*
302	30	-0.7	-2.7	K	
303	31	-0.4	+1	K	
304	33	-0.5	+0.2	K	
305	33	-0.6		K	2
306	41	-0.5		K	1
307	34	<-0.7		K	1
308	32	-0.7		K	1
309	33	-0.6	-1.6	K	
310	33	-0.3	-1.2	K	
311	35	-0.7	-0.8	K	
312	36	-0.5	-5	K	
314	36	-0.4	-2	K	1
315	33	-0.5	-1	K	
316	32	-0.4	-2	K	
318	39	-0.7	-3	K	
320	37	-0.5	0	K	
322	31	-0.3	-0.5	K	
324	24	-0.5	-2	K	
325	28	-0.3	-2	K	

* See footnotes on Table I.

CARINA (CONT.)

ℓ	V	b	dV/db	Obs	Notes
326	31	-0.4	-0.5	K	
326.5	28	-0.6		K	1
327	29	-0.6	+0.5	K	
327.5	37	-0.7	-2.5	K	1
328	37	-0.6	-4	K	1
329	34	-0.6		K	
330	32	-0.8	-1.6	K	
331	33	-0.3	0	K	
332	31	-0.5		K	
333	34	-0.7		K	1

TABLE IV: FAR OUTER ARM

ℓ (deg.)	V (km/sec.)	b (deg.)	dV/db (km/sec-deg)	Obs	Notes
26	-36	+0.5	-0.4	H*	
30	-45	+2.5	-1	H	
36	-50	+1.4	-5	H	
40	-60	+1.7	+1	H,K	
45	-66	+2.5	-1	H,K	
55	-68	+2.5	-2.5	H	
60	-77	+2.6	-1	H	
65	-85	+2.7	0	H	
80	-89	+2.3	-1	H	
86	-90	+2.0	-0.3	H	
90	-91	+2.5	-2.5	H	
95	-95	+2.5	-2.3	H	
100	-93	+2.6	+0.5	H	
105	-95	+2.2	+0.3	H	
110	-97	+2.0	0	H	
115	-98	+1.8	+2	H	1*
121	-90	+1.6	0	H	5
125	-87	+2	-1	H	5
132	-78	+1.3	-1	H	
136	-74	+2.6	-0.7	H	
145	-74	+1.0	-1	H	
146	-70	+1	+0.6	H	

*See footnotes on Table I

TABLE V: NORTHERN SAGITTARIUS ARM

(near)

ℓ (deg.)	V (km/sec)	b (deg)	dV/db (km/sec-deg,)	Obs.	Notes.
16					
20	22	+0.3	-0.8	H, K*	4*
22.3	15	+0.2	+0.3	S	1
23.3	20	+0.2	0	S	1
24.3	19	+0.2		S	1
25	18	-0.2	+2.5	K	1
25.3	22	+0.2	-0.3	S	1
26	21	0	0	H	4
26.3	21	+0.6	-0.5	S	1
27.3	22	+1	-0.6	S	1
28.3	22	+0.5	0	S	1
29.3	26	+0.2	-0.3	S	1
30	24	+0.5	0	H, K	
30.3	20	+0.4		S	1
31	26	+0.5	-3.7	K	4
31.3	25	+1.0	+0.6	S	
32	19	+0.3	-0.2	K	
32.3	24	+0.3	0	S	1
33	27	+0.4	-1.5	K	
33.3	22	+0.5	+0.7	S	
34	22	+0.5	0	K	
34.3	25	+0.4		S	
35	23	+0.1	-1.3	K	
35.3	29	+0.2	-0.2	S	
36	33	+0.3	-0.4	H	
36.3	33	+0.1	-0.5	S	
37.3	28	+0.5	-0.8	S	1
38.3	29	+0.7	0	S	1
39	26	+0.4	0	K	

* See Footnotes in Table I

NORTHERN SAGITTARIUS ARM (NEAR) (CONTINUED)

ℓ	V	b	dV/db	Obs	Notes
39.3	28	+0.1	0	S	
40	36	+0.1	0	H,K	
40.3	31	+0.3	-0.6	S	1
41.3	33	0	-0.3	S	
42.3	32	+0.1	-0.2	S	
43.5	36	-0.5	-1	B	3
45	34	+0.7	-0.3	B,H,K	1
46.5	32	+2	-1.3	B	3
48	46	-0.4	+0.3	B	
49.5	48	-0.2	+0.6	B	3
50	52	-0.2	0	K	
51	45	+0.3	-0.5	B,H	
52.5	49			B	

TABLE VI: NORTHERN SAGITTARIUS ARM (FAR)

ℓ (deg.)	V (km/sec)	b (deg.)	dV/db (km/sec-deg.)	Obs	Notes
28.3	42	0		S*	5*
29.3	45	-0.3	-1	S	
30	46	0	-0.7	H,K	
30.3	42	0	-0.3	S	
31	42	+0.2	0	K	5
31.3	44	+0.2	-1	S	
32	50	+0.4	0	K	
32.3	47	+0.5	0	S	4
33	53	+0.3	0	K	
33.3	52	+0.1	-1.5	S	
34	50	0	0	K	
34.3	46	0	+0.5	S	4
35	52	0	0	K	
35.3	51	+0.1	-0.6	S	
36	52	-0.1	-0.5	H,K	
36.3	54	-0.4	-0.8	S	4
37.3	57	-0.1		S	
38.3	56	-0.2	0	S	
39	60	-0.2	-1.2	K	
39.3	61	-0.2	-1	S	
40	65	-0.4	-1.3	H,K	
40.3	64	-0.3	-0.6	S	
41.3	62	-0.4	0	S	
42.3	60	-0.3	0	S	
43.5	60	-0.4	0	B	3
45	60	-0.3	-0.4	B,H,K	1
46.5	59	-0.3	0	B	
48	57	-0.3	-1	B	
49.5	55	+0.1	-0.7	B	3
50	53	-0.2	+0.1	K	1
51	53	0	-0.6	B,H	

*See footnotes on Table I

TABLE VII: SCUTUM ARM (NEAR)

ℓ (deg)	V (km/sec)	b (deg)	dV/db (km/sec-deg)	Obs	Notes
20	56	-0.3	+6	H,K*	
22.3	55	-0.5	0	S	5*
23.3	55	-0.5	-0.7	S	1
24.3	59	-0.4	+1	S	
25	50	+0.2	-2	K	
25.3	56	-0.2	-1	S	
26	60	-0.3	-1.5	S	
26.3	61	-0.1	+1	H	
27.3	64	0	-0.2	S	5
28.3	67	+		S	
29.3	74	0	-1	S	
30	75	-0.4	+0.3	K,H	4
30.3	76	-0.5	-0.3	S	
31	79	0	-0.5	K	1
31.3	79		-0.2	S	3
32	79	+0.1	0	K	
32.3	80	+0.1	+0.2	S	
33	84	+0.1		K	2
33.3	81	0	+0.4	S	
34	89	0	+0.5	K	
34.3	86	+0.2	+0.2	S	
35	84	+0.1	+1	K	
35.3	84	0	+0.5	S	
36	80	+0.4	-2.3	H,K	
36.3	80	+0.2	-0.3	S	

* See footnotes on Table I.

TABLE VIII: SCUTUM ARM (FAR)

ℓ (deg)	V (km/sec)	b (deg)	dV/db (km/sec-deg)	Obs	Notes
20	95	+0.1	0	H,K*	4*
22.3	94	+0.2	+0.6	S	5
23.3	97	+0.1	+0.1	S	
24.3	96	-0.4	+0.5	S	
25	98	+0.1	+1.5	K	
25.3	94	-0.5	-1.5	S	
26	95	0	-5	H	
26.3	98	+0.1	-7	S	
27.3	92	+0.2	0	S	
28.3	94	-0.2	+0.2	S	
29.3	94	+0.2	0	S	
30	92	-0.2	-0.3	H,K	1
30.3	97	-0.2		S	
31	96	-0.1	0	K	
31.3	96	0	0	S	
32	100	0.0	0	K	1
32.3	100	+0.2	+0.6	S	
33	90	+0.1	+1.2	K	
33.3	93	+0.2	0	S	
34	90	+0.1	+2	K	
34.3	89	+0.2	+0.2	S	

* See footnotes on Table I.

TABLE IX: 3-KPC ARM

ℓ (deg)	V (km/sec)	b (deg)	dV/db (km/sec-deg)	Obs	Notes
336	-114	-0.2	-3.5	K*	
337	-118	-0.1	0	K	1*
338	-115	-0.1	0	K	
339	-122	-0.2	0	K	
340	-120	-0.1	+0.7	K	
341	-125	+0.1			4
342	-128	-0.1	-5	K	
343	-122	+0.2	0	K	
344	-116	+0.2	0	K	1
345	-117	-0.1			4
346	-117	0			4
347	-118	+0.1			4
348	-115				5
349	-113	+0.3	-4	K	
350	-106	+0.3	-5	K	
351	-101	+0.2	-6	K	
352	- 91	0	-1	K	
353	- 87	-0.2	-5	K	
354	- 85	-0.2	-5	K	
355	- 77	+0.2	-6	K	
355.5	- 75	+0.3	-3	K	
356	- 68	-0.1	-2	K	
356.5	- 68	+0.1	-3	K	
357	- 72	-0.1	-5	K	
357.5	- 61	-0.1	-3.5	K	
358	- 58	0	-3	K	
358.5	- 60	-0.1	0	K	
359	- 57	-0.2	0	K	

* See footnotes on Table I.

TABLE X: SOUTHERN SAGITTARIUS ARM (NEAR)

ℓ (deg)	V (km/sec-deg)	b (deg)	dV/db (km/sec-deg)	Obs	Notes
306	-37	+0.2	-3	K*	1*
307	-32		-4.4	K	1
308	-38		-5	K	
309	-33		-2.5	K	1
310	-40	+0.5	-2	K	2
312	-42	+0.4	+1	K	1
314	-44	-0.2	-2	K	1,2
315	-48	0.0	0	K	1,2
316	-50	+0.1	-2.3	K	1,2
318	-47	+0.1	+1.7	K	1,2
322	-34	+0.5	+5	K	1
324	-48	0	+2	K	1
325	-45	0	+3	K	
326	-34			K	5
326.5	-34			K	5
327	-34			K	5
327.5	-32			K	5
328	-38	>+0.3	0	K	
329	-23	>+0.3	-1.3	K	5
330	-25	>+0.5		K	5
331	-25	>+0.5	-2	K	5
333	-19		-0.5	K	

* See footnotes on Table I.

SOUTHERN SAGITTARIUS ARM (NEAR) (CONTINUED)

ℓ	V	b	dV/db	Obs	Notes
335	-18	> +0.1	-0.5	K	
336	-16	> +0.5	-0.5	K	1
337	-18	> +0.2	-0.4	K	1
338	-16	> +0.2	-0.4	K	1
339	-15	< -0.1	0	K	
340	-18		+0.2	K	

TABLE XI: SOUTHERN SAGITTARIUS ARM (FAR)

ℓ (deg.)	V (km/sec.)	b (deg.)	dV/db (km/sec-deg.)	Obs	Notes
314	-20	0.0	+0.6	K*	2*
315	-29	-0.2	+2	K	
316	-22	-0.2	-1	K	
318	-18	-0.3	+0.5	K	
322	-6	-0.3	-0.2	K	5
324	-4	+0.2	0	K	5
326	-5	0	-0.5	K	5
327	-5	0.0	0	K	5
327.5	-5	-0.1		K	5
328	-1	0.0	0	K	
329	-2	+0.2	-1	K	
331	-1	-0.3	0	K	
333	0	-0.2	0	K	
335	-2	-0.2	0	K	
336	+2	-0.6	+1	K	
337	+4	-0.5		K	
338	+4	-0.2		K	5
339	+8	-0.4		K	
340	+18	-0.4		K	5

*See footnotes in Table I

TABLE XII: NORMA (NEAR)

ℓ (deg)	V (km/sec)	b (deg)	dV/db (km/sec-deg)	Obs	Notes
322	-75	+0.2	0	K*	
324	-75	+0.2	-1	K	
325	-80			K	
326	-87	+0.4		K	
326.5	-88	+0.4		K	
327	-85	+0.4		K	
327.5	-85	+0.2	+5	K	3*
328	-86	+0.5	+3	K	3
329	-86	+0.4	+3	K	3
330	-88	+0.3		K	
331	-82	+0.1	+4	K	
333	-82	+0.2	0	K	5
334	-85	+0.1		K	5
335	-85	+0.2	+?	K	5
336	-85		0	K	5
337	-75	+0.1	-5	K	5
338	-58	0		K	5

* See footnotes on Table I.

TABLE XIII

OVERESTIMATES OF GALACTIC THICKNESS AS A FUNCTION OF DISTANCE FOR TELESCOPES OF DIFFERING BEAM WIDTHS

HPBW / $2b_{\frac{1}{2}}$ *	Thickness Overestimate (%)	Distance: Large Telescope (HPBW = 12') (kpc)	Distance: Small Telescopes (HPBW = 2°) (kpc)
0	0	0	0
$\frac{1}{4}$	3	17	1.7
$\frac{1}{2}$	12	35	3.5
3/4	20	52	5.2
1	41	70	7.0
2	123	140	14.0
3	316	210	21.0

* In this column, the beam width of the telescope (HPBW) is compared to the angular width of the source ($2b_{\frac{1}{2}}$). Distances in columns three and four are computed on the basis of a spiral arm source width of 300 pc.

REFERENCES

Bok, B. J., 1971, Highlights of Astronomy 2, 63 (Dordrecht-Holland: D. Reidel Publishing Co.)

Bolton, J. G., Stanley, G. J., and Harris, D. E., Publ. Astron. Soc. of the Pacific 70, 417

Burton, W. B., 1970, Astron & Astrophys Suppl. 2, 291

Burton, W. B. and Shane, W. W., 1970, IAU Symposium Proceedings 38, 97 (Dordrecht-Holland: D. Reidel Publishing Co.)

Clark, B. G., Radhakrishnan, V., and Wilson, R. W., 1961, Observations of Caltech Radio Observatory at Owens Valley #3

Clark, B. G., 1965, Ap J 142, 1398

De Jager, G., 1970, Nature 225, 622

Dieter, N. H., 1964 A J 69, 288

Dieter, N. H., 1965 A J 70, 552

Falgarone, E., and Lequeux, J., 1973, Astron & Astrophys 25, 253

Field, G. B., Goldsmith, D. W., and Habing, H. J., 1969, Ap J Letters, 155, L149

Fujimoto, M. and Miyamoto, Y., 1969, Publ. Astron. Soc. Japan 21, 194

Fujimoto, M. and Tanahashi, Y., 1971, Publ. Astron. Soc. Japan 23, 7

Fujimoto, M. and Tanahashi, Y., 1971, Publ. Astron. Soc. Japan 23, 13

Goldreich, P. and Lynden-Bell, D., 1965, MN 130, 97

Grahl, B. H., 1960, Mittelungen Sternwate Bonn, #28

Grahl, B. H., Hackenberg, O., and Mebold, U., 1968, Beitr. Radioastronomie 7, 1

Gum, C. S., Kerr, F.J., and Westerhout, G., 1960, MN 121, 132

Harten, R., 1971, Ph. D. thesis, Univ. of Maryland

Henderson, A. P., 1966, Latitude-Velocity Maps, long. 16° to 230°, lat. -10° to +10°, Astronomy Program, Univ. of Maryland

Henderson, A. P., 1967, Ph. D. thesis, Univ. of Maryland

Heiles, C., 1967, Ap J Suppl. 15, 97

Hindman, J. V., and Kerr, F. J., 1969, Aust. J. Phys. Supp. 18

Hunter, C. and Toomre, A., 1969, Ap J 155, 747

Hulst, H. C. van de, 1967, Ann Rev Astron & Astrophys 5, 167

Kardashev, N., Lozinskaya, T., and Sleptsova, 1964, Sov A J 8, 479

Kerr, F. J., 1965, chapter in Galactic Structure, vol. V of Stars and Stellar Systems, ed. by L. Aller and B. McLaughlin, Univ. of Chicago Press

Kerr, F. J., 1969a, Ann Rev Astron & Astrophys 7, 39

Kerr, F. J., 1969b, Aust. J. Phys. Astrophys Suppl 9, 1

Kerr, F. J., Hindman, J. V., and Gum, C. S., Aust. J of Phys 12, 270

Kerr, F. J. and Westerhout, G., 1965, in Galactic Structure, vol. V of Stars and Stellar Systems, ed. by L. Aller and B. McLaughlin, Univ. of Chicago Press

Landau, L., and Lifschitz, E. L., Fluid Mechanics, Reading, Mass. Addison-Wesley (1959)

Lin, C. C. and Shu, F., 1964, Ap J 140, 646

Lin, C. C., Shu, F., and Yuan, C., 1969, Ap J 155, 329

Lindblad, P., 1972, Latitude-Velocity Maps, Astronomy Program, Univ. of Maryland

Makarova, S., Sov A J 8, 485 (1964)

Manchester, R. M., 1972 Ap J 172, 43

Mathewson, D. S., 1968, Ap J Letters 153, L47

McGee, R. X., and Milton, Janice, 1964, Aust. J of Phys 17, 128

Mebold, U., 1972, Astron & Astrophys 19, 13

Oort, J. H., 1962, in Interstellar Matter in Galaxies, ed. L. Woltjer, Benjamin Press, NY

Oort, J. H., Kerr, F. J., and Westerhout, G., 1961, MN 121, 123

Parenago, P. P., 1955, Astron-Zhu., 32, 226

Piddington, F., 1973, Ap J 179, 755

Roberts, M., 1970, IAU Symposium Proceedings 44, 12 (Dordrecht-Holland: D. Reidel Pub. Co.)

Roberts, W. W., 1969, Ap J 158, 123

Roberts, W. W., and Yuan, C., 1970, 161, 887

Rohlfs, K., 1971, Astron & Astrophys 12, 43

Rougoor, G. W., 1964, BAN 17, 381

Rougoor, G. W., and Oort, J. H., 1959, Paris Symp. on Radio Astron

Rougoor, G. W., and Oort, J. H., 1960, Proc. Nat. Acad. of Sci. 46, 1

Schmidt, M., 1957, BAN 13, 247

Schmidt, M., 1965, in Galactic Structure, vol. V of Stars and Stellar Systems, Ed. by L. Aller and B. McLaughlin, Univ. of Chicago Press

Shane, W. W., 1970, Ph. D. dissertation, Leiden Univ., p. 55

Shane, W. W., 1971, Astron & Astrophys Suppl. 4, 1 and 315

Shu, F. 1968, Ph. D. thesis, Harvard Univ.

Shu, F., Milione, V., Gebel, W., Yuan, C., Goldsmith, D. W., and Roberts, W. W., 1972, Ap J 173, 557

Takakubo, K., 1967, BAN 19, 125

Vandervoort, P., 1970, Ap J 161, 67

Westerhout, G., 1957, BAN 13, 201

Westerhout, G., 1970, in Galactic Astronomy (New York: Gordon and Breach) 1, 167

Weaver, H., IAU Symposium Proceedings 38, ed. by W. Becker, and G. Contopoulos, (New York: Springer-Verlag)

Weaver, H., 1973, Astron & Astrophys Supp 8, 1

Yuan, C., 1969, Ap J 158, 871

Yuan, C., 1970, IAU Symposium Proceedings 38, 391
(Dordrecht-Holland: D. Reidel Publishing Company)

Yuan, C. and Wallace, Lance, 1973, Ap J 185, 453